# STUDY OF NON-STATIONARY SIGNAL MODELS FOR OPTICAL FIBER BASED SENSORS

*By*

**MANOJ KUMAR SAXENA**

**Enrolment No: ENGG03201004001**

**Raja Ramanna Centre for Advanced Technology, Indore**

*A thesis submitted to the*

*Board of Studies in Engineering Sciences*

*In partial fulfillment of requirements*

*for the Degree of*

**DOCTOR OF PHILOSOPHY**

*of*

**HOMI BHABHA NATIONAL INSTITUTE**

**June, 2016**

# HOMI BHABHA NATIONAL INSTITUTE

## Recommendations of the Viva Voce Committee

As members of the Viva Voce Committee, we certify that we have read the dissertation prepared by **Shri Manoj Kumar Saxena** entitled **"Study of Non-stationary Signal Models for Optical Fiber Based Sensors"** and recommend that it may be accepted as fulfilling the thesis requirement for the award of Degree of Doctor of Philosophy.

| | | |
|---|---|---|
| Chairman-Prof. D. N. Badodkar | Badodkar 6/3/17 | Date: 06/03/2017 |
| Guide / Convener-Prof. S.V.G. Ravindranath | 6/3/17 | Date: 06/03/2017 |
| Examiner-Prof. Pradip Sircar | Sircar | Date: 06/03/2017 |
| Member 1-Prof. A. P. Tiwari | 06/3/17 | Date: |
| Member 2-Prof. A. K. Bhattacharjee | AKBhattacharjee | Date: 06/03/2017 |
| Member 3-Prof. Arup Banerjee | Arup Banerjee | Date: 06/03/2017 |
| Technology Advisor-Shri R. Arya | Rarya | Date: 06/03/2017 |

Final approval and acceptance of this dissertation is contingent upon the candidate's submission of the final copies of the thesis to HBNI.

I hereby certify that I have read this thesis prepared under my direction and recommend that it may be accepted as fulfilling the thesis requirement.

For Arup Banerjee

**Date:** 06/03/2017
**Place:** Indore

**Prof. S.V.G. Ravindranath**
**(Guide)**

# STATEMENT BY AUTHOR

This dissertation has been submitted in partial fulfillment of requirements for an advanced degree at Homi Bhabha National Institute (HBNI) and is deposited in the Library to be made available to borrowers under rules of the HBNI.

Brief quotations from this dissertation are allowable without special permission, provided that accurate acknowledgement of source is made. Requests for permission for extended quotation from or reproduction of this manuscript in whole or in part may be granted by the Competent Authority of HBNI when in his or her judgment the proposed use of the material is in the interests of scholarship. In all other instances, however, permission must be obtained from the author.

Manoj Kumar Saxena

# DECLARATION

I, hereby declare that the investigation presented in the thesis has been carried out by me. The work is original and has not been submitted earlier as a whole or in part for a degree / diploma at this or any other Institution / University.

Manoj Kumar Saxena

# List of Publications arising from the thesis

## Journal

1. "Empirical mode decomposition-based detection of bend-induced error and its correction in a Raman optical fiber distributed temperature sensor", Manoj Kumar Saxena, S. D. V. S. J. Raju, R. Arya, R. B. Pachori, S. V. G. Ravindranath, S. Kher, S. M. Oak, *IEEE Sensors Journal*, **2016**, *16* (*5*), 1243-1252.

2. "Empirical mode decomposition based dynamic error correction in SS covered 62.5/125 μm optical fiber based distributed temperature sensor", Manoj Kumar Saxena, S. D. V. S. J. Raju, R. Arya, R. B. Pachori, S. V. G. Ravindranath, S. Kher, S. M. Oak, *Optics & Laser Technology*, **2015**, *67*, 107-118.

3. "Raman optical fiber distributed temperature sensor using wavelet transform based simplified signal processing of Raman backscattered signals", Manoj Kumar Saxena, S. D. V. S. J. Raju, R. Arya, R. B. Pachori, S. V. G. Ravindranath, S. Kher, S. M. Oak, *Optics & Laser Technology*, **2015**, *65*, 14-24.

4. "Optical fiber distributed temperature sensor using short term Fourier transform based simplified signal processing of Raman signals", Manoj Kumar Saxena, S. D. V. S. J. Raju, R. Arya, S. V. G. Ravindranath, S. Kher, S. M. Oak, *Measurement*, **2014**, *47*, 345-355.

5. "Microcontroller based Raman optical fiber distributed temperature sensor and alarm system", Manoj Kumar Saxena, S. D. V. S. J. Raju, R. Arya, S. V. G. Ravindranath, S. Kher, S. M. Oak, *Journal of the Instrument Society of India*, **2014**, *44* (*1*), 28-31.

# Conferences

1. "Temperature error due to discontinuity in sensing fiber and its compensation in fiber distributed temperature sensor", Manoj Kumar Saxena, S. D. V. S. J. Raju, J. Kishore, R. Arya, S. V. G. Ravindranath, S. Kher, S. M. Oak, In: Proceedings of 39th National Symposium on Instrumentation (NSI) - 39, Haridwar, 15-17 Oct, 2014.

2. "Study of compact and portable fiber optic distributed temperature sensor based on Raman effect", S. D. V. S. J. Raju, M. K. Saxena, S. Kher, J. Kishore, S. Kher, and S. M. Oak, In: Proceedings of International Conference on Optics and Optoelectronics (ICOL) - 2014, Dehradun, 5-8 March, 2014, pp. 72.

3. "Microcontroller based Raman optical fiber distributed temperature sensor and alarm system", Manoj Kumar Saxena, S. D. V. S. J. Raju, J. Kishore, R. Arya, S. V. G. Ravindranath, S. Kher, S. M. Oak, In: Proceedings of 38th National Symposium on Instrumentation (NSI) - 38, Hubli, 24-26 Oct, 2013, pp. 86.

4. "Short term Fourier transform based compensation of Raman signals with background slope in an optical fiber distributed temperature sensor", Manoj Kumar Saxena, S. D. V. S. J. Raju, J. Kishore, R. Arya, S. Kher, S.V.G. Ravindranath, S. M. Oak, In: Proceedings of DRDO Sponsored 8th Control Instrumentation and System Conference (CISCON) - 2011, Manipal, 3-5 Nov, 2011, pp. 579.

Manoj Kumar Saxena

Dedicated

To

My Parents,

Wife

&

Children

# ACKNOWLEDGEMENTS

This thesis is a result of about five years of hard work and throughout this period I received a lot of support and encouragement from numerous sources**.** First and foremost, I am greatly indebted to The Almighty God for His grace. I am highly thankful to my supervisor Dr. S.V.G. Ravindranath, Professor, Electrical Sciences, Homi Bhabha National Institute, Mumbai and Ex-Head, Electronics Section, Atomic and Molecular Physics Division, Bhabha Atomic Research Centre, Mumbai who has been instrumental in the successful completion of this thesis. He has been very supportive and a source of encouragement during the entire period of the thesis. This research work and thesis would not have been possible without the active support, keen interest and untiring efforts of my technology advisor Shri R. Arya, Scientific Officer/$H^+$ and Head, Solid State Laser Electronics Section, Raja Ramanna Centre for Advanced Technology (RRCAT), Indore. Long discussions with him on technical matters, analysis of the experimental data, scientific interpretation of the results and manuscript writing for journals enhanced the quality of my work by a large factor. The contributions of my supervisor and technology advisor are beyond the purview of the acknowledgement.

My deep regards are due for Dr. S. Kher, Head, Fiber Sensors Lab., Solid State Laser Division (SSLD), RRCAT, Indore who motivated me to work hard and do the best possible. He provided all the necessary infrastructure and ideas behind the physics of fiber temperature sensors. Without his help and support, I would not have started so promptly in the laboratory. I wish to express my sincere thanks to Dr. S. M. Oak, Professor, HBNI, Outstanding Scientist and Ex-Head, SSLD, RRCAT and Dr. K. S. Bindra, Head, SSLD, RRCAT for permitting me to pursue my Ph.D. and keen interest in my research work.

I wish to thank Dr. R. B. Pachori, Associate Professor, Discipline of Electrical Engineering, Indian Institute of Technology Indore, Indore for introducing me to the new and vibrant field of non-stationary signal processing. He took a keen interest in the development of signal processing models for Raman optical fibers sensors and encouraged me whenever I interacted with them. He was available to me to clear my doubt even after the office hours.

I am thankful to Dr. P. D. Gupta, Ex-Director, RRCAT, Indore and Dr. P. A. Naik, Director, RRCAT, Indore for constant encouragement and support. I take this opportunity to thank Dr. D. D. Bhawalkar, Founding Director, RRCAT for his initiative in the field of optical fiber sensors at RRCAT.

I extend my appreciation to my colleague Shri S. D. V. S. Jagannadha Raju, Scientific Officer/E, Fiber Sensors Lab., SSLD, RRCAT for fruitful discussions and his help during the experiments. I wish to thank Shri Jai Kishore, Scientific Assistant/E, Fiber Sensors Lab., SSLD, RRCAT for his help in fabrication of mechanical assemblies like fiber holders, electrical heaters and optical fiber spool handling tool.

I am grateful to Dr. D. N. Bododkar, Associate Director, DMAG & Head, DRHR, BARC, Dr. A. P. Tiwari, Head, HRDD, BARC and Dr. A. K. Bhattacharjee, RCnD, BARC for their critical advice and valuable time spent in monitoring the yearly progress of the research work. I thank Dr. S. B. Roy, Head, MAASD & Ex-Dean-Academic, HBNI, RRCAT for setting up the annual review committee and valuable guidance. I also thank Dr. Arup Banerjee, Dean-Aademic, HBNI at RRCAT & Head, Human Resources Development Section and Dr. Avijit Chowdhury, Head, BARC Training School at RRCAT for their help and support.

Thank you, Dr. M. S. Ansari, Head, High Power Laser Electronics Lab., RRCAT, Dr. R. P. Yadav, Scientific Officer/F, Accelerator Control Division, RRCAT and Dr. Ambar Kumar Choubey, Scientific Officer/D, SSLD, RRCAT for sharing your experience and the help.

I am thankful to Homi Bhabha National Institute, Raja Ramanna Centre for Advanced Technology and Department of Atomic Energy for providing the opportunity to pursue this research.

My parents, Shri N. K. Saxena and Smt. C. K. Saxena have always been a constant source of inspiration. Their advice, words and presence has been a source of motivation and have played a great role in my life, carrier, and now the Ph. D. work.

Last but not the least, I wish to thank my wife Seema, son Ayan and daughter Navika who have witnessed the pain and excitement I experienced while pursuing this work in last six and half years. I could not have succeeded without their love and support.

Manoj Kumar Saxena

# CONTENTS

# Homi Bhabha National Institute

## SYNOPSIS OF Ph. D. THESIS

**1. Name of the Student:** Manoj Kumar Saxena

**2. Name of the Constituent Institution:** Raja Ramanna Centre for Advanced Technology

**3. Enrolment No.:** ENGG03201004001

**4. Title of the Thesis:** Study of Non-stationary Signal Models for Optical Fiber Based Sensors

**5. Board of Studies:** Engineering Sciences

## SYNOPSIS

A novel and nearly ideal approach to employ optical fibers to perform the job of transducers for a wide variety of sensing applications has given rise to a new family of sensors viz. optical fiber based sensors. Optical fiber based sensors are sensing devices where light propagating inside an optical fiber is modified in response to an external physical, chemical or biological effect [1]. Small size, immunity to electromagnetic interference/radio frequency, corrosion resistance and the ability to be embedded with the object for which the parameter is being sensed make optical fiber based sensors an attractive alternative to their conventional counterparts [2]. If there are so many points to be monitored, distributed sensors certainly have an upper edge over conventional point sensors due to their lower complexity and cost per monitored point [3]. Scattering principles such as Brillouin [4] and Raman effects [5] have been employed in distributed measurement of various parameters like strain and temperature using optical fiber.

In this thesis, focus is on development of an optical fiber based distributed temperature sensor (OFDTS) that has the ability of providing temperature values as a continuous function of distance along the length of optical fiber. In an OFDTS, every bit of fiber plays the dual role of sensing element and data transmitting medium. The fiber can replace numerous isolated sensors and wires allowing reduced complexity and cost in temperature measurement [6].

In addition to fire detection, OFDTSs have attracted the attention as a means of temperature monitoring of power cables, long gas pipelines, bore holes, tunnels and critical installations like oil wells, refineries, induction furnaces, process control industries and secondary sodium coolant loop of fast breeder test reactor [7-11] etc.

Basic principle of temperature measurement using OFDTS involves Raman scattering [5] in conjunction with optical time domain reflectometry (OTDR) [12]. The OTDR principle allows estimation of the location of hot zones whereas Raman scattering permits measurement of temperature of the hot zones in the fiber. The sensing fiber is coupled to laser pulses and ratio of backscattered anti-Stokes (AS) and Stokes (St) light signals generated due to Raman scattering is monitored for temperature measurement [13].

During the design and development of an OFDTS, several issues were encountered and were successfully addressed using non-stationary signal processing techniques. Some of the issues which have been discussed and addressed in the thesis are briefly described below.

The first issue is related to the difficulty of dynamic self-calibration of OFDTS to obtain the correct distributed temperature profile [10]. In dynamic self-calibration, experimental value of ratio (*R=Amplitude of AS signal/Amplitude of St signal*) is dynamically modified by a

reference ratio value obtained at some known temperature of calibration zone, chosen from the sensing fiber itself. However, temperature of calibration zone itself may change unless it is controlled by a dedicated setup. Therefore, it is required that calibration zone should be maintained at a constant temperature which needs additional temperature control arrangement resulting in increased complexity of the OFDTS. In this work, new methodologies have been proposed and implemented which provide freedom from keeping the calibration zone at constant temperature. The second issue is the non-identical fiber attenuation along the fiber length for AS and St signals due to difference in their optical wavelengths [10, 13, and 14]. The attenuation difference between AS and St signal results in an error in distributed temperature ($T$) profile with respect to the fiber length and therefore needs to be corrected. The third issue is related to the drift in AS and St signals with time caused by variations in laser power and/or laser-fiber coupling. Therefore, any previously stored reference values of AS and St signals for calibration zone can no longer be used as reference for distributed temperature measurement at a later stage. Due to this reason, the dynamic self-calibration has been devised and incorporated in the present work to take care of this issue. The fourth issue is related to denoising of AS and St signals and the resulting spatial inaccuracy in the location of hot zones [15]. In order to obtain better temperature accuracy without increasing the acquisition time, AS and St signals need to be denoised by digital filters. However, conventional Fourier denoising of Raman AS and St signals causes spatial inaccuracy which in turn yields erroneous information about location of hot zones [15]. Therefore, new denoising schemes which do not cause additional spatial inaccuracies in AS and St signals need to be developed. Such techniques have been developed and discussed in this thesis. The fifth issue is related to distributed temperature measurement in presence of an undesired bend in sensing fiber. In an OFDTS, distributed temperature profile is measured correctly assuming that sensing fiber is free from any discontinuity. However, in real applications, as

the time passes, the fiber attenuation is affected when the sensing fiber undergoes perturbations such as bends, tensions or compressions which cause discontinuity in AS and St signals [16]. In case the sensing fiber undergoes a bend, significant temperature error will be introduced in the temperature profile of fiber zone that exists after the bend. Therefore, automatic detection and determination of the location of the bend is crucially important to detect and estimate the error in distributed temperature profile. A novel technique for detection of bend induced error and its compensation has been proposed and implemented in the present work.

Literature survey reveals that in order to compensate the error caused by the difference in attenuation between AS and St signals several schemes have been proposed. These schemes include the use of Rayleigh in place of St signal [17], loop back [10] and double-ended (DE) configuration [18] where both ends of sensing fiber are accessed by the OFDTS. Lee [14] and Suh *et al.* [19] suggested the schemes based on the use of two laser sources. A better correction method using one light source and one light detector has also been proposed by Hwang *et al.* [16] which requires attachment of a carefully designed reflective mirror at the far fiber-end of sensing fiber. A scheme combining DE configuration and detection of AS signal has also been devised recently in the above context [20]. These schemes provide better temperature measurement accuracy but with an increase in complexity.

From the point of view of digital signal processing, electrical versions of AS and St signals are non-stationary signals. In the present work emphasis has been made on the development of new techniques using three different non-stationary signal processing models like short-term Fourier transform (STFT) [21], discrete wavelet transform (DWT) [22] and empirical mode decomposition (EMD) [23] for resolving above mentioned issues. The contemporary

work related to non-stationary signal processing for OFDTS carried out by other researchers are also briefly described.

In previous years, Guang-yong *et al.* [24] has applied wavelet transform directly on the output (temperature vs. distance) data of a developed OFDTS. The wavelet transform was used for denoising of output data rather than using it for preprocessing of input experimental Raman AS and St signals. The temperature range demonstrated in this experiment was 20-35 °C only. Xiaobing and Jiangtao [25] presented a useful wavelet transform based denoising technique to extract temperature information from a noisy temperature vs. distance data of an OFDTS for an improved temperature range of 29-110 °C. However, the study [25] does not use the wavelet transform to eliminate the temperature error caused by fiber attenuation difference between AS and St signals (second issue) and for this reason distributed temperature profile has an unwanted downward slope. Also, the calibration zone has to be kept at a constant temperature and thus first issue remains unattended. On the other hand, in the present work, above mentioned issues have been addressed using DWT. Recently, Wang *et al.* [26] presented an improved denoising technique based on wavelet transform modulus maxima (WTMM) to decrease the temperature measurement error. An off-line algorithm supported by wavelet transform was also proposed by Hou *et al.* [27] to eliminate noisy part of Raman signals at a single temperature (room temperature) only. The off-line nature of the algorithm used in above study [27] makes it unsuitable for automated operation of OFDTS. Also, extraction of distributed temperature information from Raman signals has not been demonstrated in this study. None of the above studies [24-27] reports use of wavelet transform for dynamic self calibration of OFDTS. Henderson *et al.* [28] analyzed the output from an OFDTS using continuous wavelet transform and cross-wavelet transform to obtain hydrologic insight using an off-the-shelf OFDTS (Model: Lios 2000/4000) that

works on the principle of optical frequency domain reflectometry (OFDR). It may be noted that in most of the studies, emphasis is on the wavelet based post processing of the data available at the output of an OFDTS. However, the present work focuses on DWT based preprocessing of input raw AS and St signals and addresses first four issues simultaneously. Some studies also report the use of DWT for signal demodulation in OFDTS based on fiber Bragg gratings [29]. Fourier wavelet regularized deconvolution (ForWaRD) [30, 31] and total variation deconvolution [32] have also been proposed to improve the spatial resolution of OFDTS. Soto *et al.* [33] have recently reported wavelet based image processing that allows a significant improvement in signal to noise ratio (SNR) of Brillouin optical time-domain analyser based fiber distributed sensors. The literature available on the application of EMD in Raman OFDTS is limited. Recently, Zhong *et al.* [34] studied the application of EMD in OFDTSs. They used EMD only for cancellation of noise in Raman AS and St signals. On the other hand, in the present work, the EMD based technique has been proposed and implemented to address all the above five issues successfully.

This thesis presents various techniques based on non-stationary signal processing to address different issues. First, a technique based on STFT has been proposed. It successfully addresses first three issues i.e. dynamic self-calibration, non-identical fiber attenuation and variation of AS and St signals with time. However, fourth and fifth issues could not be addressed using STFT. Next, wavelet transform based methodology has been proposed to apply the features of DWT for addressing various issues. In addition to first three issues, wavelet based technique could successfully address the fourth issue also. The inherent de-noising capability of wavelet processing allows better accuracy with lower acquisition time. The proposed methodology makes use of a dynamic self-calibration circuitry and an algorithm designed and developed in the present work. Based on the proposed wavelet

transform based technique, a prototype Raman OFDTS system has been designed and developed using 200/220 µm sized optical fiber. The thesis also describes an OFDTS developed using low core sized 62.5/125 µm Stainless Steel (SS) covered Multimode fiber with EMD based signal processing technique for Raman AS and St signals to address the first four issues. With the use of SS covering the developed OFDTS is suitable for field applications. Simultaneous de-noising of AS and St signals offered by DWT and EMD processing yields better SNR of these signals and allows reduced error in temperature measurement without any increase in acquisition time. The proposed techniques also ensure inherent smoothening of AS and St signals and thus do not require an additional algorithm for this purpose as required in earlier technique [15]. The thesis also describes the design and development of a microcontroller and Raman OFDTS based zone specific temperature alarm system which is useful in control room of a process plant and opens the possibility of designing a novel fiber based distributed temperature controller. Finally, the error in distributed temperature profile measurement caused by a bend in sensing fiber (fifth issue) is analyzed in detail. In practice, it is difficult for the user to visually identify the presence of the bend and estimate its location from AS and St signals directly. This thesis presents a novel automatic and dynamic technique using EMD for detection of bend and its location using area of analytic form of intrinsic mode functions [23, 35] for St signal. Further, a technique to compensate the error in distributed temperature measurement is also demonstrated. The conclusion with a brief discussion on the scope for possible future research work is also presented in the thesis.

Research highlights of the presents work are:

- Study of STFT and its application in addressing the various issues involved in design and development of Raman OFDTS.

- Study of DWT based methodology to apply its features for addressing various issues related to Raman OFDTS and development of a prototype OFDTS system using 200/220 µm sized optical fiber for the temperature range of 25-300 °C with temperature accuracy of ± 3.5 ºC, spatial resolution of 1 m over the length of ~ 200 m.
- Study of EMD based technique for the design and development of a field usable rugged prototype OFDTS using SS covered, standard sized 62.5/125 µm fiber.
- Study and analysis of error in distributed temperature measurement caused by a bend in sensing fiber. A novel automatic and dynamic technique using EMD has been devised for detection of bend and its location using area of analytic IMFs of St signal. A technique to compensate the error in distributed temperature measurement is also presented.

**References**

[1] Culshaw B., "Basic concepts of optical fiber sensors," In: Dakin J., Culshaw B. (eds.), "Optical Fiber Sensors: Principle and Components - vol. 1," Artech House Inc., Norwood, MA, 1998, pp. 9-24.

[2] Grattan K. T. V., Sun T., "Fiber optic sensor technology: Introduction and overview," In: Grattan K. T. V., Meggitt B. T. (eds.), "Optical Fiber Sensor Technology: Fundamentals," Kluwer Academic, London, 2000, pp. 1-44.

[3] Grattan K. T. V., Sun T., "Fiber optic sensor technology: An overview," Sensors and Actuators A Physical 82 (2000), pp. 40–61.

[4] Culshaw B., Kersey A., "Fiber-optic sensing: A historical perspective," Journal of Lightwave Technology 26 (2008), pp. 1064-1078.

[5] Long D. A., "The Raman Effect," John Wiley, England, 2002, pp. 49-131.

[6] Zhao X. F., Li L., Ba Q., Ou J. P., "Scour monitoring system of subsea pipeline using distributed Brillouin optical sensors based on active thermometry," Optics & Laser Technology 44 (2012), pp. 2125-2129.

[7] Rogers A. J., "Distributed optical-fiber sensors for the measurements of pressure, strain and temperature," Physics Reports 169 (1988), pp. 99-143.

[8] Yilmaz G., Karlik S. E., “A distributed optical fiber sensor for temperature detection in power cables,” Sensors & Actuators A Physical 125 (2006), pp. 148-155.

[9] Hurtig E., Großwig S., Kühn K., “Fiber optic temperature sensing: Application for subsurface and ground temperature measurements,” Tectonophysics 257 (1996), pp. 101-109.

[10] Höbel M., Ricka J., Wüthrich M., Binkert Th., “High-resolution distributed temperature sensing with the multiphoton-timing technique,” Applied Optics 34 (1995), pp. 2955-2967.

[11] Pandian C., Kasinathan M., Sosamma S., Babu Rao C., Jayakumar T., Murali N., Raj B., “Looped back fiber mode for reduction of false alarm in leak detection using distributed optical fiber sensor,” Applied Optics 49 (20) (2010), pp. 3869-3874.

[12] Vo T. D., He J., Magi E., Collins M. J., Clark A. S., Ferguson B. G., Xiong C., Eggleton B. J., “Chalcogenide fiber-based distributed temperature sensor with sub-centimeter spatial resolution and enhanced accuracy,” Optics Express 22 (2014), pp.1560-1568.

[13] Dakin J. P., Pratt D. J., Bibby G. W., Ross J. N., “Distributed optical fiber Raman temperature sensor using a semiconductor light source and detectors,” Electronics Letters 21(13) (1985), pp. 569-570.

[14] Lee C. E., “Self-calibrating technique enables long-distance temperature sensing,” Laser Focus World 43 (2007), pp. 101-117.

[15] Chakraborty A. L., Kher S., Chaubey S., Nathan T. P. S., “Bidirectional frequency-domain digital filtering to simultaneously improve temperature resolution and eliminate spatial inaccuracy of a distributed temperature sensor,” Optical Engineering 43 (2004), pp. 2724-2729.

[16] Hwang D., Yoon D. J., Kwon I. B., Seo D. C., Chung Y., “Novel auto-correction method in a fiber-optic distributed-temperature sensor using reflected anti-Stokes Raman scattering,” Optics Express 18 (2010), pp. 9747-9754.

[17] Stoddart P. R., Cadusch P. J., Pearce J. B., Vukovic D., Nagrajah C. R., Booth D. J., “Fiber optic distributed temperature sensor with an integrated background correction Function,” Measurement Science and Technology 16 (2005), pp. 1299-1304.

[18] Fernandez A. F., Rodeghiero P., Brichard B., Berghmans F., Hartog A. H., Hughes P., Williams K., Leach A. P., “Radiation-tolerant Raman distributed temperature monitoring system for large nuclear infrastructures,” IEEE Transactions on Nuclear Science 52 (2005), pp. 2689-2694.

[19] Suh K., Lee C., “Auto-correction method for differential attenuation in a fiber-optic distributed-temperature sensor,” Optics Letters 33 (2008), pp. 1845-1847.

[20] Soto M. A., Signorini A., Nannipieri T., Faralli S., Bolognini G., “Impact of loss variations on double-ended distributed temperature sensors based on Raman anti-Stokes signal only,” Journal of Lightwave Technology 30 (2012), pp.1215-1222.

[21] Cohen L., “Time-Frequency Analysis,” Prentice Hal PTR, New Jersey, 1995, Chapter 7.

[22] Mallat S. G., “A theory for multiresolution signal decomposition: The wavelet representation,” IEEE Transaction on Pattern Analysis & Machine Intelligence 11 (1989), pp. 674-693.

[23] Huang N. E., Shen Z., Long S. R., Wu M. C., Shih H. H., Zheng Q., Yen N., Tung C. C., Henry H. L., “The empirical mode decomposition and Hilbert spectrum for nonlinear and nonstationary time series analysis,” Proceedings of the Royal Society A 454 (1998), pp. 903-995.

[24] Guang-yong X., Jian-ping Y., Kun-jun Z., Wen M., “Monitoring data processing of distributed optical fiber temperature sensor based on multi-wavelet,” In: Proceedings of the International Workshop on Education Technology and Training & International Workshop on Geoscience and Remote Sensing; 2008, pp. 203-206. (doi:10.1109/ETTandGRS.2008.60)

[25] Xiaobing L., Jiangtao G., “Wavelet analysis in distributed optical fiber temperature sensor,” In: Proceedings of the Asia Communications and Photonics Conference (ACP/ IPOC); 2013, paper code AF21.3.

[26] Wang Z., Chang J., Zhang S., Luo S., Jia C., Sun B., Jiang S., Liu Y., Liu X., Lv G., Liu Z., “Application of wavelet transform modulus maxima in Raman distributed temperature sensors,” Photonic Sensors 4 (2) (2014), pp. 142-146.

[27] Hou S., Jian Y., Chen Y., Han L., “Signal processing of single-mode fiber sensor system based on Raman scattering,” In: Proceedings of the 2nd International Conference on Advanced Computer Control; 2010, pp. 176-181.

[28] Henderson R. D., Day-Lewis F. D., Harvey C. F., “Investigation of aquifer-estuary interaction using wavelet analysis of fiber-optic temperature data,” Geophysical Research Letters 36 (2009), pp. 1-6. (doi:10.1029/2008GL036926)

[29] Wong A. C. L., Peng G. D., “Applications of discrete wavelet transform in optical fiber sensing,” In: Olkkonen H. (eds.), “Discrete wavelet transforms-biomedical applications,” In Tech, Shanghai, 2011, pp. 221-248.

[30] Bahrampour A. R., Maasoumi F., “Resolution enhancement in long pulse OTDR for application in structural health monitoring,” Optical Fiber Technology 16 (2010), pp. 240-249.

[31] Bahrampour A. R., Moosavi A., Bahrampour M. J., Safaei L., “Spatial resolution enhancement in fiber Raman distributed temperature sensor by employing ForWaRD deconvolution algorithm,” Optical Fiber Technology 17 (2011), pp. 128-134.

[32] Bazzo J. P., Pipa D. R., Martelli C., Vagner da Silva E., Cardozo da Silva J. C., “Improving spatial resolution of Raman DTS using total variation deconvolution,” IEEE Sensors Journal 16 (11) (2016), pp. 4425-4430.

[33] Soto M. A., Ramírez J. A., The´venaz L., “Intensifying the response of distributed optical fibre sensors using 2D and 3D image restoration,” Nature Communications 7 (2016), Article No. 10870. (doi: 10.1038/ncomms10870)

[34] Zhong Y. P., Zhang Q., Zhou D., "Distributed optical fiber Raman signal noise cancellation based on empirical mode decomposition," Applied Mechanics and Materials 198 (2012), pp. 1621-1626.

[35] Donghoh K., Hee-Seok O., "EMD: A package for empirical mode decomposition and Hilbert spectrum," The R. Journal 1 (1) (2009), pp. 40-46.

## Publications in Refereed Journals:

### a. Published

1. "Empirical mode decomposition-based detection of bend-induced error and its correction in a Raman optical fiber distributed temperature sensor", **Manoj Kumar Saxena**, S. D. V. S. J. Raju, R. Arya, R. B. Pachori, S. V. G. Ravindranath, S. Kher, S. M. Oak, IEEE Sensors Journal, **2016**, *16* (*5*), 1243-1252.

2. "Empirical mode decomposition based dynamic error correction in SS covered 62.5/125 μm optical fiber based distributed temperature sensor", **Manoj Kumar Saxena**, S. D. V. S. J. Raju, R. Arya, R. B. Pachori, S. V. G. Ravindranath, S. Kher, S. M. Oak, Optics & Laser Technology (Elsevier), **2015**, *67*, 107-118.

3. "Raman optical fiber distributed temperature sensor using wavelet transform based simplified signal processing of Raman backscattered signals", **Manoj Kumar Saxena**, S. D. V. S. J. Raju, R. Arya, R. B. Pachori, S. V. G. Ravindranath, S. Kher, S. M. Oak, Optics & Laser Technology (Elsevier), **2015**, *65*, 14-24.

4. "Optical fiber distributed temperature sensor using short term Fourier transform based simplified signal processing of Raman signals", **Manoj Kumar Saxena**, S. D. V. S. J. Raju, R. Arya, S. V. G. Ravindranath, S. Kher, S. M. Oak, Measurement (Elsevier), **2014**, *47*, 345-355.

5. "Microcontroller based Raman optical fiber distributed temperature sensor and alarm system", **Manoj Kumar Saxena**, S. D. V. S. J. Raju, R. Arya, S. V. G. Ravindranath, S. Kher, S. M. Oak, Journal of the Instrument Society of India, **2014**, *44* (*1*), 28-31.

## Conference Presentations:

1. "Temperature error due to discontinuity in sensing fiber and its compensation in fiber distributed temperature sensor", **Manoj Kumar Saxena**, S. D. V. S. J. Raju, J. Kishore, R. Arya, S. V. G. Ravindranath, S. Kher, S. M. Oak, In: Proceedings of 39th National Symposium on Instrumentation (NSI) - 39, Haridwar, 15-17 Oct, 2014.

2. “Study of compact and portable fiber optic distributed temperature sensor based on Raman effect”, S. D. V. S. J. Raju, **M. K. Saxena**, S. Kher, J. Kishore, S. Kher, and S. M. Oak, In: Proceedings of International Conference on Optics and Optoelectronics (ICOL) - 2014, Dehradun, 5-8 March, 2014, pp. 72.

3. “Microcontroller based Raman optical fiber distributed temperature sensor and alarm system”, **Manoj Kumar Saxena**, S. D. V. S. J. Raju, J. Kishore, R. Arya, S. V. G. Ravindranath, S. Kher, S. M. Oak, In: Proceedings of 38th National Symposium on Instrumentation (NSI) - 38, Hubli, 24-26 Oct, 2013, pp. 86.

4. “Short term Fourier transform based compensation of Raman signals with background slope in an optical fiber distributed temperature sensor”, **Manoj Kumar Saxena**, S. D. V. S. J. Raju, J. Kishore, R. Arya, S. Kher, S.V.G. Ravindranath, S. M. Oak, In: Proceedings of DRDO Sponsored 8th Control Instrumentation and System Conference (CISCON) - 2011, Manipal, 3-5 Nov, 2011, pp. 579.

Manoj Kumar Saxena
Date: 21-03-2016

# LIST OF FIGURES

**Chapter 1**

There is no figure in Chapter 1.

**Chapter 2**

There is no figure in Chapter 2.

**Chapter 3**

**Chapter 4**

**Chapter 5**

**Chapter 6**

**Chapter 7**

There is no figure in Chapter 7.

**Appendix A**



**Appendix B**

**Appendix C**



**Appendix D**

# LIST OF TABLES

## Chapter 1

There is no Table in Chapter 1.

## Chapter 2

There is no Table in Chapter 2.

## Chapter 3



## Chapter 4

## Chapter 5



## Chapter 6



## Chapter 7

There is no Table in Chapter 7.

### Appendix A

There is no Table in Appendix A.

**Appendix B**

There is no Table in Appendix B.

**Appendix C**

There is no Table in Appendix C.

**Appendix D**

There is no Table in Appendix D.

# LIST OF ACRONYMS

| | |
|---|---|
| AM-FM | Amplitude and frequency modulated |
| AS | anti-Stokes |
| CTM | Central tendency measure |
| CWT | Continuous wavelet transform |
| ℂWT | Complex dual tree wavlet transform |
| DAQ | Data acquisition card |
| DC | Direct current |
| DE | Dual-ended |
| DFT | Discrete Fourier transform |
| DPSSL | Diode pumped solid state laser |
| DSCU | Dynamic self-calibration unit |
| DWT | Discrete wavelet transform |
| EA | Electrical amplifiers |
| EEG | Electroencephalogram |
| EMD | Empirical mode decomposition |
| FFT | Fast Fourier transform |
| FBTR | Fast breeder test reactor |
| FIR | Finite impulse response |
| ForWARD | Fourier wavelet regularized deconvolution |

| | |
|---|---|
| FWHM | Full width half maxima |
| GPIB | General purpose interface bus |
| HHT | Hilbert–Huang transform |
| IDFT | Inverse DFT |
| IFFT | Inverse Fast Fourier transform |
| IIR | Infinite impulse response |
| IMF | Intrinsic mode function |
| KWST | Kruskal-Wallis statistical test |
| MATLAB | Matrix Laboratory |
| OFDR | Optical frequency domain reflectometry |
| OFDTS | Optical fiber distributed temperature sensor |
| OTDR | Optical time-domain refelectometry |
| PCI | Peripheral component interconnect |
| PD | Photodiode |
| P-I-D | Proportional integral derivative |
| PMT | Photomultiplier tube |
| SNR | Signal to noise ratio |
| SS | Stainless Steel |
| St | Stokes |
| STFT | Short term Fourier transform |

# Chapter 1

# Introduction

Light plays a very important role in our daily life. The importance of light is evident by the United Nations' announcement of celebrating the year 2015 as the International Year of Light and Light-based Technologies (IYL 2015). Further, the optical fibers [1] are the main guiding media to carry light wave from one place to other and play a vital role in everyone's day to day life. Apart from their usage in communication, optical fibers are novel and nearly ideal approach to perform the job of transducers for a wide variety of sensing applications which give rise to a new family of sensors known as optical fiber based sensors. Optical fiber based sensors are essentially a means whereby light guided within an optical fiber can be modified in response to an external physical, chemical or biological influence [2]. Various qualities of optical fiber based sensors like small size, immunity to electromagnetic interference/radio frequency, corrosion resistance and the ability to be embedded with the object for which the parameter is being sensed equip them to be an attractive alternative to conventional sensors [2-5]. If there are so many points to be monitored, distributed sensors are found to have an upper edge over conventional point sensors due to their lower complexity and cost per monitored point [5-7]. Brillouin [3, 8] and Raman scattering [9] principles have been widely employed in distributed measurement of various parameters like strain and temperature using optical fiber.

In this thesis, focus is on development of an optical fiber based distributed temperature sensor (OFDTS) using Raman scattering. An OFDTS has the ability of providing temperature values as a continuous function of distance along the length of optical fiber [10]. In an OFDTS, every bit of fiber plays the dual role of sensing element and data transmitting medium. The

fiber can replace numerous isolated sensors and wires allowing reduced complexity and cost in temperature measurement [11]. OFDTSs have attracted the attention as a means of temperature monitoring of power cables, long pipelines, bore holes, tunnels and critical installations like oil wells, secondary sodium loop of fast breeder test reactor (FBTR), refineries, induction furnaces and process control industries [12-17] etc.

Basic principle of temperature measurement using OFDTS involves Raman scattering [9] in conjunction with optical time domain reflectometry (OTDR) [18-20]. The OTDR principle allows estimation of the location of hot zones in the fiber whereas Raman scattering permits measurement of temperature of the hot zones. The sensing fiber is coupled to laser pulses and ratio of backscattered anti-Stokes (AS) and Stokes (St) light signals, generated due to Raman scattering in the fiber, is monitored for temperature measurement [15, 21].

### 1.1 Motivation and objectives

In this thesis, non-stationary signal [22] processing models to address various issues encountered in the development of Raman scattering based OFDTS have been extensively investigated. Study of these issues and tackling them appropriately define the objectives for the thesis. Keeping in view the various applications and advantages of OFDTS over their conventional counterparts, development of new methodologies to address these issues motivate researchers to pursue research in the field of OFDTS. The non-stationary signal models studied in this work are based on short term Fourier transform (STFT) [23-25], discrete wavelet transform (DWT) [26, 27] and empirical mode decomposition (EMD) [28]. The various issues are briefly described below.

The first issue is related to the difficulty of dynamic self-calibration of OFDTS to obtain the correct distributed temperature profile [15]. In dynamic self-calibration, experimental value of ratio profile (*R=Amplitude of AS signal/Amplitude of St signal*) is dynamically modified by a reference ratio value obtained at some known temperature of calibration zone, chosen from the sensing fiber itself. However, temperature of calibration zone itself may change unless it is controlled by a dedicated setup. Therefore, it is required that calibration zone should be maintained at a constant temperature which needs additional temperature control arrangement resulting in increased complexity of the OFDTS. In present work, new methodologies have been proposed and implemented which provide freedom from keeping the calibration zone at constant temperature. The second issue is the non-identical fiber attenuation along the fiber length for AS and St signals due to difference in their optical wavelengths [15, 21 and 29]. The attenuation difference between AS and St signal results in an error in distributed temperature (*T*) profile with respect to the fiber length and therefore needs to be corrected. The third issue is related to the drift in AS and St signals with time caused by variations in laser power and/or laser-fiber coupling. Therefore, any previously stored reference values of AS and St signals for calibration zone can no longer be used as reference for distributed temperature measurement at a later stage. Due to this reason, the dynamic self-calibration has been devised and incorporated in the present work to take care of this issue. The fourth issue is related to denoising of AS and St signals and the resulting spatial inaccuracy in the location of hot zones [30]. In order to obtain better temperature accuracy without increasing the acquisition time, AS and St signals need to be denoised by digital filters. However, conventional Fourier denoising of Raman AS and St signals causes spatial inaccuracy which in turn yields erroneous information about location of hot zones [30]. Therefore, new denoising schemes which do not cause additional spatial inaccuracies in AS and St signals need to be developed. Such techniques have been developed and discussed in this thesis. The

fifth issue is related to distributed temperature measurement in presence of an undesired bend in sensing fiber. In an OFDTS, distributed temperature profile is measured correctly assuming that sensing fiber is free from any discontinuity. However, in real applications, as the time passes, the fiber attenuation is affected when the sensing fiber undergoes perturbations such as bends, tensions or compressions which cause discontinuity in AS and St signals [31]. In case the sensing fiber undergoes a bend, significant temperature error will be introduced in the temperature profile of fiber zone that exists after the bend. Therefore, automatic detection and determination of the location of the bend is crucially important to detect and estimate the error in distributed temperature profile. A novel technique for detection of bend induced error and its compensation has been proposed and implemented in the present work.

### 1.2 Contribution of thesis

This thesis presents various techniques based on non-stationary signal processing to address different issues. First, a technique based on STFT has been proposed [32]. It successfully addresses first three issues i.e. dynamic self-calibration, non-identical fiber attenuation and variation of AS and St signals with time. However, fourth and fifth issues could not be addressed using STFT. Next, wavelet transform based methodology has been proposed [33] to apply the features of DWT for addressing various issues. In addition to first three issues, wavelet based technique could successfully address the fourth issue also. The inherent de-noising capability of wavelet processing allows better accuracy with lower acquisition time. The proposed methodology makes use of a dynamic self-calibration circuitry and an algorithm designed and developed in the present work. Based on the proposed wavelet transform based technique, a prototype Raman OFDTS system has been designed and

developed using 200/220 µm sized optical fiber as sensing element. The thesis also describes an OFDTS developed using low core sized 62.5/125 µm Stainless Steel (SS) covered Multimode sensing fiber with EMD based signal processing technique for Raman AS and St signals to address the first four issues [34]. With the use of SS covering the developed OFDTS is suitable for field applications. Simultaneous de-noising of AS and St signals offered by DWT and EMD processing yields better signal to noise ratio (SNR) of these signals and allows reduced error in temperature measurement without any increase in acquisition time. The proposed techniques also ensure inherent smoothening of AS and St signals and thus do not require an additional algorithm for this purpose as required in earlier technique [30.]. The thesis also describes the design and development of a microcontroller and Raman OFDTS based zone specific temperature alarm system [35] which is useful in control room of a process plant and opens the possibility of designing a novel fiber based distributed temperature controller. Finally, the error in distributed temperature profile measurement caused by a bend in sensing fiber (fifth issue) is analyzed in detail. In practice, it is difficult for the user to visually identify the presence of the bend and estimate its location from AS and St signals directly. This thesis presents a novel automatic and dynamic technique [36] using EMD for detection of bend and its location using area of analytic form of intrinsic mode functions [28, 37] for St signal. Further, a technique to compensate the error in distributed temperature measurement is also demonstrated. The thesis concludes with a brief discussion on the scope for possible future research work.

Important contributions of the present thesis are:

- Study of STFT and its application in addressing the various issues involved in design and development of Raman OFDTS.
- Study of DWT based methodology to apply its features for addressing various issues related to Raman OFDTS and development of a prototype OFDTS system using

200/220 µm sized optical fiber for the temperature range of 25-300 °C with temperature accuracy of ± 3.5 ºC, spatial resolution of 1 m over the length of ~ 200 m.

- Study of EMD based technique for the design and development of a field usable rugged prototype OFDTS using SS covered, standard sized 62.5/125 µm fiber.
- Study and analysis of error in distributed temperature profile measurement caused by a bend in sensing fiber. In an OFDTS, it is required to detect and compensate the temperature error caused by the bend. In practice, it is difficult for the user to visually identify the presence of the bend and estimate its location from AS and St signals directly. The thesis presents a novel automatic and dynamic technique using EMD for detection of bend and its location using a new feaure called ‘area’ of analytic intrinsic mode functions (IMFs) for St signal. Further, it is demonstrated that the proper selection of the additional calibration zone after the detected bend makes it possible to use rest of the fiber for obtaining correct temperature profile.

# Chapter 2

# Literature survey

OFDTS systems based on Raman scattering are particularly attractive for obtaining a graphical or pictorial presentation of temperature information [8, 10]. Such sensor systems permit monitoring the magnitude of temperature and also its variation along the length of continuous uninterrupted optical fiber and offer a powerful and economical means of covering a large number of locations within a significant area. Compared to point sensor based network OFDTS makes use of optical fiber that itself acts as sensing element as well as data career and thus may reduce the complexity and cost largely. Optical time domain reflectometry (OTDR) and Raman scattering are the main concepts to understand the technologies to be implemented for realizing a practically working Raman OFDTS system. The earliest form of distributed sensor was the optical OTDR (or lidar) concept to examine the continuity and attenuation of optical fibers from a measurement of the backscattering versus time characteristic when a short pulse of light is launched into a fiber waveguide [18, 19]. OTDR in conjuction with polarized light source had been used for the measurement of spatial distribution of magnetic and electric fields, pressure and temperature by Rogers [20]. The basic method of OTDR was devised by Baronski *et al.* in the year 1976 [18]. OTDR technique in fiber involves the launching of short laser pulses into the fiber under test via a directional coupler, which also serves to couple the backscattered light fraction, captured and returned via the fiber, to the optoelectronic transducer.

When a monochromatic radiation or radiation of very narrow frequency band is scattered by a solid then the scattered light not only consists of the radiations of incident frequency but also the radiations of frequencies above and below that of incident frequency. This form of

scattering in which the optical frequency of incident beam undergoes a definite change was observed and studied by Sir C. V. Raman in 1928 and is called Raman effect [9, 38]. Raman scattering is an in-elastic scattering of photon. The spectrum of scattered light consists of optical signals of the same optical frequency (or wavelength) as the incident beam (called Rayleigh lines) as well as additional weak Raman optical signals of changed wavelength (called Raman AS or St lines).

OFDTS involves measurement of two parameters: time of flight using OTDR and intensity of backscattered Raman scattering. The short interrogating laser pulses are launched into the sensing fiber and the profiles of backscattered optical AS and St signals are monitored for measurement of distributed temperature profile of fiber. The Raman signals are inherently weak (of the order of pW) and need amplification by several orders (~$10^7$) of magnitude. The ratio ($R$) of more-temperature-sensitive AS intensity ($I_{AS}$) to less-temperature-sensitive St intensity ($I_{St}$) is then used to determine the unknown absolute temperature ($T$) of the zone for which these intensities have been measured. Parameter ($R$) is expressed as [15, 21]:

$$R = \frac{I_{AS}}{I_{St}} = \left(\frac{\lambda_{St}}{\lambda_{AS}}\right)^4 \exp\left(-\frac{B}{T}\right) \tag{2.1}$$

where,

$$B = \frac{hc\nabla}{k} \tag{2.2}$$

In Eq. (2.1), parameter $k$ is the Boltzmann constant ($1.38064852 \times 10^{-23}$ J/K), $h$ the Planck constant ($6.62607004 \times 10^{-34}$ J-s), $c$ the speed of light in vacuum ($3\times10^8$ m/s), $\nabla$ the wave number separation between one of the Raman components (AS or St) and Rayleigh scattering light for a given fiber. For Silica fiber ($\nabla = 440$ cm$^{-1}$). Therefore, $B$ is a constant for a given fiber. Parameters $\lambda_{St}$ and $\lambda_{AS}$ are St and AS wavelengths respectively and are also known for a given combination of pump laser wavelength and sensing fiber type. Thus, all the parameters

in Eq. (2.1) are known and it should be, in principle, possible to measure unknown distributed temperature (*T*) profile in Kelvin.

In Eq. (2.1), the measurement of the ratio (*R*) should provide an absolute indication of the temperature of the medium, irrespective of the light intensity, the launch conditions, the fiber geometry and composition of the fiber. In practice, however, a correction has to be made for the difference between attenuation profiles between AS and St wavelengths [10, 21]. In the first experimental demonstration of OFDTS methodology, a pulsed argon-ion laser was used in conjunction with Corning telecommunication grade 50/125 μm graded index fiber [10]. The ratio of AS and St intensities is a strong function of temperature but both the signals have a decay due to fiber attenuation. The direct implication of the above effect is the downward sloping pattern in parameter *R* and hence in distributed temperature along the fiber length which causes error in temperature measurement. Dakin *et al.* [21] also indicated the need of small allowance for different fiber attenuation at each wavelength for a long fiber to get corrected ratio profile and in turn correct distributed temperature profile for longer fiber.

During the design and development of an OFDTS, several issues are encountered which need proper addressing. The objective for the thesis is to address these major issues using non-stationary signal processing methods. Some of the major issues which have been discussed and addressed in this thesis may be described in detail as below.

### 2.1 Issue No. 1

The first issue is related to difficulty of dynamic self-calibration to obtain the correct distributed temperature profile. Dynamic self-calibration is required because of the difference

in theoretical and experimental values of the ratio (*R*) at various temperature values. The reason for this difference is explained below.

At 25 °C (for example), obtaining theoretical value of 0.1747 for *R* requires that the optoelectronic conversion using photomultiplier tubes (PMT) (e.g. PMT-R5108, Hamamatsu) detectors, the beam splitting and the subsequent light coupling into AS and St detectors (described in Section 2.3) are in such a way that relation St = 5.72×AS is maintained for backscattered AS and St signals while traveling the path from fiber to the final stage of detection. However, due to non-ideal behavior of various optical components in the path and band nature of AS and St signals, above relation does not hold. The relation gets deteriorated at every stage in the path. For example, the cathode radiant sensitivity of a PMT for AS wavelength and St wavelength is 0.95 mA/W and 0.2 mA/W respectively which causes St current to be approximately 5 times less compared to AS current. Non-ideal performance of beam splitters and optical filters also does not support the above ideal relation. As a result, the cumulative effect of various components makes experimental values of *R* to be different from theoretical one.

Direct use of experimental values of *R* in Eq. (2.1) will yield highly erroneous and unacceptable temperature profile (*T*). Hence Eq. (2.1) needs to be modified to obtain correct values. Modification is done by dynamic self-calibration in which experimentally obtained ratio values are referenced with respect to a ratio value obtained at some known temperature of the calibration zone. The calibration zone is chosen from sensing fiber itself [15].

### 2.2 Issue No. 2

The second issue is the non-identical fiber attenuation along the fiber length for Raman AS and St signals due to difference in their wavelengths [10, 21]. In the present system, the difference between two wavelengths is ~100 nm if excitation laser of wavelength 1064 nm is utilized in OFDTS. The lower optical wavelength signal (AS) experiences higher attenuation in comparison to higher optical wavelength signal (St) while travelling in sensing optical fiber. This attenuation difference results in an unwanted downward slope in ratio (*R*) profile and finally in unknown temperature (*T*) profile with respect to fiber length. It may be noted that downward slope in ratio (*R*) profile causes additional errors in unknown temperature (*T*) profile of fiber and should be corrected.

### 2.3 Issue No. 3

Amplitude of AS and St signals varies with time due to slow variations/drifts in laser power and laser-fiber coupling. Also, the temperature of calibration zone itself may change unless it is controlled by a dedicated setup. Therefore, any previously stored reference values of AS, St signals and calibration zone temperature can no longer be used as reference for temperature measurement at a later stage [15].

### 2.4 Issue No. 4

In order to obtain a better temperature resolution without increasing the acquisition time and hence the response time of OFDTS, Raman AS and St signals need to be denoised by digital filters to improve SNR. Conventional finite impulse response/infinite impulse response

(FIR/IIR) based Fourier filtering of Raman signals causes spatial inaccuracy in locating the hot-zones which in turn yields erroneous information about the location of hot zones [30].

### 2.5 Issue No. 5

The calibration of Raman OFDTS is performed using temperature of the reference (calibration) zone located at the start of the sensing fiber. It is assumed that sensing fiber in an OFDTS is free from any bend, break etc. when measurement of distributed temperature profile is carried out. This allows uniform decay in AS and St signals. However, in real applications, the fiber loss may get affected by the bend in fiber which causes discontinuity in AS and St signals [31]. If the distributed temperature profile is still calibrated by using the same calibration zone, temperature profile of the fiber zone that exists after the bend will be highly erroneous. Therefore, detection of the bend, temperature error caused by that bend and compensation of the error is of utmost importance. Unfortunately, users find it difficult to identify the bend by merely looking at AS and St signals. It means just visual inspection of AS and St signals is not enough to identify the presence and location of bend. Therefore, on-line automatic detection of localized bend, even if it occurs during the measurement cycle, is crucially important to obtain the correct distributed temperature profile. A suitable method also needs to be devised to compensate the bend induced error.

### 2.6 Overview of existing methods for addressing the various issues and present work in above context

Literature survey reveals that many methods have been suggested to address the above mentioned issues over the time. Stoddart *et al.* [39] proposed to use Rayleigh instead of St

from the backscattered spectrum to avoid the temperature measurement error due to differential attenuation caused by the optical fiber for AS and St signal wavelengths. This provided better results but could not eliminate the error caused by the differential attenuation completely. The dual-ended (DE) configuration (i.e. both ends of sensing fiber are connected to OFDTS unit) [40] and dual laser source schemes [29, 41] have also been proposed to take care of the difference in attenuation between AS and St. These schemes have resulted in improvements but add complexity and need double length of fiber, extra distributed temperature sensor (DTS) with an optical switch and two costly lasers. A correction method to take care of the difference in attenuation for AS and St signals has been proposed with only one light source and one light detector but requires attachment of a carefully designed reflective mirror at the far fiber-end of the sensing fiber [31]. A more sophisticated correction technique [42] based on detection of AS signal alone in combination with DE configuration has been investigated. This has provided better results for temperature monitoring of very long fibers but with increased complexity. OFDTSs based on above schemes are important and to certain extent become mandatory in situations where sensing fiber is exposed to the severe radiation environment or hydrogen darkening in oil wells. Requirements for less demanding situations like temperature measurement in steam pipelines of turbines, electrical cables; temperature profiling of big buildings, gas pipelines and mines etc. can be met by the technique based on digital signal processing. Modern and new techniques based on digital signal processing have been studied and proposed in the present work which will enable the extraction of useful distributed temperature information from experimental Raman signals in a rather simple way.

From the point of view of digital signal processing, electrical versions of AS and St signals are non-stationary signals. In the present work emphasis has been made on the use of

advanced non-stationary signal processing methods like STFT [23-25], DWT [26, 27] and empirical mode decomposition (EMD) [28]. These methods have been used for pre-processing of Raman AS and St signals to address the above mentioned issues of Raman OFDTS successfully.

In previous years, Guang-yong *et al.* [43] has applied wavelet transform directly on the output (temperature vs. distance) data of a developed OFDTS. The wavelet transform was used for denoising of output data rather than using it for pre-processing of input experimental Raman AS and St signals. The temperature range demonstrated in this experiment was 20-35 °C only. Xiaobing and Jiangtao [44] presented a useful wavelet transform based denoising technique to extract temperature information from a noisy temperature vs. distance data of an OFDTS for an improved temperature range of 29-110 °C. However, the study [44] does not use the wavelet transform to eliminate the temperature error caused by fiber attenuation difference between AS and St signals (second issue) and for this reason distributed temperature profile has an unwanted downward slope. Also, the calibration zone has to be kept at a constant temperature and thus first issue remains unattended. On the other hand, in the present work, above mentioned issues have been addressed using DWT. Recently, Wang *et al*. [45- Photonic Sensors] presented an improved denoising technique based on wavelet transform modulus maxima (WTMM) to decrease the temperature measurement error. An off-line algorithm supported by wavelet transform was also proposed by Hou *et al.* [46] to eliminate noisy part of Raman signals at a single temperature (room temperature) only. The off-line nature of the algorithm used in above study [46] makes it unsuitable for automated operation of OFDTS. Also, extraction of distributed temperature information from Raman signals has not been demonstrated in this study. None of the above studies [43-46] reports use of wavelet transform for dynamic self calibration of OFDTS. Henderson *et al.* [47] analyzed

the output from an OFDTS using continuous wavelet transform and cross-wavelet transform to obtain hydrologic insight using an off-the-shelf OFDTS (Model: Lios 2000/4000) that works on the principle of optical frequency domain reflectometry (OFDR). It may be noted that in most of the studies, emphasis is on the wavelet based post processing of the data available at the output of an OFDTS. However, the present work focuses on DWT based pre-processing of input raw AS and St signals and addresses first four issues simultaneously. Earlier, an experimental technique based on curve fitting with extrapolation [48] has also been suggested to address some of the above mentioned issues. Unfortunately, it is not a truly automatic measurement technique because of the involvement of human operator and requirement of a large calibration zone. Some studies also report the use of DWT for signal demodulation in OFDTS based on fiber Bragg gratings [49]. Fourier wavelet regularized deconvolution (ForWaRD) [50, 51] has also been proposed to improve the spatial resolution of OFDTS. A new mathematical technique based on total variation deconvolution has been recently proposed by Bazzo *et al.* [52] for enhancement of spatial resolution. Soto *et al.* [53] have recently reported wavelet based image processing that allows a significant improvement in SNR of Brillouin optical time-domain analyser based fiber distributed sensors. The literature available on the application of EMD in Raman OFDTS is limited. Zhong *et al.* [54] studied the application of EMD in OFDTSs. They used EMD only for cancellation of noise in Raman AS and St signals. On the other hand, in the present work, the EMD based technique has been proposed and implemented to address all the above five issues.

Conventional method of detecting bend in fiber is to observe Rayleigh backscattered light in OTDR mode. However, it is not possible to rely on Rayleigh light in OFDTS system since it is filtered out. Rayleigh light has a little role to play in temperature determination and for this reason it is filtered out. A loop back arrangement suggested by Fernandez *et al.* [40] may also

be used to detect the bends and cracks in fiber. In their proposed system, laser pulses were injected into both the ends of the fiber. The traces obtained by injecting the pulses into the second end of the fiber are used as a reference to discriminate any abnormality like bend in the main sensing fiber. The looped back fiber mode has also been used for reduction of false alarm in leak detection using distributed optical fiber sensor [55]. However, in such cases, only half of the total fiber length is utilized for distributed temperature sensing. Hwang *et al.* [31] demonstrated a technique to eliminate the effect of local losses caused by the bending in sensing fiber by using reflected AS signal from the mirror located at the far fiber end. The advantage of this technique is that loop back arrangement of sensing fiber can be avoided. Ravet *et al.* [56] made use of Brillouin spectrum in order to detect the cracks in a fiber optics sensor. But the incorporation of such a sophisticated technique requires inclusion of Brillouin optical time domain analysis (BOTDA) [57] based interrogator unit which will increase the complexity and cost of the OFDTS.

The present thesis attempts to find out the solutions to the above mentioned issues in rest of the chapters. Chapter 3 of the thesis presents an overview of various types of fiber sensors and theory of Raman Effect followed by study of STFT and its application in addressing various issues for Raman OFDTS [32]. Chapter 4 first introduces the wavelet transform and then describes how its features can be applied to address various issues for Raman OFDTS [33]. The inherent de-noising capability of wavelet processing allows better accuracy with lower acquisition time. Based on the proposed wavelet based technique, a prototype Raman scattering based OFDTS system has been designed and developed. Chapter 5 describes an OFDTS using low core standard sized 62.5/125 µm SS covered Multimode fiber with EMD based signal processing of Raman AS and St signals [34]. The EMD pre-processor dynamically minimizes the error in temperature measurement caused by the difference in

attenuation to AS and St signals offered by the optical fiber. Simultaneous de-noising of AS and St signals offered by the EMD based pre-processor yields better SNR of these signals and thus reduced error in temperature measurement without any increase in acquisition time. Unlike wavelet based technique, EMD based technique is a data driven technique and does not require selection of basis function in advance. Chapter 5 also presents automated and dynamic self-calibration of distributed temperature sensor with the proposed EMD based preprocessor. The use of proposed EMD based pre-processor has been demonstrated to develop an OFDTS with a sensing fiber which is suitable for field applications. Proposed techniques, described in above Chapters, are more automatic compared to technique proposed earlier [32]. Proposed DWT and EMD techniques also ensure inherent smoothening of AS and St signals and thus do not need an additional algorithm for this purpose [30].

Chapter 5 also describes the design and development of a microcontroller (89V51RD2) and Raman OFDTS based zone specific temperature alarm system for 100 m length [35**].** Such an alarm system is very useful in the control room of a process plant and opens the possibility of designing a novel fiber based distributed temperature controller. The alarm system has been successfully tested for 10 zones in a 100 m long sensing fiber for different temperature values.

In Chapter 6 the error in distributed temperature profile measurement caused by a bend in sensing fiber (issue No. 5) is analyzed in detail. This Chapter presents a novel automatic and dynamic technique [36] using EMD for detection of bend and its location using a new feature called ‘area’ of analytic IMFs **[**37, 28] for St signal. Also, it is demonstrated that the error in temperature measurement for rest of the fiber that exists after the bend can be compensated by properly considering an extra calibration zone after the detected bend [36].

Chapter 7 presents the conclusion of the thesis and scope for future work. Details of STFT, Continuous wavelet transform and EMD are presented in Appendix A, B and C repectively. Appendix D presents the schematic diagram of PMT based detector circuit for AS and St signals and circuit diagram of dynamic self calibration system.

# Chapter 3

# Optical fiber based sensors and STFT based pre-processing of Raman signals

## 3.1 Optical fiber based sensors: reasons for using such sensors

In general, optical fiber based sensors can measure a physical, chemical or biological parameter by monitoring the modulation of light propagating inside the fiber. Light from an optical source is launched into a fiber via a stable coupling mechanism and guided to the point at which the measurement is to be carried out. At this point, light may be allowed to exit the fiber and modulated in a separate zone before being re-launched into the same fiber. Such an arrangement is called extrinsic sensor. On the other hand, light may continue to propagate inside fiber and is modulated in response to the measurand but still remains guided by fiber. This type of arrangement is known as intrinsic sensor. Fig. 3.1 depicts the examples of extrinsic and intrinsic optical fiber sensors [3]. In most intrinsic sensors, the fiber acts as sensing element and the communication channel. Such an arrangement facilitates various convenient solutions.

## 3.2 Optical fiber sensor configuration and types

A general classification of optical fiber sensors can be done based on their configuration schemes. There are three possible configuration schemes in which fiber sensors can be utilized [6]:

- Point
- Distributed
- Quasi-distributed

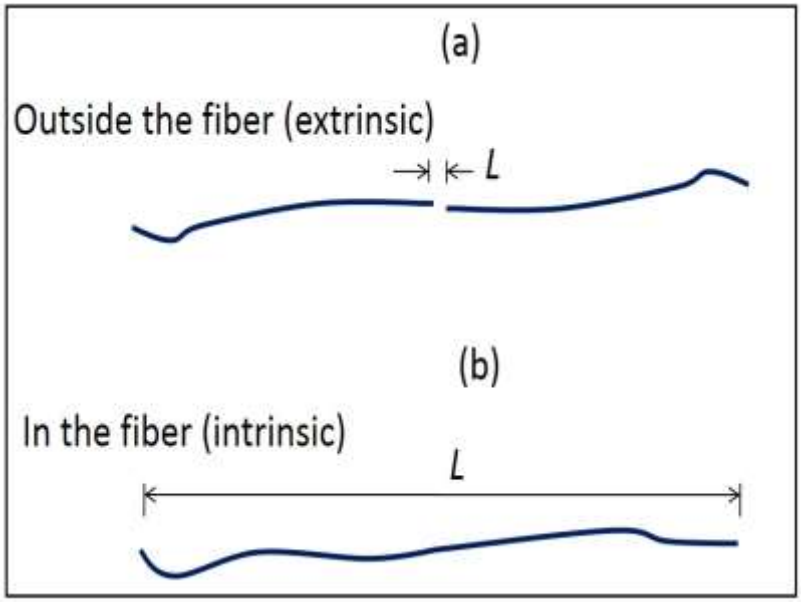


*Fig. 3.1. Extrinsic and intrinsic sensors. (a) extrinsic: light emerges from the fiber into a modulation zone (here applied to the interferometric measurement of distance changes) (b) intrinsic where the light remains in the fiber from source to detector [3].*

The most common and familiar requirement of a sensor system is the measurement of a particular measurand at a particular location which is usually achieved with a point sensor. Fig. 3.2 illustrates the above three major sensor schemes. Fig. 3.2(a) depicts a point sensor based on optical fiber temperature sensor where the luminescent active material at the distant end of the fiber responds to a temperature change applied to the optical fiber. The other arrangement is where sensor devices are designed in such a way that they can discriminate in terms of space which in turn allows the measurand to be determined along the sensing fiber length itself. This type of scheme is popularly known as distributed sensor and can be

schematically illustrated in Fig. 3.2(b). The third configuration of sensor that lies 'in between' the point and distributed sensors is termed as quasi-distributed sensor and is depicted in Fig. 3.2(c). In quasi-distributed scheme measurand information is made available at particular points only and not at every point along the length of the fiber.

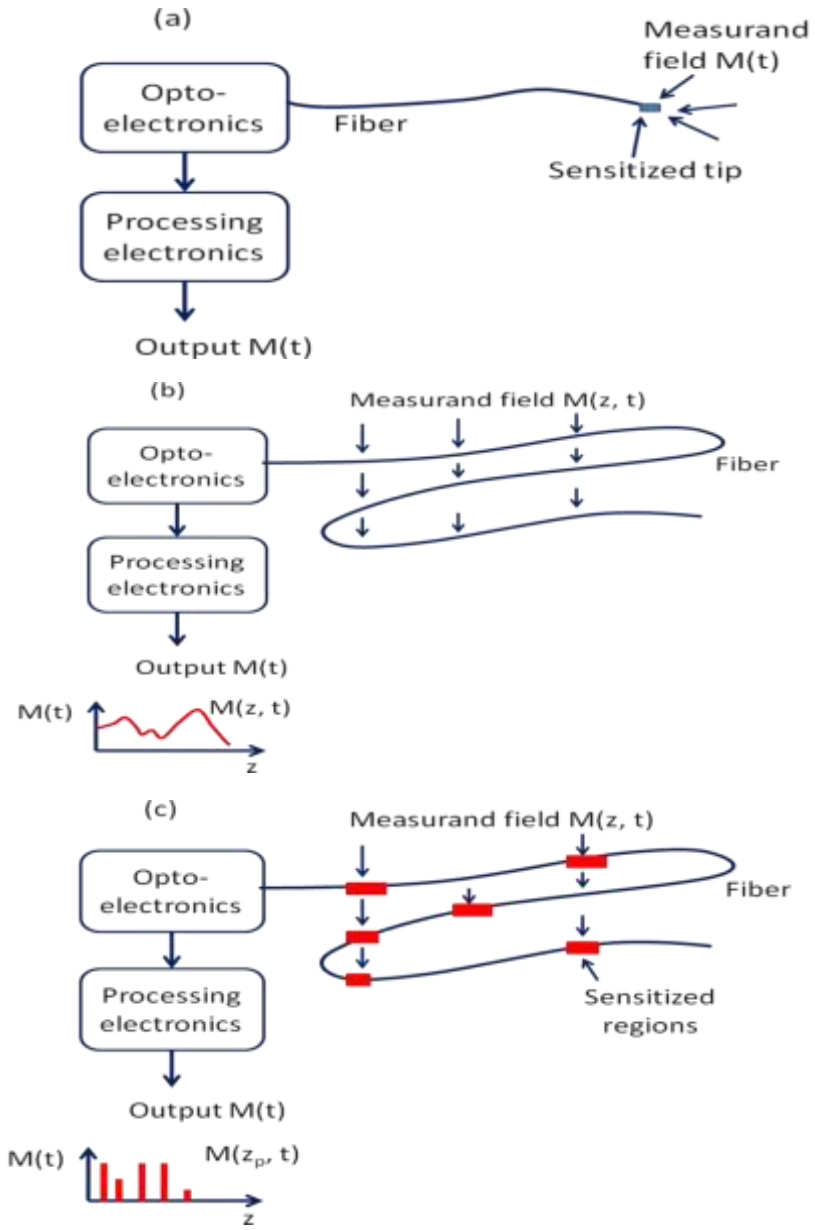


*Fig. 3.2. Various sensor configurations: (a) point (b) distributed and (c) quasi-distributed sensing [6].*

In the present work, focus is kept on the development of distributed sensor scheme which is

intended for temperature sensing and such a system is termed as OFDTS. The temperature is the measure of the average kinetic energy of particles in a substance and is the result of the motion of particles. Temperature increases as the energy of this motion increases. Several considerations drive the need for OFDTS. Temperature sensors are sometimes needed to operate in strong electromagnetic fields. Sensors with metallic leads will experience eddy currents in such environments which will create both noise and the potential for heating of the sensor which in turn add further inaccuracy in the temperature measurement. Fiber optics temperature sensors do not use metallic transducers and thus allow minimized heat dissipation by conduction and provide quick response. Since fiber based sensors are less perturbing to the environment and therefore have the potential for better accuracy [7].

### 3.3 Optical fiber based distributed temperature sensors (OFDTS)

OFDTS systems provide a continuous profile of the temperature distribution along the fiber cable [52]. OFDTS systems mainly make use of Raman and Brillouin scattering. OFDTS systems based on Raman scattering have gained popularity for practical applications owing to their low cost and great stability in comparison to distributed temperature sensor systems based on Brillouin scattering [52]. Following are the main concepts to understand the technologies to be implemented for realizing a practically working Raman OFDTS system.

#### 3.3.1 Optical time domain reflectometry (OTDR)

As outlined earlier, OTDR relies on measurement of round-trip time of the launched laser pulse for the event of interest to measure the spatial location of the event. As with a conventional radar system, the distance ($z$) is directly related to the round-trip time ($t$) taken

by laser pulse which is given by:

$$t = \frac{2z}{V_g} \tag{3.1}$$

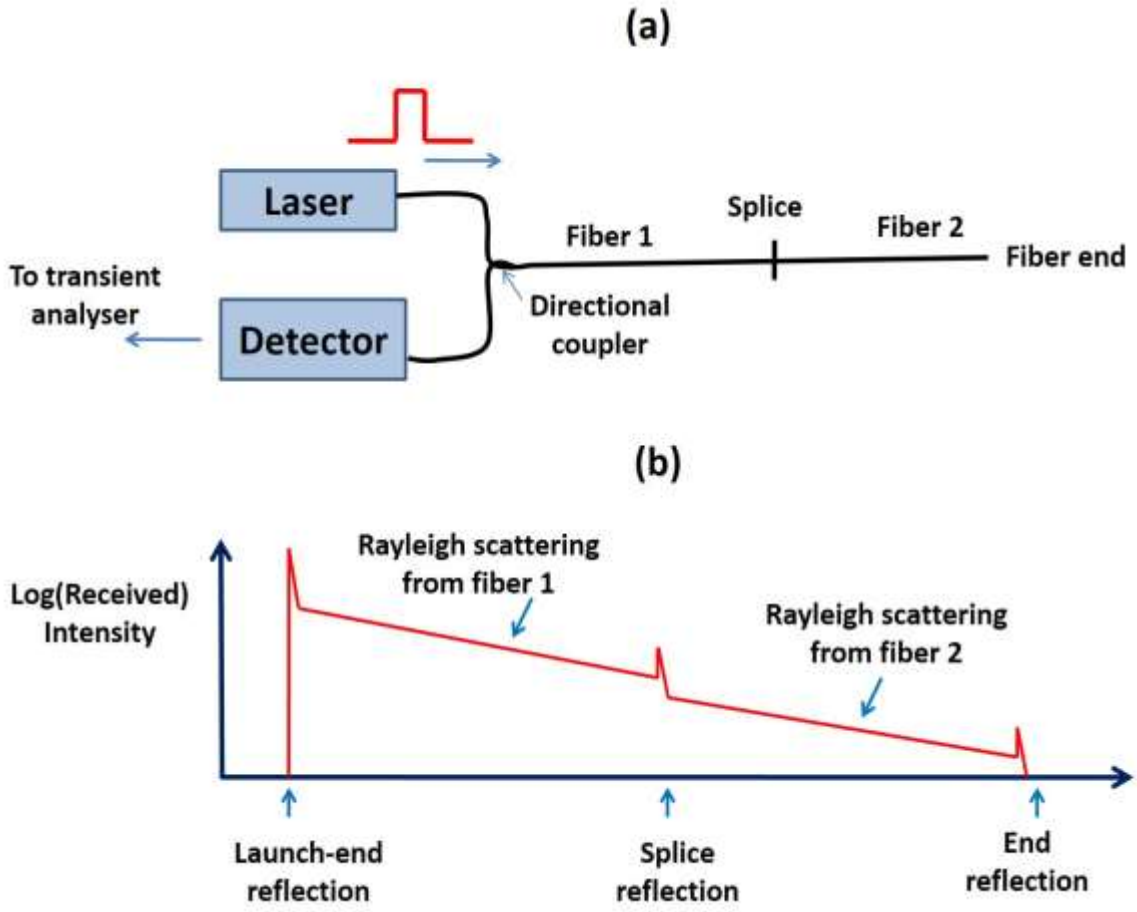


*Fig. 3.3. Basic concept of OTDR (a) optical arrangement (b) OTDR return signal [10].*

where, $V_g$ is the guided wave velocity in the fiber. Therefore, the temporal variation of the detected signal may be used to determine the variation of attenuation of fiber employed in OTDR. Fig. 3.3 (a) shows the basic concept of OTDR method using Rayleigh back scattered light [10]. As shown in Fig. 3.3(b) Rayleigh back scattered light carries the signature of the

event in the fiber. Here, the event is change of refractive index at start, splice and end of fiber. Hence, Rayleigh backscattered light can be used for estimating the location of start of fiber, splice and end of fiber by identifying the Rayleigh reflections from launch end, splice and fiber-end respectively. The Rayleigh backscattered light is separated from input laser with the help of a directional coupler and is analyzed by a transient analyser.

### 3.3.2 Raman Effect and its salient features

Raman Effect [9, 38] is a phenonmenon in which a monochromatic radiation undergoes a change in frequency after scattering by a solid. Because of change in frequency of incident photon, Raman Effect is considered as an in-elastic scattering of photon. If $\nu_i$ is the frequency of the incident radiation and $\nu_s$ is that of the light scattered by a given molecular species, then the Raman shift ($\nabla$) is defined as: $\nabla = \nu_i - \nu_s$. The Raman shift, also known as the wave number shift (expressed in $cm^{-1}$) is the characteristic of the substance producing the scattering and does not depend on the frequency of the light employed. When:

(i) $\nabla$ is positive, $\nu_s < \nu_i$, Raman spectrum is said to consist of St lines.

(ii) $\nabla$ is negative, $\nu_s > \nu_i$, Raman spectrum is said to consist of AS lines.

St lines are frequently much more intense than the AS lines. Raman shift generally lies within the range of 100-3000 $cm^{-1}$ which falls in far and near infra-red regions of the spectrum. This leads to conclude that the changes in energy of the scattered light in Raman Effect correspond to the energy changes accompanying rotational and vibrational transitions in a molecule.

The spectrum of scattered light consists of following components:

(i) Lines of the same optical frequency (or wavelength) as the incident beam. These are called Rayleigh lines.

(ii) Additional weak lines of changed optical frequency (or wavelength). Lines on low wavelength side are called AS lines while those on the high wavelength side are called St lines.

(iii) Raman scattered line intensity is ~$10^{-3}$ times of the Rayleigh line intensity.

(iv) St line intensity is approximately 4-5 times higher than AS line intensity.

Following are the salient features of Raman spectra which make it different from Fluorescence spectra:

(i) Spectral lines have frequencies greater and lesser than the incident frequency. This feature is different from Fluorescence spectra in which line frequency is always less than the incident frequency.

(ii) Raman s**p**ectra arise due to scattering of light by the vibrating molecules. Whereas, fluorescence spectra arise due to absorption of light by vibrating molecules.

(iii) It is the polarizability of the molecule which determines whether the material is Raman active or not. For fluorescence, the molecule must possess permanent dipole moment.

### 3.3.3 Quantum theory of Raman Effect

In scattering, due to the absorption of the incident radiation by scattering molecule, they are raised to a higher energy state. Now if they return to their original state then frequency of radiation emitted is same as that of incident light: but if they return to a higher state or lower vibrational or rotational level, the frequency of scattered radiation is lesser or greater than that of the incident radiation. The amount of this difference is equivalent to the difference in vibrational or rotational energy states. If a molecule is in its initial (lower) state $E^{¨}$ and is exposed to incident radiation of frequency $\nu_i$ $cm^{-1}$. The absorption of this incident radiation

would raise this molecule to a level in which its energy is ($E''+ hc\nu_i$ ). If the molecule returns to a level of energy $E'$, lying above the level $E''$, by losing energy $hc\nu_s$ and emitting (scattered) radiation having observed frequency $\nu_s$. It follows then

$$E'' + hc\nu_i - hc\nu_s = E'$$

$$E' - E'' = hc(\nu_i - \nu_s)$$

$$= hc\,\nabla \qquad (3.2)$$

Eq. (3.2) shows that Raman shift ($\nabla$) is equal to the difference in energy of the two levels represented by $E'$ and $E''$. It is obvious that sign of $\nabla$ depends upon $(E'-E'')$. If $E'>E''$or in other words, if the molecule initially is in lower state when it absorbs energy of incident light, St lines of Raman spectrum (for which $\nabla$ should be positive) are produced. On the other hand, if the molecule is initially in upper state $E'$ and then returns to the lower state $E''$ after emission of scattered Raman radiation, then $\nabla$ is negative and hence Raman spectrum will consist of AS lines.

It may be noted that frequency shifts of Raman lines, their intensity and polarization are characteristics of the scattering substance. Classically, St and AS lines should have equal intensity. However, experiments confirm that St lines are more intense. It can be explained on the basis of quantum theory of Raman Effect: St lines have transition which are more probable as there are plenty of molecules in the ground state at room temperature. On the other hand, the number of molecules at room temperature is quite less in upper state which is responsible for AS lines.

For Silica fiber $\nabla$ is 440 $cm^{-1}$. The value of AS wavelength ($\lambda_{AS}$) and St wavelength ($\lambda_{St}$) when the laser of wavelength ($\lambda_i$) is employed as pump source, can be calculated using Eqs. (3.3) and (3.4) respectively.

$$\frac{1}{\lambda_{AS}} = \frac{1}{\lambda_i} + \nabla \tag{3.3}$$

$$\frac{1}{\lambda_{St}} = \frac{1}{\lambda_i} - \nabla \tag{3.4}$$

### 3.3.4 Basic Raman OFDTS schemean

Fig. 3.4 depics the basic block diagram of Raman OFDTS [10]. A pulsed laser is used as an excitation source. The backscattering of laser light takes place from each and every point of

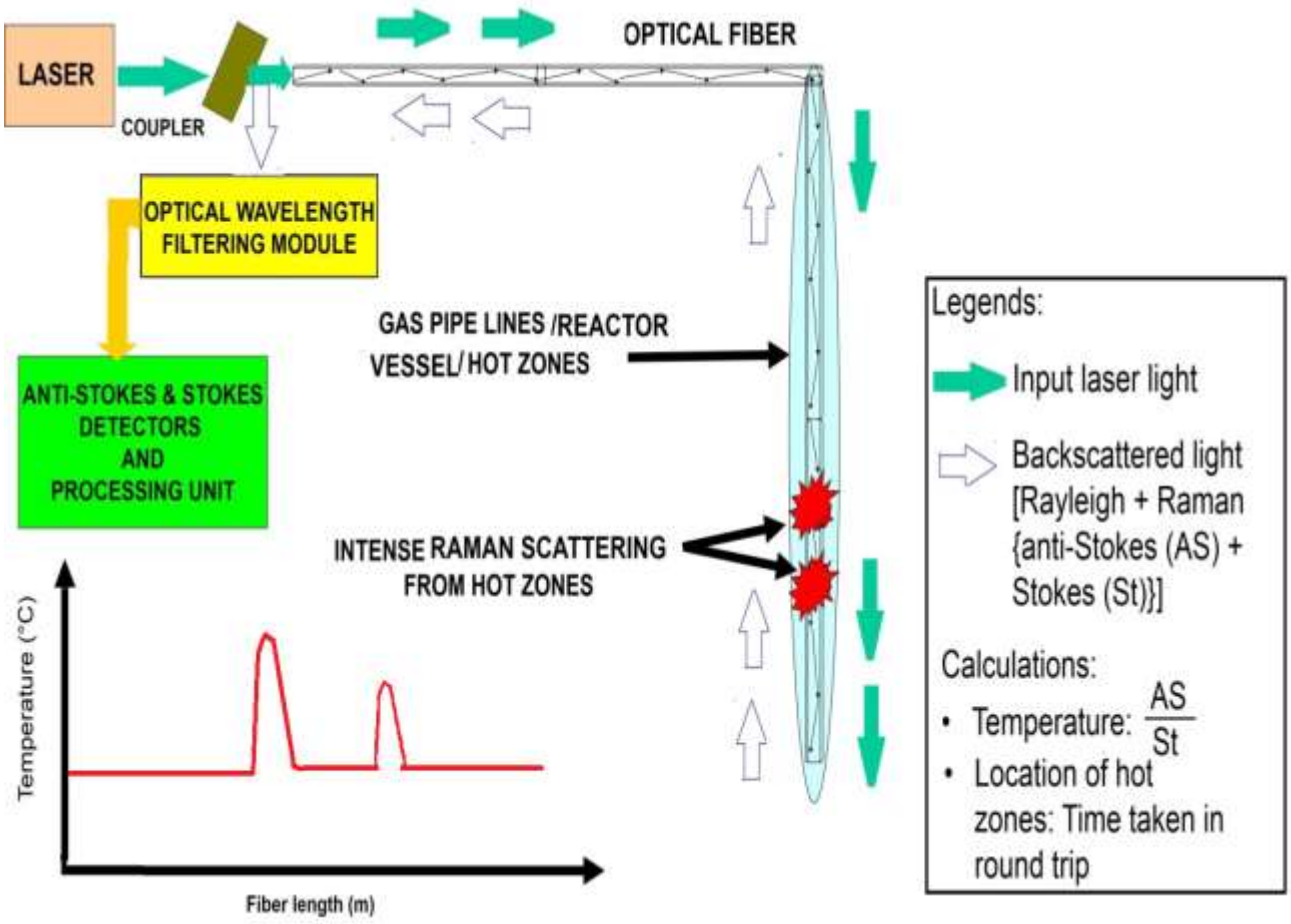


*Fig. 3.4. Basic block diagram of Raman OFDTS. Temperature of a hot zone is derived by the ratio of the anti-Stokes (AS) to Stokes (St) intensities and location using time taken by laser pulse in round trip up to hot zones (OTDR principle) (Concept taken from Ref. [10]).*

the sensing fiber. The backscattered light consists of Rayleigh and Raman (AS and St) light signals. Raman AS and St signal profiles along fiber length are obtained by OTDR principle after optical filtering using wavelength filtering module and are processed for plotting final distributed temperature profile along the fiber length.

### 3.4 Non-stationary signal processing methods

Mathematical transformations are applied to signals to obtain further information from the signals that is not readily available in their raw form. In many cases, the most useful information remains hidden in the frequency contents of the signal. Generally, Fourier transform is used to find the frequency contents of a signal [22]. Need for other transforms comes from the very important property of a time domain signal which is called stationarity of the signal. Stationary signals are ones for which frequency contents do not change in time. In this case, there is no need to know at what times what frequency components exist since all frequency components are present at all the times. On the other hand, the signals in which frequency does not remain constant and varies with time are called non-stationary signals.

To deal with non-stationary signals, there are many transforms [22]. Short-term Fourier transform (STFT), wavelet transform and empirical mode decomposition are the main non-stationary signal models which are employed to analyze non-stationary signals. The study of above non-stationary signal methods for resolving various issues involved in the development of Raman OFDTS is the subject matter of the present thesis. First, it is demonstrated that how STFT can be applied to address various issues.

### 3.5 Short term Fourier transform (STFT) based signal pre-processing of Raman AS and St signals

The optical Raman AS and St lights are converted into electrical signals by opto-electronic transducers. The obtained electrical AS and St signals are in time domain and are non-stationary in nature. Conventional Fourier transform has limitation that it is not suitable for analyzing non-stationary signals and signals having time varying direct current (dc) component. To deal with such signals, short term (or time) Fourier transform (STFT) is utilized [23-25]. In STFT, the signal is divided into small segments by windowing, where these segments of signals can be assumed to be stationary. The width of the window must be equal to the segment of the signal where signal is stationary and dc component is assumed to be constant. This window function is first located at the very beginning of the signal and its product with signal is computed. Then this product is assumed to be just another signal for which Fourier transform is computed. Next step would be shifting this window to a new location, multiplying with the signal and taking Fourier transform of the product. This procedure is followed until the end of the signal is reached. In real world, since analog signals (e.g. AS and St) after digital conversion by data acquisition (DAQ) card are aperiodic and discrete, Fourier transform can be replaced by a transform which is especially designed for use with discrete data. Such a transform is known as discrete Fourier transform (DFT) [58]. Detailed information on STFT is available in Appendix A.

#### 3.5.1 Removing variable slope of a signal using fast Fourier transform

DFT is used in many applications because of its ability to transform a time-series into its equivalent frequency representations. The fast Fourier transform (FFT) is one of the most

optimized algorithms that are used to compute DFT.

The *N* point DFT, *X(k)* of a time sampled signal *x(n)*

$$x(n) = x_0, x_1, x_2, \dots, x_k, \dots, x_{N-1} \tag{3.5}$$

is given by the following expression [58]

$$X(k) = \sum_{n=0}^{N-1} \left[ x(n) e^{-\frac{j2\pi kn}{N}} \right], \qquad 0 \leq k \leq N-1 \tag{3.6}$$

And the inverse DFT (IDFT) is given by

$$x(n) = \frac{1}{N} \sum_{k=0}^{N-1} \left[ X(k) e^{\frac{j2\pi kn}{N}} \right], \qquad 0 \leq n \leq N-1 \tag{3.7}$$

where, *N* is number of samples in the signal.

The first value of the transformed series that is *X(0)* is the lowest frequency component of the time-series and is called the trend of the signal. Leaving a trend in the signal adds a dc component which is mainly responsible for the slope of the signal. It may be noted that vectors in MATLAB [59] are indexed from 1 to *N* instead of 0 to *N-1*, the DFT and IDFT computed in the MATLAB program make use of *X(1)* for computation of the trend [60].

### 3.5.2 Experimental setup and data acquisition

The detailed block diagram of the experimental setup developed in the laboratory which has been used to obtain actual Raman AS and St signals from sensing fiber is depicted in Fig. 3.5 [10, 61 and 62]. A pulsed diode-pumped solid-state laser (DPSSL) (Model: DTL-324QT, Make: Laser Export, Russia) with laser wavelength of 1064 nm and pulse width of 10 ns is used as an excitation source to generate Raman scattering in the optical fiber. The laser operates at pulse energy of 100 µJ with a pulse repetition rate of 1 kHz. The laser is coupled

to a sensing fiber which is a 200/220 µm sized Multimode Polyimide coated silica fiber with numerical aperture of 0.22 and core refractive index of 1.5.

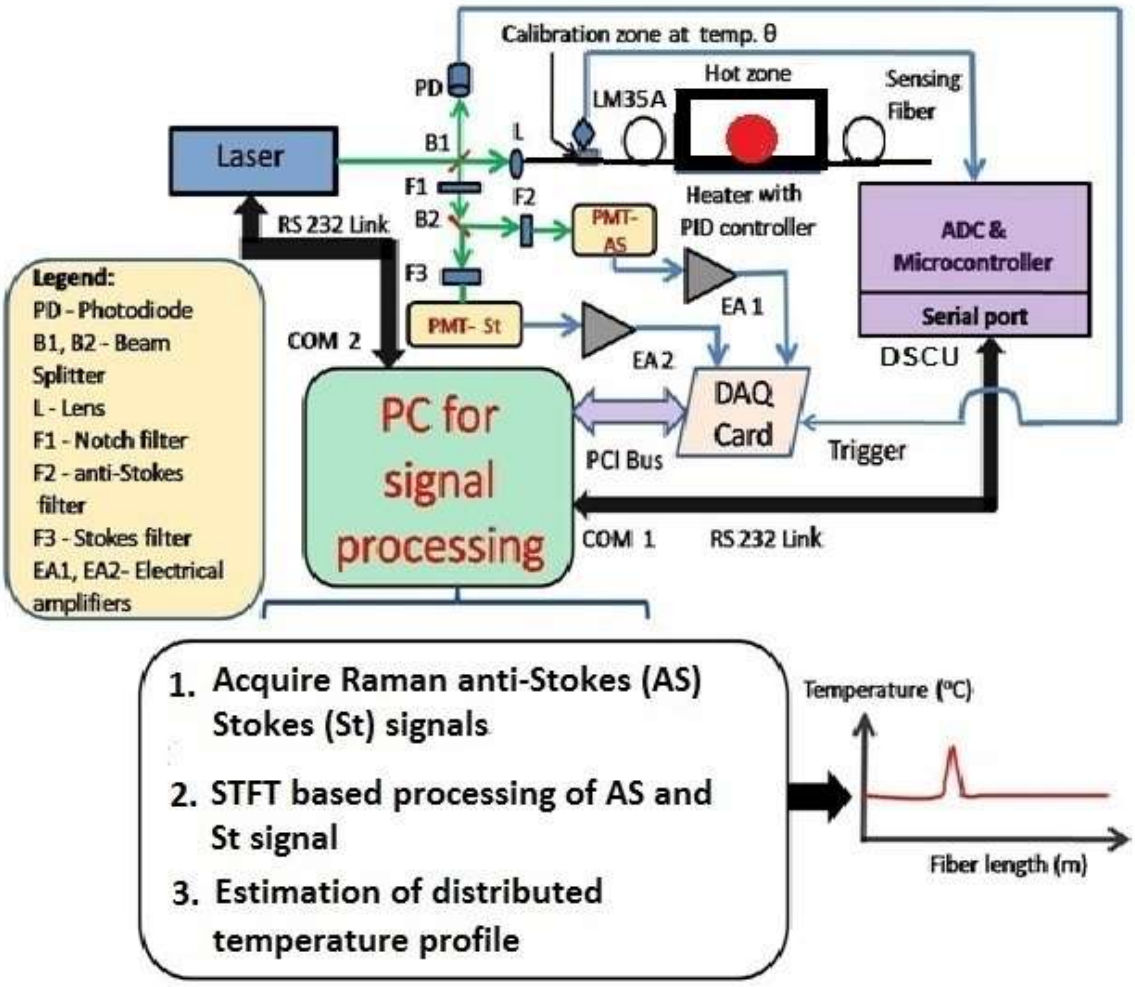


*Fig.3.5. Block diagram of experimental set-up developed in laboratory (Concept taken from Ref. [10, 61 and 62]).*

An initial 1 m long section of the sensing fiber is kept reserved as calibration zone. Laser light is coupled to optical fiber using lens (L) with focal length of 8 mm and numerical aperture of 0.5. Backscattered spectrum from sensing fiber which consists of Rayleigh,

Raman AS and Raman St optical signals is split by a 50:50 beam splitter (B1). A holographic super notch filter (F1) with center wavelength of 1064 nm attenuates the undesired Rayleigh signal in the backscattered light. This light is further split into two parts by another beam splitter (B2). The split parts of backscattered light are filtered by an optical filter (F2) with center wavelength of 1020 nm to get AS signal and by an optical filter (F3) with centre wavelength of 1110 nm to obtain St signal. These optical AS and St signals are converted into electrical signals with the help of photomultiplier tubes PMT-AS and PMT-St respectively. Both PMTs (Model: R5108, Make: Hamamatsu, Japan) have spectral response of 400-1200 nm. Photomultiplier tubes are transducer which convert optical signals into electrical signals. The amplitudes of electrical AS and St signals, at the start of fiber are -560 μV and -960 μV respectively. These amplitudes correspond to the room temperature. The electrical signals are amplified by electrical amplifiers EA1 and EA2 (Model: SR445A, Make: Stanford Research Systems, USA)) with gain setting of 25 for each signal. The amplified electrical output signals of PMTs are fed to a high bandwidth peripheral component interconnect (PCI) bus [63] based DAQ card system (Model: CS85G, Make: Gage, USA) which digitizes both the Raman signals at a sampling rate of 1GSamples/s. The digitized signals are accessed by personal computer (PC) in MATLAB environment. The DAQ card is triggered externally by output of a photodiode (PD) on which a part of pump laser through beam splitter (B1) is allowed to fall. A temperature measurement system based on precision integrated-circuit sensor LM35A, analoge to digital converter (ADC) ADC0848 and a microcontroller (89V51RD2) has also been developed in the present work. It is named as dynamic self-calibration unit (DSCU). The Schematic diagrams of PMT based detectors and circuit diagram of DSCU are presented in Appendix D. The DSCU is connected to serial port (COM1) of the main PC through RS232 link. A software using MATLAB has been developed to read the latest value of $\theta$ and update it in the main program for determining the

unknown temperature *(T)* profile for the whole fiber length. Another serial port (COM2) of PC is used to control the laser operation (ON/OFF), laser pulse energy and repetition rate of DPSSL.

To test the performance of the developed OFDTS, 1 m long section from sensing fiber was selected as hot zone for temperature measurement. This hot zone is located at 190 m from the laser end of the fiber. Hot zone was heated with the help of an electric heater having 930 W electrical power, controlled by a proportional-derivative-integral (P-I-D) controller (Model: PID528, Make: Selec Controls, India) and solid state relay (Model: G3NE, Make: Omron, Japan). Fig. 3.6 shows the schematic diagram of the heater's cross section whereas Fig. 3.7 shows the photograph of the heater.

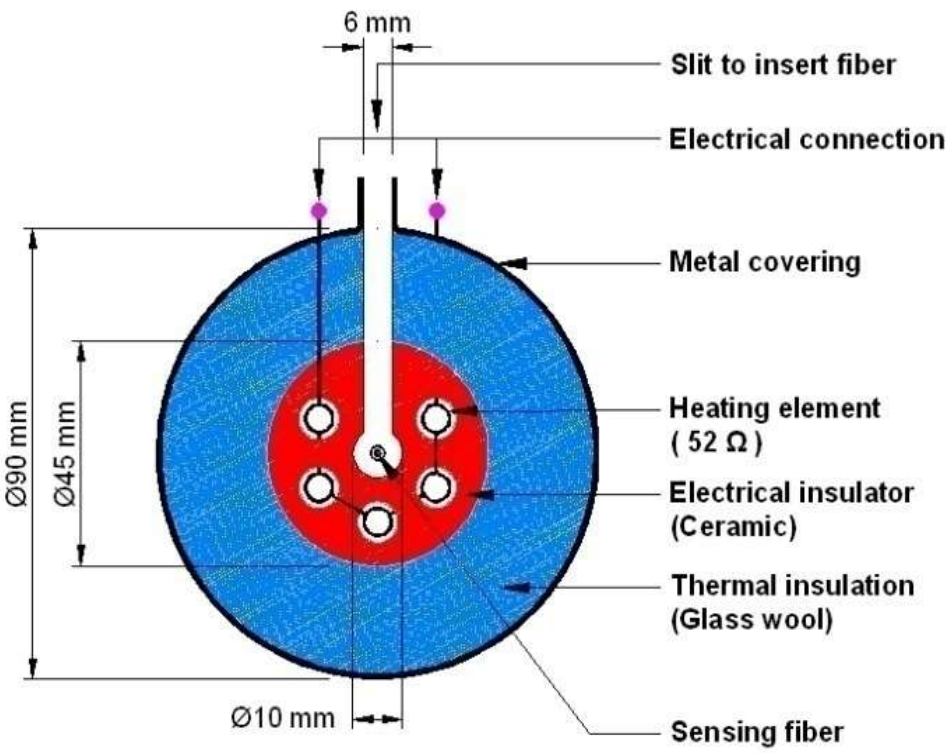


*Fig. 3.6. Schematic diagram of the cross section of the electrical heater.*

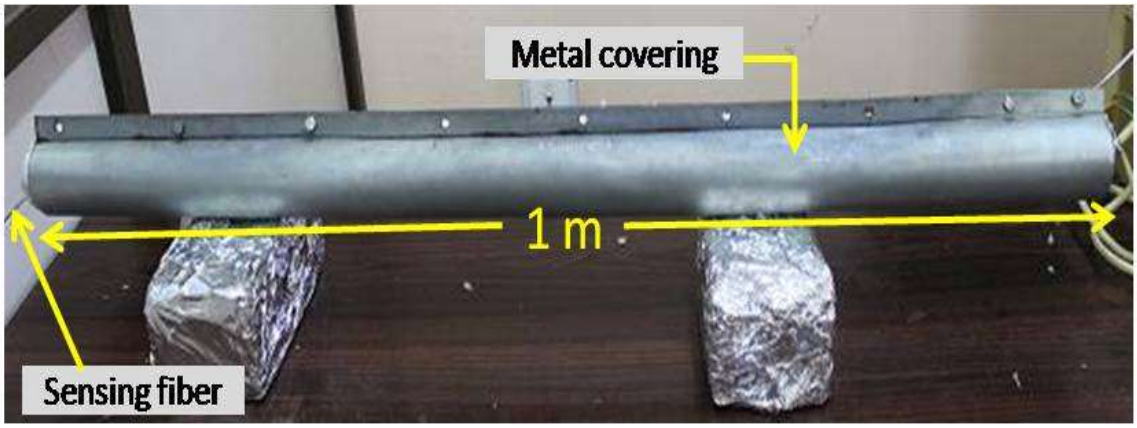


*Fig. 3.7. Photograph of the electrical heater.*

For the present study, hot zone was kept at 105 ˚C and allowed to stabilize for ~ 30 minutes while the remaining fiber was kept at room temperature (~ 24.5 ˚C). The reference temperatures of various zones in the fiber were measured by thermocouple based thermometers (Model: Digirad71, Make: Radix, India) placed in the close vicinity of fiber. This setup is utilized to check whether OFDTS, developed using proposed STFT technique, is able to measure temperature, width and location of hot zones with sufficient accuracy.

### 3.6 Experimental Raman AS and St signals

The amplified and averaged AS and St signals obtained from the experimental set up are shown in Fig. 3.8. Th upper (black) curve represents AS signal whereas lower (red) curve corresponds to St signal. The total number of samples in AS and St signal are 2048 for 204.8 m length of fiber. In a fiber having refractive index ($n$) following OTDR relation between relation between length (z) and number of samples ($N$) obtained from sampling rate ($S$) holds true.

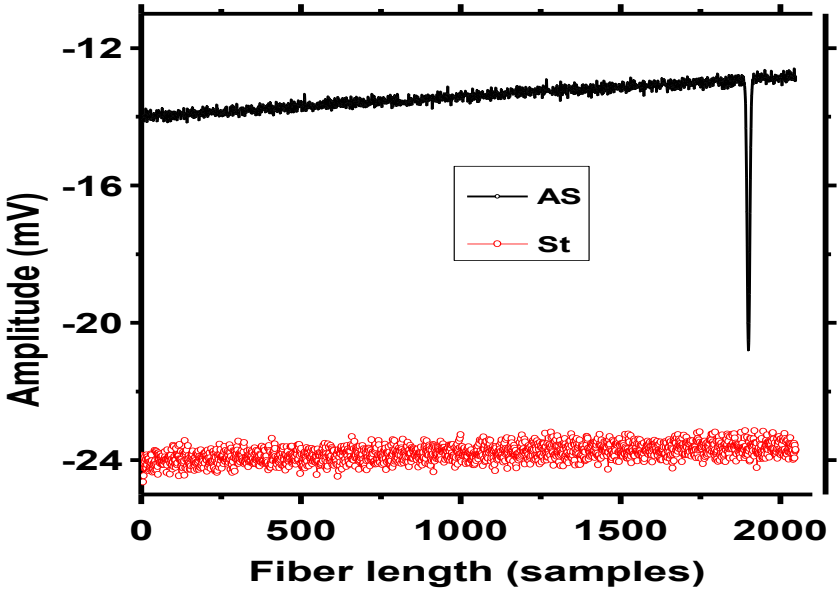


*Fig. 3.8. Experimental AS (upper curve) and St (lower curve) signals* (*On horizontal-axis, 10 samples ≡ 10 ns ≡ 1m*).

$$z = \frac{cN}{2nS} \tag{3.8}$$

In the present system, AS and St signals are of 2.048 μs duration for 204.8 m long silica fiber. Since AS and St signals are sampled at a sampling rate of 1 G Samples/s, each of them will be represented by 2048 samples. Therefore, for the present experiment, 10 samples ≡ 10 ns ≡ 1m relation works well. The hot zone located at 190 m appears at sample number 1900 as shown in AS (upper curve) of Fig. 3.8.

If Eq. (2.1) is directly used for distributed temperature profile measurement using AS and St signals presented in Fig. 3.8 a highly erroneous and unacceptable temperature profile, as shown in Fig. 3.9, will be obtained. It measures the room temperature of 24.5 °C at the start of fiber as 456 °C and room temperature of 25 °C at the end of fiber as 380 °C. Moreover,

temperature of hot zone (kept at 105 °C) is measured as 1064 °C. Therefore, it is required to modify Eq. (2.1) in order to achieve correct temperature profile. As discussed in Section 1.1, the incorrect distributed temperature profile using Eq. (2.1) is due to issue No. 1.

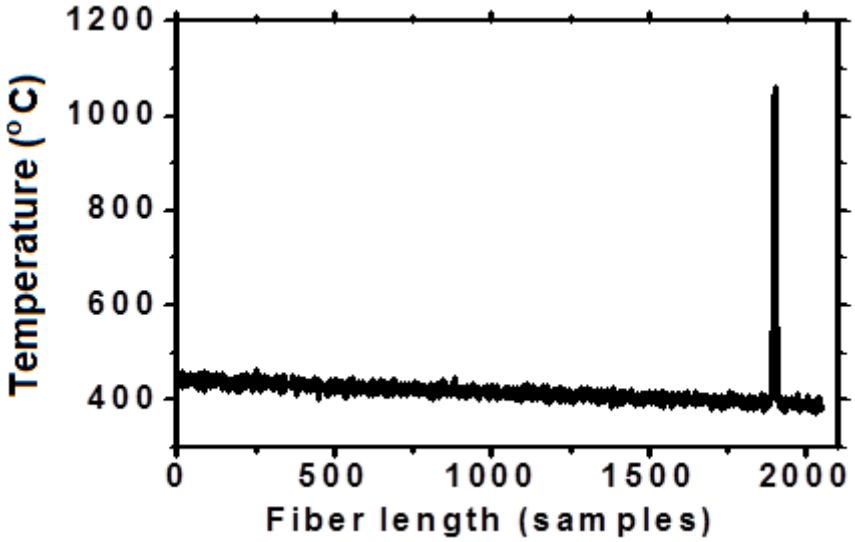


*Fig. 3.9. Erroneous distributed temperature profile measured with Eq. (2.1) using AS and St signals presented in Fig. 3.8* (*On horizontal-axis, 10 samples ≡ 10 ns ≡ 1 m*).

As discussed in Chapter 2, issue No. 2 and 3 also need to be addressed. The issue of differential attenuation (issue No. 2) is taken up first. Then issue No. 1 and 3 are addressed together by modifying Eq. (2.1). The issue No. 2 can be resolved by using the proposed algorithm, proposed in this work.

It is proposed to address issue No. 2 by first minimizing the slopes of both the signals to significantly low values. This is achieved by removing the varying amount of background from AS and St signals. The basic steps of the proposed algorithm are as described below.

1. Divide AS and St signals into small rectangular windowed sections in time sample domain. Each windowed signal may be represented by *x(n).*

2. Using FFT algorithm for Fourier transform, calculate *X(n)* of the windowed section.
3. Make background of the windowed signal zero by setting *X(0)* to zero. This gives modified FFT of signals *[X'(n)]* of the windowed section.
4. Take inverse Fourier transform using IFFT algorithm corresponding to *X'(n)* of the windowed section to obtain its modified time domain version.
5. Repeat step 2-4 for each windowed section.
6. Concatenate all modified time domain versions of windowed sections.
7. Obtain slope free time domain signals by adding a constant equivalent to a value to the average of first 10 samples of the signal obtained in step 1.

The AS and St signals after having pre-processed using above algorithm are depicted in Fig. 3.10. A rectangular window of size 200 samples was chosen. Unprocessed AS and St signals are also shown for comparison. It may be observed that varying amount of DC component from AS and St signals has been minimized.

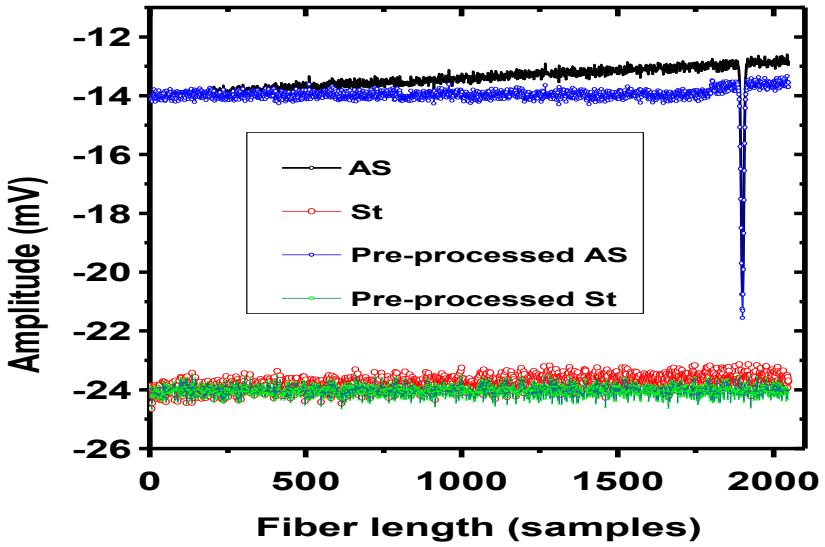


*Fig. 3.10. Pre-processed AS (upper curve) and St (lower curve) signals. Original AS and St signals of Fig. 3.8 are also shown (On horizontal-axis, 10 samples ≡ 10 ns ≡ 1m).*

The issue No. 1 can be addressed by referencing the ratio profile at unknown temperature to the ratio value at known temperature of the calibration zone of fiber [15]. In case, calibration zone is kept at some known absolute room temperature ($\theta$), the quotient of the ratio profile ($R_T$) at unknown temperature ($T$) for an arbitrary zone and the ratio value ($R_\theta$) at the calibration zone temperature ($\theta$) can be calculated with the help of Eq. (2.1) and is given by the following expression:

$$\frac{R_T}{R_\theta} = e^{-B\left(\frac{1}{T}-\frac{1}{\theta}\right)} \tag{3.9}$$

where, $\theta$ is measured in Kelvin.

On simplification, *T (°C)* is given by the following expression [29, 64]:

$$T\,(^\circ C) = B.\left[\frac{1}{\left(B.\frac{1}{\theta} - \ln R_T + \ln R_\theta\right)}\right] - 273.15 \tag{3.10}$$

The numerical value of $B$ can be calculated using Eq. (2.2). Thus, in Eq. (3.10), parameters $B$ and $\theta$ are known. Therefore, Eq. (3.10) will yield unknown temperature profile ($T$) for complete fiber length provided profiles of $R_T$ and value of $R_\theta$ are available. $R_\theta$ is the ratio value of AS to St signal (AS/St) for the calibration zone of length 1 m chosen from sensing fiber at the laser end. However, some caution has to be exercised while calculating $R_T$ profile for complete fiber length. In Eq. (3.10), it is assumed that $R_T$ (AS/St) profile for complete fiber length is calculated after wavelength dependent attenuation difference between AS and St signals has been corrected (issue No. 2). In other words, AS and St signals must have either same slope or should be 'slope free' before they are used in Eq. (3.10). The ideal situation would be when both AS and St signals do not have background contribution and are thus free from any slope caused by fiber attenuation. It is known that the electrical version of AS (and St) signal has a slope due to fiber attenuation [10] which means that removing the

slope will eliminate the fiber attenuation from these signals. In sample domain, this slope can be eliminated from AS (and St) signal with the help of STFT based processing described above.

Even if Eq. (3.10) is used in lieu of Eq. (2.1) using unprocessed AS and St signals (shown in Fig. 3.8), an erroneous distributed temperature profile is obtained. Such a profile is shown in Fig. 3.11 in red colour. However, it is much better temperature profile shown in Fig. 3.9 which was obtained using Eq. (2.1). Therefore, it is necessary to pre-process AS and St signals (Fig. 3.8) and then use them in Eq. (3.10). The experimental method to achieve the background of AS and St signals is to monitor and store both the signals at the start of the experiment when there were no hot zones in the fiber and whole fiber was at room temperature. However, in real life situations, at a later moment, levels of AS and St signals may be different from their stored values because of the variation in laser power and laser-fiber coupling. Therefore, the temperature calculation algorithm should be able to dynamically recover the background (i.e. room temperature versions of AS and St signals) from real time signals available at the time of measurement of temperature. Moreover, the temperature of calibration zone ($\theta$) must also correspond to the latest values of AS and St signal for the calibration zone. Measuring the most recent value of $\theta$ along with the most recent corresponding values of AS and St signals (to obtain $R_\theta = AS/St$) for calibration zone and using these parameters in Eq. (3.10) is called dynamic self calibration (issue No. 1). It is performed on every fresh measurement of unknown distributed temperature ($T$) for whole fiber length and makes the temperature measurement independent of variation in laser power and laser-fiber coupling (issue No. 3). The DSCU has been developed to measure $\theta$ on every fresh measurement for profile of $T$. It eliminates the need of keeping the calibration zone at a constant temperature using isothermal bath and thus associated complicated arrangement for

isothermal bath could be avoided.

### 3.7 Results of distributed temperature profile measurement using proposed STFT based technique

STFT based signal pre-processing for AS and St signals has been implemented to obtain pre-processed AS and St signals. These signals were used in Eq. (3.10) to obtain the correct temperature profile. Fig. 3.11 presents the final corrected distributed temperature profile for complete fiber length of 204.8 m in black colour. The temperature ($\theta$) of the calibration zone was measured to be 24.5 °C by DSCU. The zoomed view at hot zone for temperature profile shown in Fig. 3.11 is available in Fig. 3.12. Temperature profile (red colour) obatained using

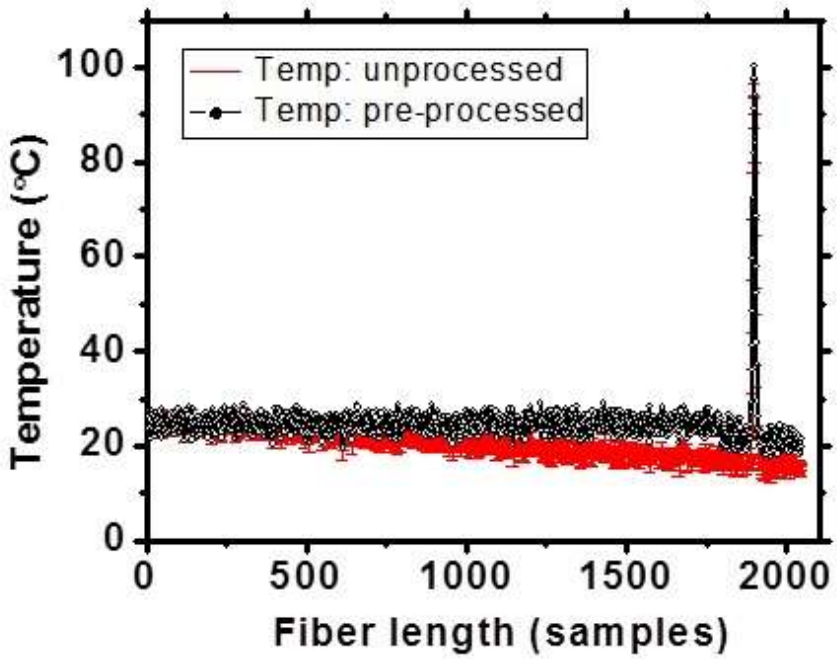


*Fig. 3.11. Distributed temperature profile obtained using Eq. (3.10) with pre-processed AS & St signals (black colour) and unprocessed AS & St signals (red colour)* (*On horizontal-axis, 10 samples ≡ 10 ns ≡ 1 m*).

Eq. (3.10) with unprocessed AS and St signals is also shown in Fig. 3.11 and 3.12. Comparison of these two temperature profiles clearly brings out the benefits of STFT based signal processing in terms of reduced errors in temperature profile measurement. The width of the hot zone in the present experiment was kept around 1 m. This information can be recovered from full width half maxima (FWHM) values measured for the peak corresponding to hot zone. The measured value of width of the hot zone comes out to be 1 m

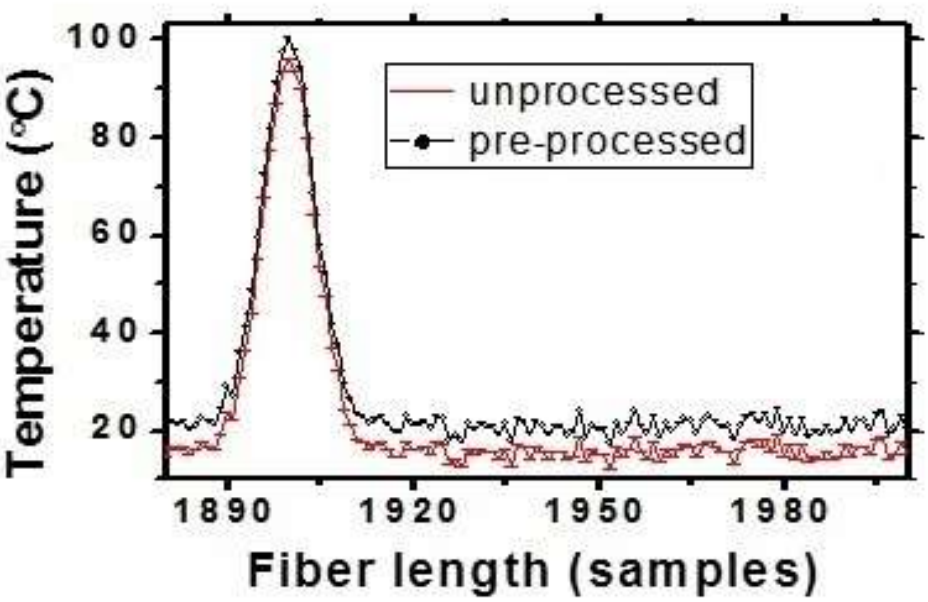


*Fig. 3.12. Zoomed view of temperature profile (shown in Fig. 3.11) at hot zone* (*On horizontal-axis, 10 samples ≡ 10 ns ≡ 1 m*).

and is shown in Fig. 3.12. This is same as the width of hot zones set while conducting the experiment. Also, the rise time (10% - 90% of peak value) of the hot zone is measured to be 1 m. These parameters indicate that the spatial resolution of the developed OFDTS is 1 m [65, 66]. Summary of some of the measurements carried out by the developed system is given in Table 3.1. Error in temperature measurement is less than 5 °C and error in location of hot zones is less than 3 cm. Thus temperature, spatial location and spatial width of two hot zones

can be recovered with reasonably small errors by STFT based pre-processing of Raman signals for the OFDTS developed in the present work. However, it may be noticed that peak-to-peak variation in measurement of room temperature along fiber length is quite high and and is measured to be 10.8 °C. The peak-to-peak variation causes additional error in temperature measurement. This is because of the noise level present in AS and St signals even after an avering of 5000 waveforms. The time spent in averaging is 100 s on an Intel Pentium-4 (1.9 GHz) processor based PC having 1 GB RAM and Windows 2000 operating system support. More number of waveforms are required to be averaged if peak-to-peak variation has to be limited. However, increased averaging causes increase in response time of OFDTS. In STFT based pre-processing, the user has to carefully choose the window size for AS and St signals in such a manner that the hot zone lies in the middle of the window. This allows better results in terms of accuracy of temperature measurement.

**Table 3.1**

Comparison of error in temperature measurement at various zones with unprocessed and STFT pre-processed Raman AS and St signals.

| Zone (Location) | Reference temperature | Measured temperature | |
|---|---|---|---|
| | | Unprocessed | Pre-processed |
| Start of fiber (Location: 0 m) | 24.5 °C | 23.0 °C | 23.0 °C |
| | Error | -1.5 °C (- 6.12%) | -1.5 °C (- 6.12%) |
| Hot zone (Location: 190 m) | 105 °C | 97.0 °C | 100.2 °C |
| | Error | -8.0 °C (- 7.6%) | -4.8 °C (- 4.5%) |
| End of fiber (Location: 204.5 m) | 25 °C | 14.2 °C | 17.7 °C |
| | Error | -10.8 °C (- 43.2%) | -7.3 °C (- 29.2%) |

The inaccuracy in temperature measurement is attributed to following sources. First, the temperature of hot zone is not uniform everywhere in entire 1 m length. The temperature is slightly less at the edges compared to its middle position. Because of this non-uniform heating of hot zones, 1 m long fiber is not fully exposed to the temperature indicated by the reference thermometer. Due to this reason, measured temperatures are different from reference thermometer readings. Second, a finite gap has to be maintained between reference thermometer's tip and sensing fiber to avoid the risk of breaking the fiber. For this reason, the temperature experienced by the sensing fiber is slightly different from the temperature sensed by the reference thermometer. Third, the final accuracy of LM35A based DSCU, used to measure calibration temperature ($\theta$) is ± 0.5 °C. This also contributes to certain error in temperature measurement. Fourth, the AS and St signals are not denoised by STFT method. This makes calculated value of parameter $R_\theta$ for the calibration zone to be slightly different from its ideal value and finally causes temperature errors.

### 3.8 Summary

This Chapter describes STFT based technique which is developed to reduce errors in measurement of temperature profile using Raman scattering based OFDTS. Error reduction is achieved by addressing the issues like difference in fiber attenuation for Raman AS and St signals and dynamic self calibration. Reduced error in temperature profile measurement for the full length of the fiber and freedom from constant temperature bath of the calibration zone are the main features of the proposed technique. In addition to the above features the developed technique also takes care of variation in laser power and/or laser power coupled to sensing fiber with time. However, apart from the fact that issue No. 4 and 5 still remain unaddressed, STFT based technique also requires manual assistance while choosing a

window size. This factor makes STFT based technique less attractive for development of an automated version of OFDTS.

# Chapter 4

# Wavelet transform based pre-processing of Raman signals for an OFDTS

## 4.1 Introduction

In Chapter 3, STFT was used to address issue No. 1-3 related to the development of OFDTS. However, issue No. 4 and 5 remain unaddressed with STFT. The present Chapter presents how various features of wavelet transform can be applied to address issue No. 1-4 simultaneously. Discussion on how to address issue No. 5 is presented in Chapter 6. The following section describes the superiority of wavelet transform [67-69] over STFT with reference to development of OFDTS.

## 4.2 Need of wavelet transform

The main limitation of STFT based processing is related to width of the window function used. In Fourier transform, there is no resolution problem in frequency domain since it is possible to know exactly what frequencies exist in the signal. Similarly, there is no time resolution problem in time domain, since value of the signal at every instant of time is well estimated. Conversely, time resolution in Fourier transform and frequency resolution in time domain have worst figures since there is no information about these parameters. The perfect frequency resolution in Fourier transform is possible because of its window used which is the kernel of the form $e^{j2\pi ft}$. Here, $f$ and $t$ are frequency and time parameters respectively. This function exists at all times from -∞ to +∞ [22]. In STFT, the window is of finite length and

covers only a portion of the signal which causes poorer frequency resolution. Poorer frequency resolution implies that it is difficult to know the exact frequency components that exist in the signal but it is possible to only know a band of frequencies that exist. Also, STFT requires manual selection of window width which makes STFT unsuitable for the development of an automated OFDTS. Wavelet transform has the ability to provide a solution to this problem. Various properties of wavelet transform are quite useful in addressing the different issues encountered while developing a Raman OFDTS. In this Chapter, the resolution of various issues by using wavelet transform is described. Development of a prototype version of OFDTS which employs wavelet transform based signal processing of Raman AS and St signals is also described in this Chapter.

The present Chapter attempts to describe the use of DWT [26, 27] based digital signal processing technique for Raman AS and St signals to address various issues described in Section 1.1. The developed DWT based technique, described here, is more automatic as no selection of calibration zone and window size by the user is required. The proposed DWT based technique also ensures smoothening of AS and St signals because of the inherent de-noising property of DWT and thus does not need an additional algorithm for this purpose. Denoising of signals is obtained as a by-product of the proposed DWT based pre-processing and no additional denoising algorithm is needed. Thus, DWT based technique provides a single solution to address multiple issues (issue No. 1 to 4) simultaneously. In the proposed technique, first, the slope free denoised versions of AS and St signals are dynamically recovered for whole fiber length from the real time experimental versions of respective signals using 'trend' finding capability of DWT. This solves the problem of non-identical fiber attenuation in AS and St signals (issue No. 2). Further, simultaneous measurement of temperature of calibration zone and corresponding AS and St

signals is carried out to resolve the issues No. 1. With DWT based signal processing, denoised AS and St signals are obtained without causing any spatial inaccuracy in the location of hot zones which is an improvement over conventional FIR/IIR based Fourier filtering (issue No. 4). Based on the proposed technique, a Raman scattering based OFDTS system has been designed and developed. The maximum temperature error of ±3.5 °C in the range of 25-295 °C with spatial resolution of 1 m over a sensing length of 204.8 m is achieved. The maximum spatial error of ±3 cm was observed in locating the hot zones placed at 190 m in the above temperature range.

### 4.3 A brief theory of wavelet transform

A wavelet is a waveform of limited duration and has an average value of zero. Unlike sinusoids that theoretically extend from $-\infty$ to $+\infty$ on time axis, wavelets have a beginning and an end. Sinusoids are smooth, predictable and are good at describing stationary signals. On the other hand wavelets are irregular, of limited duration and often non-symmetrical [68]. Thus, they are better at describing anomalies, pulses and other events that start and stop within the signal. In wavelet analysis, one uses the ability of wavelet transform to process both time and frequency together by using the compressed wavelets at low scales (high frequencies) and stretched wavelets at high scales (low frequencies). Thus, wavelet transform gives precise time information at high frequencies, precise frequency information at low frequencies and is thus found to be suitable for analyzing non-stationary signals. Mathematically, wavelets are functions that can be used to decompose an original signal into localized contributions characterized by scale parameters. The continuous wavelet transform (CWT) [70] of a signal $s(t)$, using a mother wavelet $\psi(t)$ is defined as follows.

$$CWT_s(a,\tau) = \frac{1}{\sqrt{|a|}} \int_{-\infty}^{\infty} s(t)\psi\left(\frac{t-\tau}{a}\right) dt \tag{4.1}$$

The result of CWT operation is a set of wavelet coefficients, $CWT_s$, which are functions of the scale (reciprocal of frequency) parameter ($a$) and time localization (or shifting) parameter ($\tau$). From Eq. (4.1), it is noted that in wavelet transform, signal values are weighed by wavelet basis function $\psi(t)$. This is quite different from Fourier transform where signals are weighed by the exponential of imaginary and harmonic frequency dependent arguments. The function $\psi(t)$ must satisfy the following three conditions.

1. The function should integrate to zero

i.e. $$\int_{-\infty}^{\infty} \psi(t) = 0 \tag{4.2}$$

2. The function should be square integrable or, equivalently, should have finite energy

i.e. $$\int_{-\infty}^{\infty} |\psi(t)|^2 \, dt < \infty \tag{4.3}$$

3. To ensure the existence of an inverse CWT corresponding to a forward CWT, mother wavelet must satisfy the sufficient and necessary condition, known as the admissibility condition on $\psi(t)$. It is given by following relations. If

$$C = \int_{-\infty}^{\infty} \frac{|\psi(\omega)|^2}{|\omega|} d\omega \tag{4.4}$$

and is such that $0 < C < \infty$. Then, it is possible to recover the signal $s(t)$ from its $CWT_s(a, \tau)$. In Eq. (4.4), $\psi(\omega)$ is the Fourier transform of $\psi(t)$.

It is computationally expensive to calculate the wavelet coefficients at every possible scale. Alternatively, if scale ($a$) and shift ($\tau$) are selected based on powers of two then the wavelet analysis will be much more efficient. Such scales and positions are known as dyadic scales

and positions. This type of analysis is carried out using DWT [26, 27] and is defined as:

$$DWT_s(j,k) = \frac{1}{\sqrt{|2^j|}} \int_{-\infty}^{\infty} s(t)\psi\left(\frac{t-2^j k}{2^j}\right) dt \tag{4.5}$$

where, $a$ and $\tau$ are replaced by $2^j$ and $2^j k$ respectively. More details on wavelet transform are available in Appendix B.

### 4.4 Multiresolution analysis

Mallat [26, 70] investigated wavelet decomposition of a signal from the point of view of filter design [71, 72] using multiresolution analysis (MRA). In MRA, signal components are partitioned into a number of frequency bands. MRA analysis is obtained by passing the discrete signal $s(k)$ through a series of low-pass ($G_s$) and high-pass ($H_s$) filters. Filter pairs $G_s$ and $H_s$, so called quadrature mirror filters are arranged repeatedly in a pyramidal structure with sub-sampling. The pyramidal algorithm for MRA to obtain decomposition up to the second level is illustrated in Fig. 4.1 [72].

MRA yields the so-called approximations ($cA_j$) and details ($cD_j$) which correspond to low frequency and high frequency components of the signal respectively. The next levels of decomposition of signal are obtained in an analogous way, when in place of original signal, approximation coefficients obtained from previous decomposition level are analysed. At

each step of this decomposition process, the frequency resolution gets halved. In Fig. 4.1, the frequency bands [0 to ($f_s/4$)], [($f_s/4$) to ($f_s/2$)], [0 to ($f_s/8$)] and [($f_s/8$) to ($f_s/4$)] of the original signal are represented by the coefficients *cA1*, *cD1*, *cA2* and *cD2* respectively where $f_s$ is the sampling frequency [27]. Signal reconstruction may be achieved using an inverse pyramidal algorithm involving up sampling of corresponding components [72].

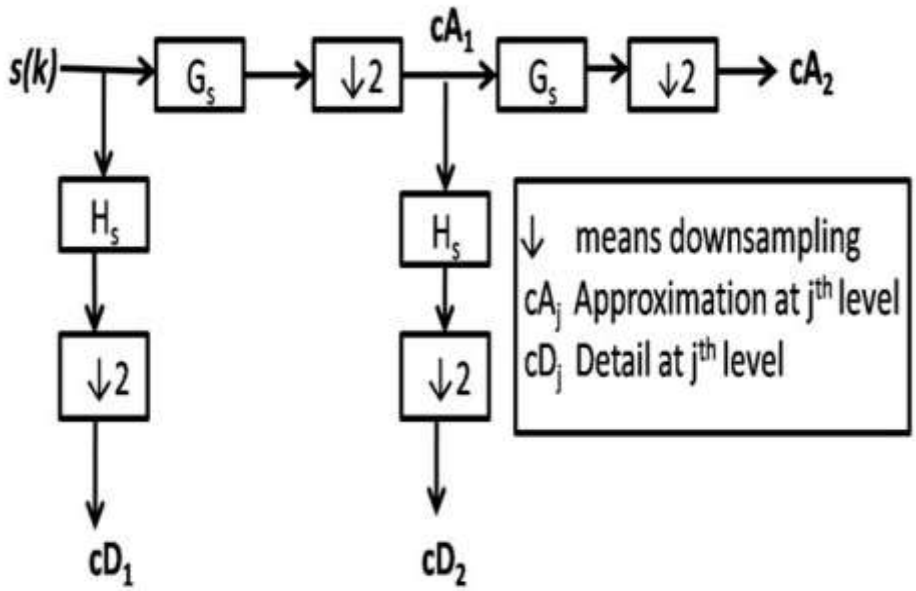


*Fig. 4.1. Pyramidal algorithm for multiresolution analysis (MRA) based decomposition of a signal up to second level [72].*

### 4.5 Finding trend of a signal using DWT

MRA of a signal decomposes the signal into various frequency bands. In present experiment, high frequency components of the signal represent noise and lower frequency components represent the slow varying parts (like background) of the signal. In a DWT based

decomposition of a signal, the lowest frequency component is termed as ‘trend’ of the signal. Thus, trend represents the slowest part of the signal and corresponds to the largest scale value. In wavelet analysis, as the scale increases, the resolution decreases which produces a better estimate of the signal trend. Another method to find trend also exists which is known as ‘manual polynomial fitting’ but its effectiveness and accuracy depends on the user’s experience [73]. On the other hand, DWT based technique is superior to ‘manual polynomial fitting’ because it does not require user’s intervention and is thus automatic.

In an OFDTS, Raman AS signal is composed of three parts: first the background signal due to optical fiber attenuation, second the main signal consisting of peak due to hot zone and third, the high frequency noise caused by stray light and various parts like laser power supply, Q-switch power supply, detection electronics etc. used in the system. Out of three parts, the second is the most useful one. As a typical case, for 204.8 m long silica fiber having a hot zone of 1 m width, located at 190 m distance, AS signal will be of 2.048 μs duration. It will have a decaying background due to fiber attenuation. Within this duration, there will be a peak of 10 ns width (corresponding to 1 m width of hot zone) located at 1.9 μs position. The above parameters (i.e. width and location) can be calculated from an OTDR relation for optical fiber and is governed by Eq. (3.1). The third parameter for peak i.e. amplitude is characterized by the temperature of the hot zone. St signal is very similar to AS but has a different background slope. The difference in the nature of the background for AS and St signals depends upon their wavelengths and fiber characteristics.

The first part of AS (or St) signal i.e. background signal is of low frequency compared to the second part (i.e. main signal) and both are well separated in the frequency domain. Therefore, DWT based trend (or background) can effectively represent the signal which is due to fiber

attenuation only. If the trend is subtracted from the original AS (or St) signal, the resulting corresponding signals will be free from fiber attenuation part. In other words, both AS and St signals will then have the same slope.

'Automatic polynomial fitting' can also be used for above purpose but, unfortunately it has poor performance especially in environments having low SNR [74]. On the other hand, wavelet based approach of finding trend outperforms in such situations. Moreover, DWT based approach requires no prior knowledge about the signal, no prior mathematical assumption of the background distribution, no selection of suitable background correction points and can handle all kinds of backgrounds [75]. This justifies the choice of wavelet based technique in the present application.

### 4.6 Denoising using DWT

In the present experiment, the mid frequency range will represent the analyte signal which is the most useful part of AS and St signals. The high-frequency components above a certain frequency level represent noise. In other words, the noise components will be represented by small wavelet coefficients at short scales in wavelet domain of the signal. Therefore, by modifying the corresponding wavelet coefficients, denoising of signal is possible. DWT based denoising is a preferred choice over Fourier transform based denoising because of its inherent better performance. This is because the former allows different parts to be filtered individually while the latter affects all data points in the same manner. A general three step procedure for wavelet denoising is [75]:

Step 1: Apply forward DWT to a noisy signal and obtain the vector ($w$) of wavelet coefficients.

Step 2: Reduce or remove those elements in *w* that are thought to be attributed to noise.

Step 3: Apply inverse WT on *w* to obtain a denoised signal.

Wavelet denoising methods, in general, use two different approaches for performing second step. These approaches are called hard thresholding and soft thresholding. The hard thresholding philosophy is to set all the wavelet coefficients below a certain threshold to zero. The soft thresholding [76], on the other hand, reduces the value (referred to as 'shrinking') of wavelet coefficients towards zero if they are below a certain threshold value. In soft-thresholding approach, for a certain wavelet coefficient $w_k$, we have:

$$w_k = sign\left|(w_k - \lambda)\right| \tag{4.6}$$

where, *sign* returns the sign of the wavelet coefficient $w_k$ and $\lambda$ is the threshold. Threshold level can be decided using the principle of Stein's unbiased risk estimate (SURE) [77].

## 4.7 Block diagram of prototype OFDTS

Using the above concepts of DWT, a prototype Raman OFDTS has been developed with better specifications and features compared to one based on STFT. Several issues as described in Section 1.1 are addressed using wavelet transform and an LM35A temperature sensor and microcontroller based DSCU, developed in-house. Fig. 4.2 shows schematic diagram of prototype Raman OFDTS using DWT. The details of the hardware components of the prototype system are as described in Section 3.5.2. However, the pre-processing of Raman AS and St signals has been carried out by DWT. This is indicated by a different block below ‘PC for signal processing’ in Fig. 4.2.

### 4.8 Determination of distributed temperature over the complete fiber length

As described in Section 3.6, Eq. (3.10) will yield temperature profile ($T$) for complete fiber length provided profiles of $R_T$ and value of $R_\theta$ are available. $R_\theta$ is determined by taking the ratio of AS to St signal (AS/St) for the calibration zone. However, AS and St signals need to be pre-processed while determining profile of $R_T$. First, the AS and St signals need to be

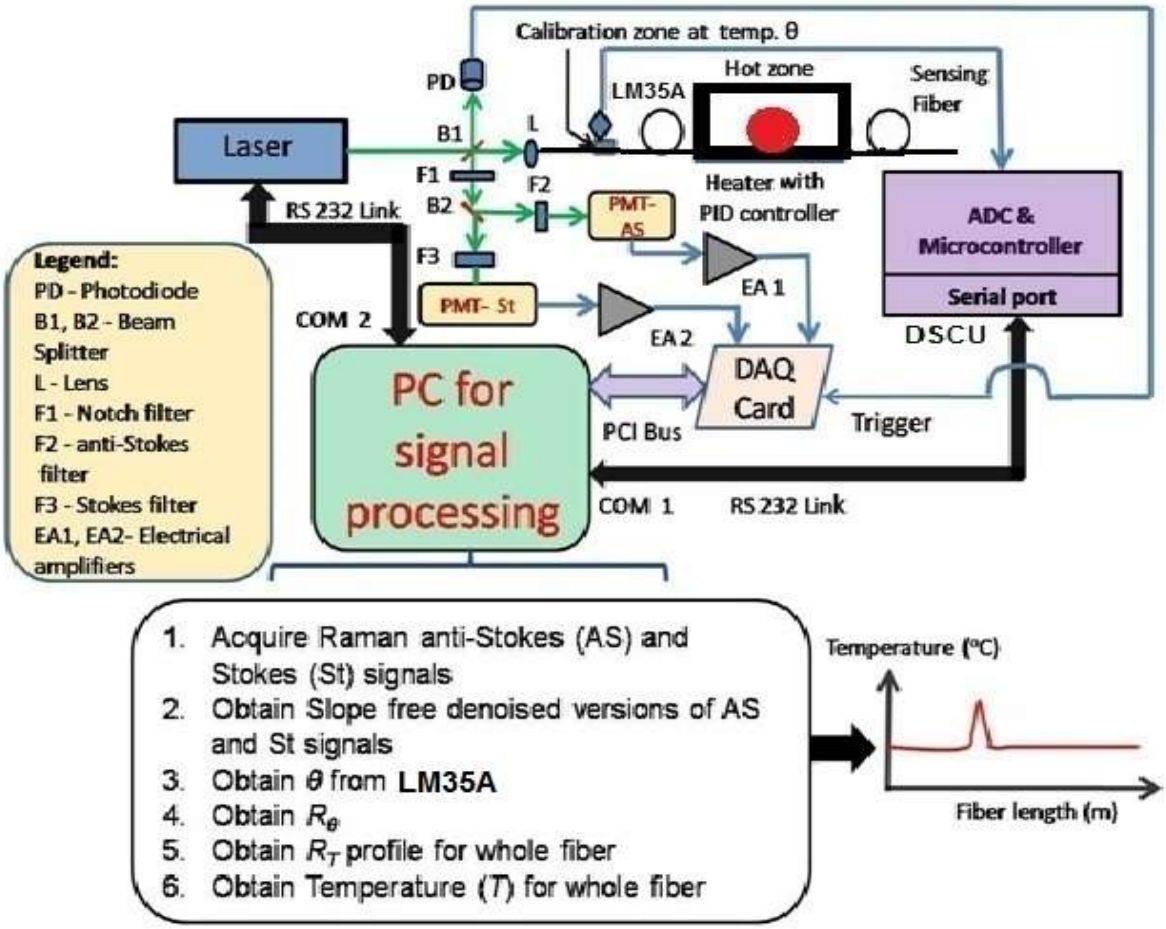


*Fig. 4.2. Block diagram of prototype Raman OFDTS using DWT based pre-processing of Raman AS and St signals.*

denoised for better SNR (issue No. 4). The denoised versions of original AS and St signals are obtained by DWT based denoising process (to be explained in Section 4.9) and are represented by symbols *DenAS* and *DenSt* respectively. Second, wavelength dependent

attenuation difference between AS and St signals should be corrected (issue No. 2). In other words, AS and St signals must have either same slope or should be 'slope free' before they are used in Eq. (3.10). The best condition is when both AS and St signals are free from any slope. Once, AS and St signals are available in sample form, their slopes can be minimized by first calculating their trend from original signals with the help of DWT based pre-processing and then subtracting it from denoised version of signals. In DWT based processing, trend is represented by the last approximation component for AS and St signals. Next, an offset given by AS (or St, as the case may be) signal value at the start of sensing fiber is added to recover a slope free denoised AS (or St) signal. Both the signals obtained in such a way will have minimum attenuation difference. This is how slope free denoised AS (represented by *SFDenAS*) and slope free denoised St (represented by *SFDenSt*) signals are obtained.

In the present system, AS and St signals are represented by 2048 samples which corresponding to 204.8 m long fiber. The DWT based trend of AS and St signals is given by the reconstruction of 11$^{th}$ approximation component in their DWT based decomposition tree. They are represented by *A11AS* and *A11St* for AS and St signals respectively (to be explained in section 4.9).

Thus, parameter $R_T$ can be expressed by Eq. (4.7).

$$R_T = \frac{SFDenAS}{SFDenSt} \tag{4.7}$$

Use of Eq. (4.7) in Eq. (3.10) will yield an unknown temperature profile (*T*) that is free from error caused by its unwanted downward slope with respect to fiber length. This is how issue No. 2 is addressed using DWT.

Issue No. 1 and 3 are taken care by dynamic self calibration method using DSCU described in Section 3.6. The dynamic self calibration is performed each time a new measurement of distributed temperature (*T*) for whole fiber length is made and thus it is able to care of variation in laser power and laser-fiber coupling.

### 4.9 Wavelet based pre-processing of experimental Raman AS and St signals

Experimentally obtained unprocessed Raman AS and St signals corresponding to the experimental setup of Fig. 4.2 are depicted in Fig. 4.3 (a) and 4.4(a) respectively. These signals are same as shown in Fig. 3.8. These signals were obtained after averaging for 5,000 times which requires approximately 100 s on an Intel Pentium-4 (1.9 GHz) processor based PC having 1 GB RAM and Windows 2000 operating system support. In order to obtain a correct distributed temperature profile using Eq. (3.10), calculation of *SFDenAS*, *SFDenSt* alongwith $R_\theta$ is necessary and is performed as described below.

In Fig. 4.3, experimentally obtained unprocessed Raman AS signal [Fig. 4.3(a)] and its DWT based decomposition (details and approximation components) are presented [Fig. 4.3 (b-m)]. DWT based decomposition was performed using 'db20' (Daubechies family) [78] orthogonal mother wavelet basis. Details components of AS signal at first, second, third level etc. are correspondingly represented by D1AS, D2AS, D3AS etc. In Fig. 4.3(m), the 11$^{th}$ approximation component is the trend of AS signal and is represented by *A11AS*.

Another point to be noted in Fig. 4.3 is that D1AS and D2AS contain high frequency noise components and therefore can be soft thresholded to obtain *DenAS*. Denoising of AS signal is performed at level 2 using the soft thresholding based procedure described in Section 4.6. An

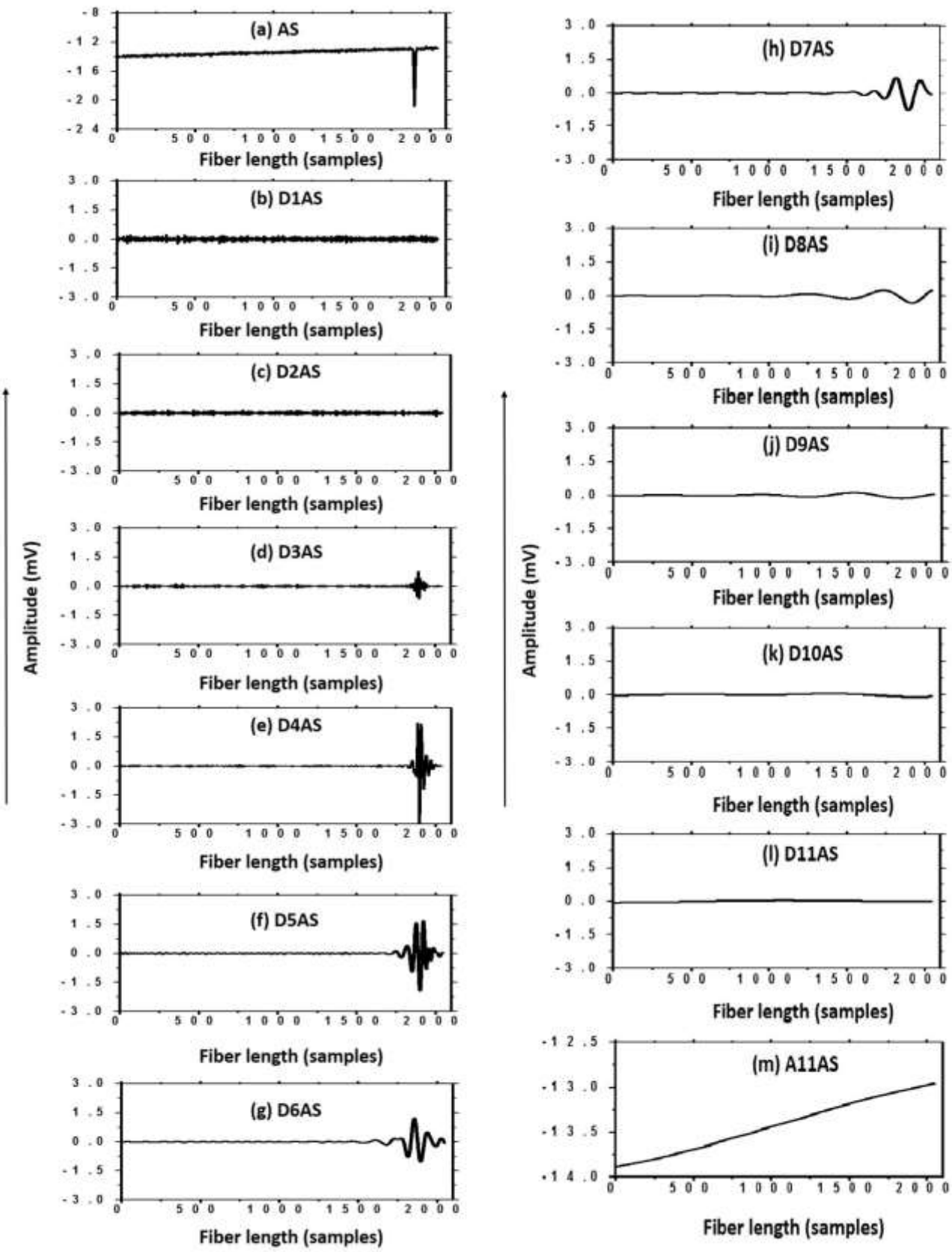


*Fig. 4.3. 'db20' wavelet based signal decomposition tree for AS signal. (a) unprocessed AS signal, (b - l) Detail components (D1AS to D11AS), and (m) 11$^{th}$ Approximation component (A11AS)* (*On horizontal-axis, 10 samples ≡ 10 ns ≡ 1 m*).

offset (*OffsetAS*) calculated from the mean of first 10 samples of *DenAS* is also obtained. In the present case, *OffsetAS* is found to be -14.022 mV. Finally, *SFDenAS* is obtained as below.

$$SFDenAS = DenAS - A11AS + OffsetAS \tag{4.8}$$

The *SFDenAS* and unprocessed AS signal are shown in Fig. 4.5 which clearly shows the desired effect of DWT based pre-processing. To appreciate the improvement in AS signal after processing, the horizontal axis has been divided into three parts. This allows a zoomed viewing of AS signal at different zones of fiber length. Clearly, *SFDenAS* is a representation of AS signal which has reduced attenuation effect caused by the fiber. It is worth emphasizing here that DWT based pre-processing of AS signal has enabled calculation of trend from noisy AS signal without any prior knowledge of its baseline function and finally yielded *SFDenAS.* Another point to be noted in Fig. 4.5 is that DWT based denoising process provides smoothening of AS signal and introduces only a negligibly small undesired shift in the location of hot zone peaks. This effect is quite different from conventional IIR/FIR based filtering which causes a significant shift in location of peaks [30]. In other words, wavelet denoising has not introduced any noticeable spatial inaccuracy in locating the hot zones. Therefore, it is better than the conventional FIR/IIR based technique.

The St signal was also pre-processed in the same manner as described for AS signal. The unprocessed St signal and its DWT based decomposition using 'db20' wavelet are presented in Fig. 4.4. The 11$^{th}$ approximation component of St signal (*A11St*) yields its trend [(Fig. 4.4(m)] and represents the background contribution to St signal caused by the fiber attenuation. The St signal was also denoised to obtain *DenSt*, with *OffsetSt* value of -24.011 mV. Finally, *SFDenSt* is obtained using Eq. (4.9).

$$SFDenSt = DenSt - A11St + OffsetSt \tag{4.9}$$

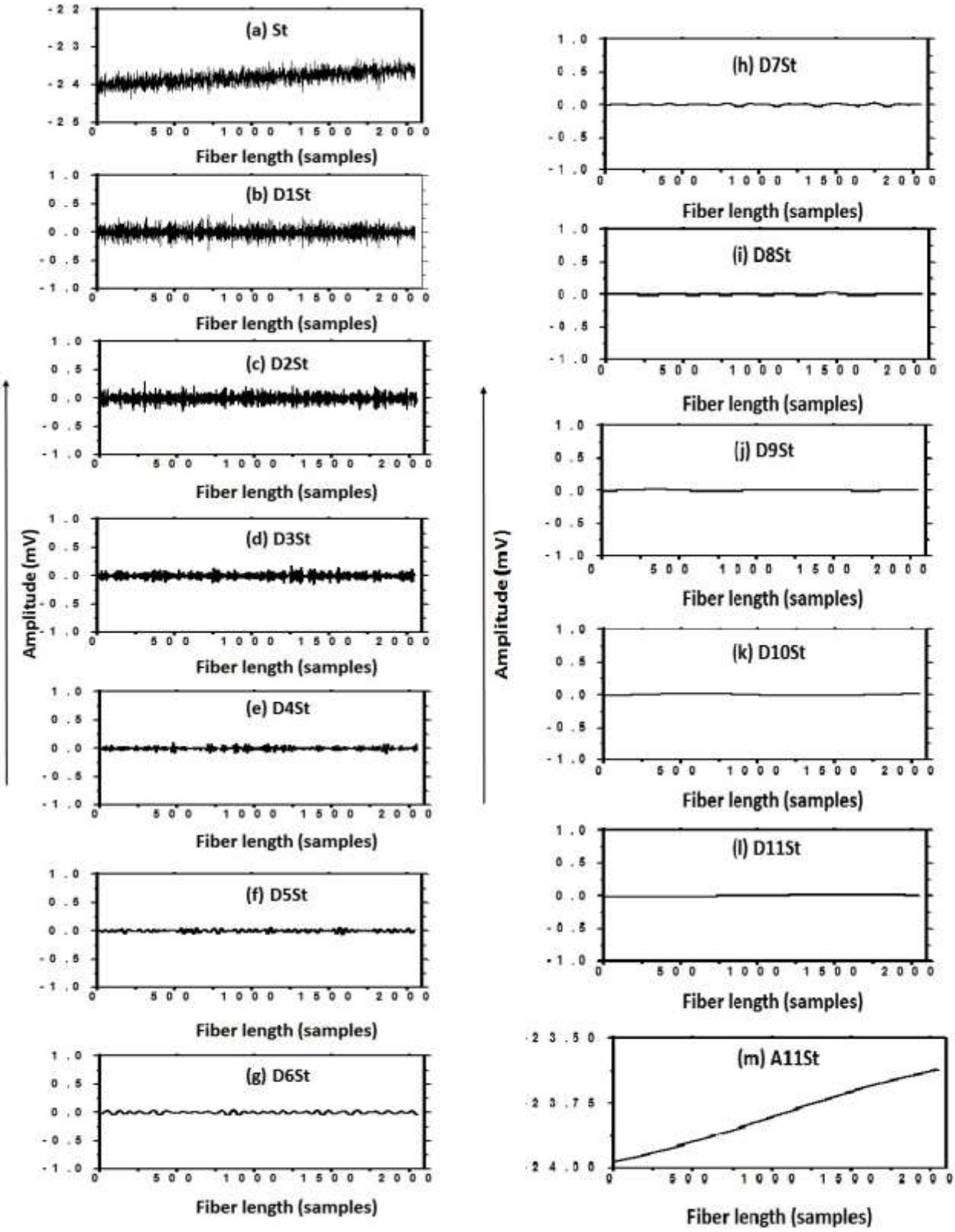


*Fig. 4.4. 'db20' wavelet based signal decomposition tree for St signal. (a) unprocessed St signal, (b - l) Detail components (D1St to D11St), and (m) 11$^{th}$ Approximation component (A11St)* (*On horizontal-axis, 10 samples ≡ 10 ns ≡ 1 m*).

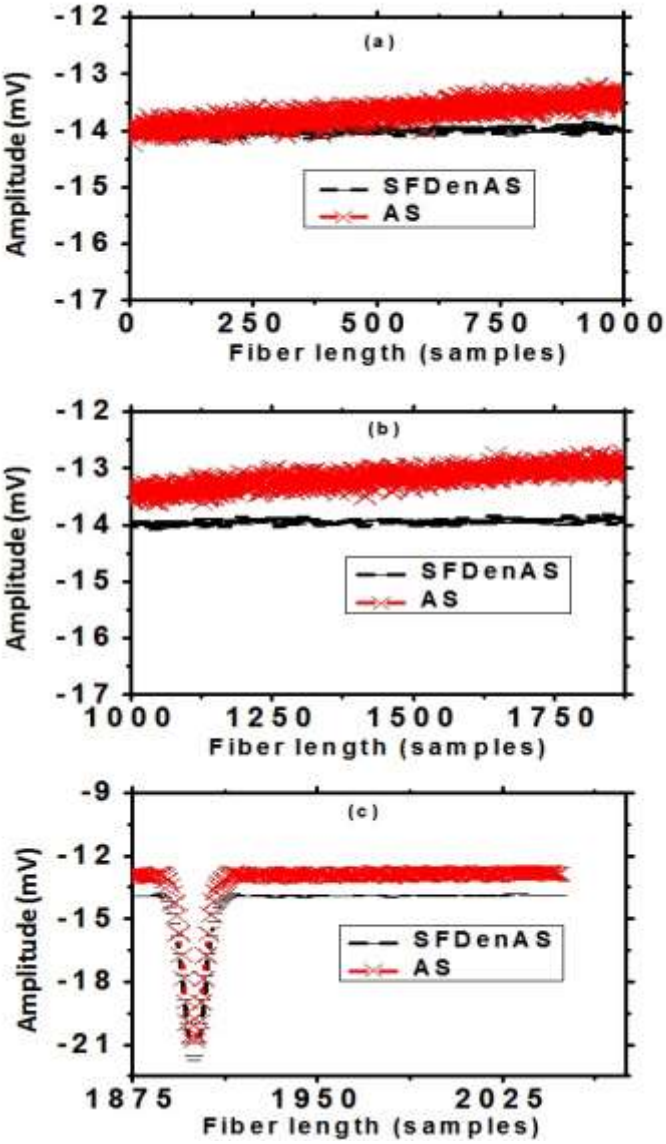


*Fig. 4.5. Unprocessed AS signal and Slope free denoised AS signal (SFDenAS) for sample No. (a) 1 to 1000 (b) 1001 to 1875 and (c) 1876 to 2048* (*On horizontal-axis, 10 samples ≡ 10 ns ≡ 1 m*).

Fig. 4.6 shows a zoomed view of different parts of the unprocessed St and *SFDenSt* signal. Using DWT based pre-processing of St signal, it has become possible to recover slope free version of St signal because of the capability of DWT of recovering trend from a noisy signal without having its prior knowledge. The parameter $R_\theta$ is calculated as the ratio of *OffsetAS* to *OffsetSt* and is found to be 0.584. The value of $\theta$ (24.5 °C) is read by LM35A based DSCU and is fed to PC through COM1. It is noted that all the parameters in Eqs. (4.7) and (3.10) are

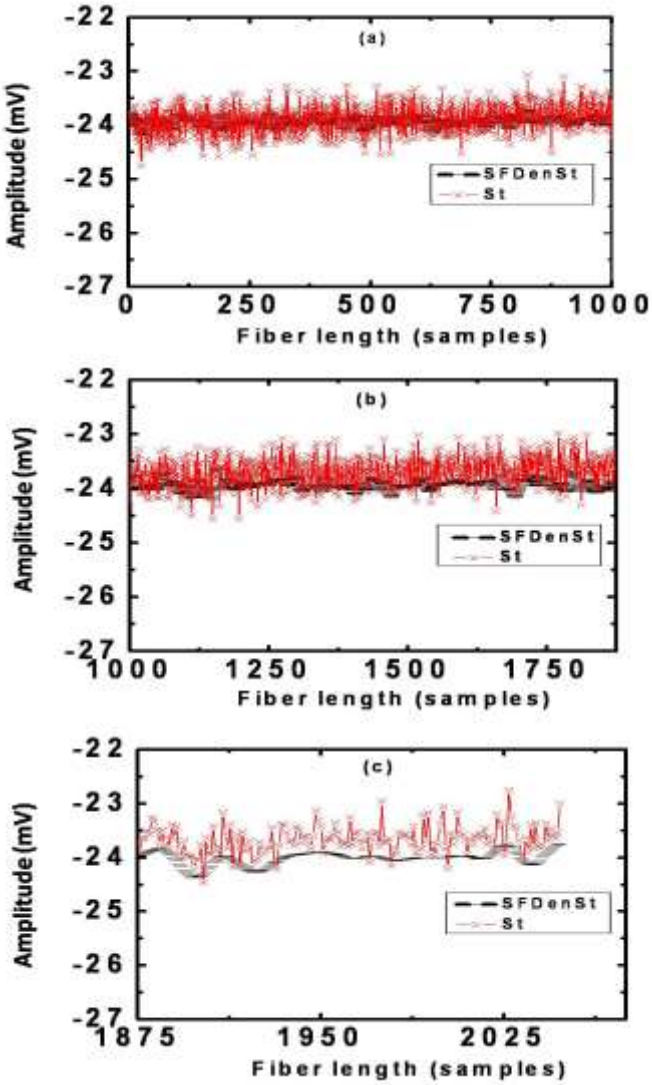


*Fig. 4.6. Unprocessed St signal and Slope free denoised St signal (SFDenSt) for sample No. (a)1 to 1000 (b)1001 to 1875 and (c)1876 to 2048 (On horizontal-axis, 10 samples ≡ 10 ns ≡ 1 m).*

now available and can, therefore, be used to yield distributed temperature profile. Next, fiber length is converted from 'number of samples' to 'm' unit using the relation, 10 samples = 1 m. Finally, distributed temperature profile *[T(°C) vs. fiber length (m)]* is obtained for the whole fiber length and is shown in Fig. 4.7

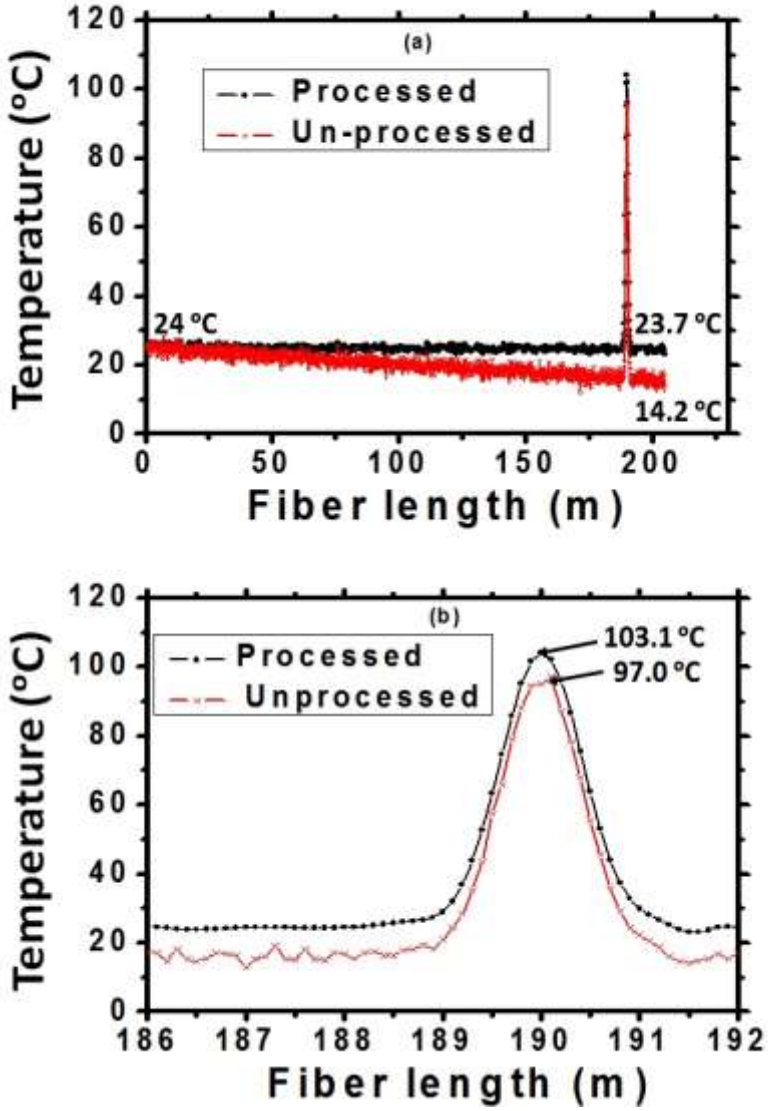


*Fig. 4.7. Distributed temperature profile with processed (black colour) and unprocessed (red colour) Raman signals (a) view for complete fiber length (b) zoomed view for hot zone.*

The time required in above described DWT based pre-processing of AS and St signals is ~5 s. The total time required in obtaining the final distributed temperature profile is the sum of averaging time (100 s), DWT based pre-processing time (5 s) and additional time (5 s) taken in computing and printing the final distributed temperature profile on PC screen. Thus, the total time required in updating the distributed temperature profile is ~110 s.

### 4.10 Results of distributed temperature measurement with DWT based pre-processed Raman signals

Distributed temperature profile for fiber length of ~205 m, obtained by Eq. (3.10) using unprocessed Raman signals of Figs. 4.3(a) and 4.4(a) is presented in Fig. 4.7 (red colour). The temperature measured at the start of the fiber, where fiber temperature is 24.5 °C, is found to be 24 °C. However, at the end of fiber (at ~205 m location), where fiber is at a temperature of 25 °C, measured temperature is 14.2 °C, showing an error of - 10.8 °C (- 43.2%). The temperature (105 °C) of hot zone is incorrectly measured as 97.0 °C (- 7.6% error) with unprocessed signals. Thus, distributed temperature obtained using unprocessed Raman signals is erroneous. It may be noted that for a longer length of fiber, say few km, the temperature errors will be even higher. For improvement in temperature measurement, experimentally obtained Raman AS and St signals are first pre-processed using proposed DWT based technique described in Section 4.9 and then they are used in Eqs. (4.7) and (3.10). Finally, the most corrected distributed temperature profile obtained using pre-processed Raman AS and St signals is shown in Fig. 4.7 (black colour). This shows a further reduction in temperature measurement errors in comparison to the errors obtained using unprocessed Raman signals (red colour). The temperature of hot zone is measured as 103.1 °C (1.8% error) whereas temperature at 205 m location is measured as 23.7 °C (5.2% error). Table 4.1 presents the comparison of error in temperature measurement at various zones using Eq. (3.10) with unprocessed and DWT pre-processed Raman signals to appreciate the improvement achieved after DWT based pre-processing. The reference temperatures of various zones were measured by thermocouple based thermometers (model: Digirad71, make: Radix, India) which were placed close to sensing fiber. If the error in temperature measurement of Table 4.1 is compared with the error in measurement using STFT (shown in

Table 3.1 ), it is found that DWT based technique allows reduced error. Also, improved peak-to-peak variation in measurement of room temperature along fiber length is measured to be 3.6 °C against 10.8 °C achieved with STFT technique.

A direct comparison of SNR values observed in the unprocessed (red) and processed (black) signals can be made by considering a fiber zone (0-188 m) which is kept at a reference temperature of 24.5 °C. SNR in unprocessed and processed signals is found to be 14.22 dB and 31 dB respectively. It is clear that SNR is improved by a factor of 2.18 after processing. If the same level of improvement in SNR, which in turn results in better temperature accuracy, is desired without DWT based pre-processing additional averaging of AS and St signals would be required. It has been observed that number of averages required is 24,000 which would require an averaging time of 480 s as opposed to 105 s with DWT based pre-processing. Thus, DWT based pre-processing allows lower processing time and yields better accuracy in temperature measurement.

It is clear from Table 4.1 that the wavelet based pre-processing of Raman signals has significantly reduced the errors in distributed temperature measurement at various zones. Also, the location of hot zone is measured to be 190 m which is same as the original value set in the experiment. The measured width of hot zone in temperature profile of Fig. 4.7 (black colour), was found to be 1 m by obtaining FWHM of the hot zone. This value matches with the width of hot zone set while conducting the experiment. Also, rise time (10%-90% of peak value) is found to be 1 m. Therefore, spatial resolution of the developed OFDTS is claimed to be 1 m. The dynamic self calibration is provided by measuring the most recent AS and St signals, their ratio ($R_\theta$) and temperature of the calibration zone ($\theta$) using DSCU. It is observed that proposed DWT based pre-processing of Raman AS and St signals and dynamic

self calibration technique have very well addressed all the issues No. 1 - 4.

**Table 4.1**

Comparison of error in temperature measurement at various zones with unprocessed and DWT pre-processed Raman signals.

| Zone (Location) | Reference temperature | Measured temperature | |
|---|---|---|---|
| | | Unprocessed | Pre-processed |
| Start of fiber (Location: 0 m) | 24.5 °C | 24 °C | 24 °C |
| | Error | -0.5 °C (- 2.04%) | -0.5 °C (- 2.04%) |
| Hot zone (Location: 190 m) | 105 °C | 97.0 °C | 103.1 °C |
| | Error | -8.0 °C (- 7.6%) | -1.9 °C (- 1.8%) |
| End of fiber (Location: 205 m) | 25 °C | 14.2 °C | 23.7 °C |
| | Error | -10.8 °C (- 43.2%) | -1.3 °C (- 5.2%) |

The above experiment was repeated at several other temperature values in the range of 25-295 °C. Fig. 4.8 shows the zoomed view of different temperature profiles of hot zones. The maximum error in temperature measurement is found to be ±3.5 °C in the range of 25-295 °C. The spatial error in the measured location of hot zones was also recorded. The maximum spatial error of ±3 cm was found in locating the hot zone for the above temperature range. In order to have a close look at the noise level in temperature profiles, a second experiment was also carried out. In this experiment, the temperature of hot zone alone was changed while rest of the fiber was kept at room temperature. Temperature profiles for complete fiber length were recorded for temperature values of 25 °C and 35 °C. These profiles are presented in Fig. 4.9. A close view of noise levels at room temperature of 25 °C shows that noise level is

well within ± 3.5 °C limit [Fig. 4.9(a)]. A zoomed view of temperature profiles at hot zone is depicted in Fig. 4.9(b).

Based on the proposed DWT based signal pre-processing technique for AS and St signals, a

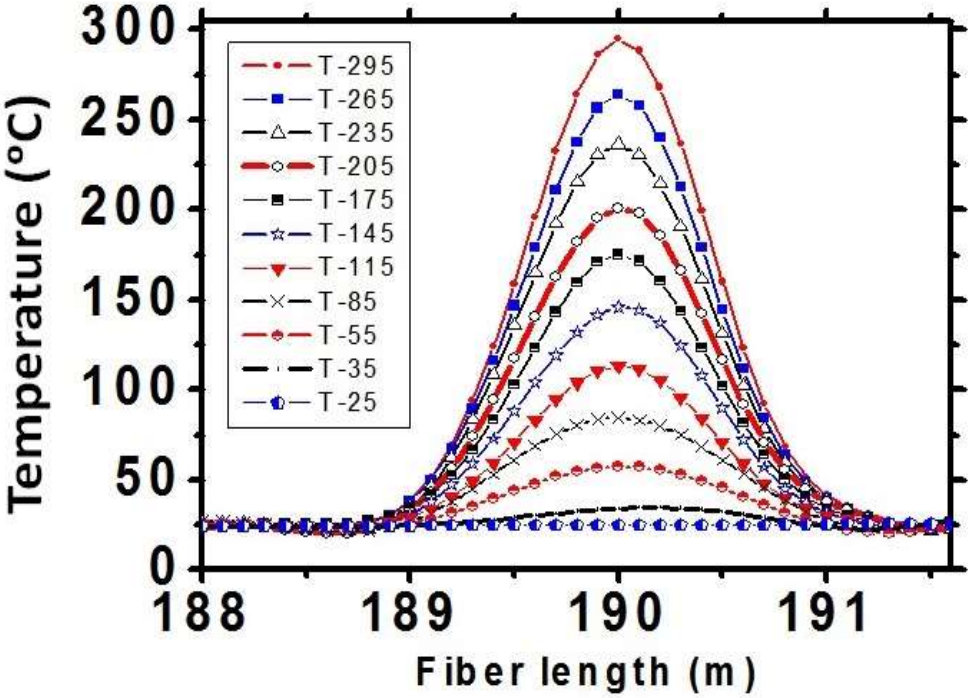


*Fig. 4.8. Zoomed view of distributed temperature (T) profile at hot zone for various temperatures in the range of 25-295 °C.*

prototype OFDTS system has been designed and developed. Fig. 4.10 depicts the photograph of the developed prototype OFDTS. It has three main parts. Part 1 is the upper portion of the system and contains laser head, optics, detectors and part of sensing fiber. Part 2 is the lower portion of the system that contains laser power supply, PMT power supplies, amplifier, laser control circuitry etc. Part 3 is known as 'Temperature profile display unit' which is basically the screen of main PC and is used for signal processing also. The distributed temperature is displayed on this screen. Fig. 4.11 shows photograph of the internal parts of the developed

OFDTS system.

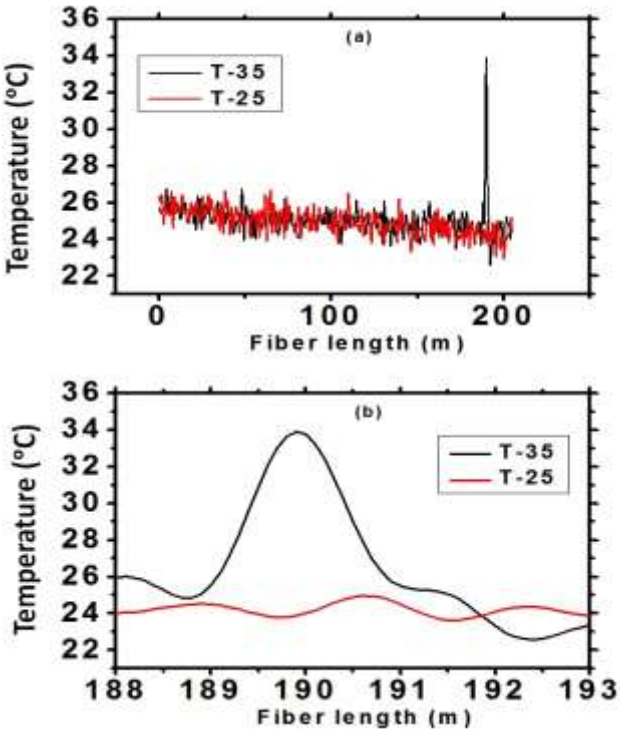


*Fig. 4.9. Distributed temperature (T) profile with hot zone kept at 25 °C and 35 °C and rest of the fiber at room temperature (a) view for complete fiber length (b) zoomed view for hot zone.*

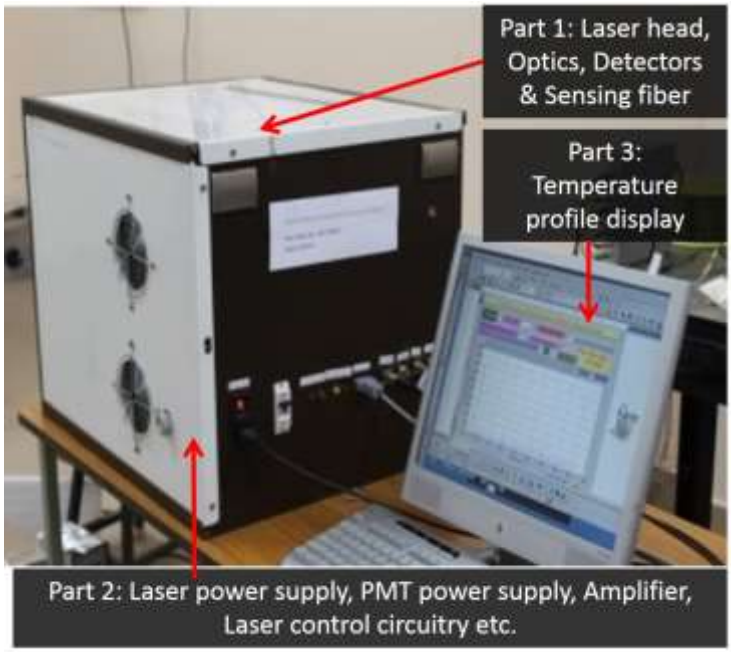


*Fig. 4.10. Photograph of the developed prototype OFDTS.*

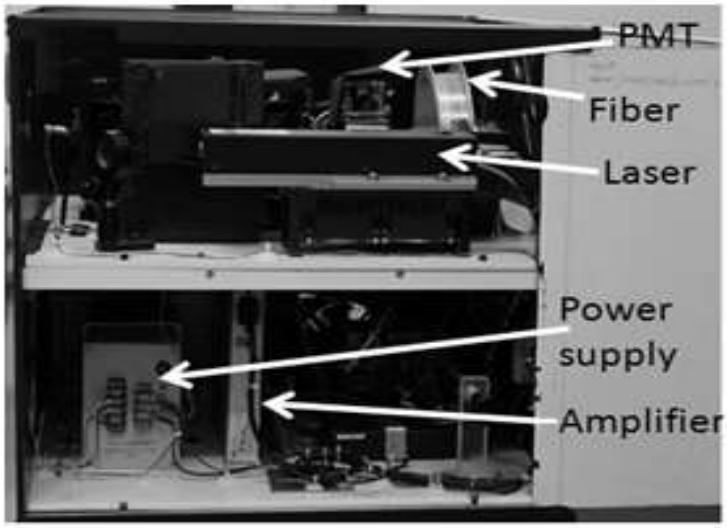


*Fig. 4.11. Photograph of the internal parts of the developed OFDTS system.*

A user friendly graphical user interface (GUI) [79], shown in Fig. 4.12, has also been developed in MATLAB for easy and automated operation of OFDTS. The GUI takes care of all the signal processing steps in the back end and displays temperature as a continuous function of fiber length at the front end. The 'Enable' button in GUI initializes the DAQ Card, checks the availability of laser trigger, and if found available, makes the system ready for measurement. After selecting the color of temperature plot and desired time of record etc., custom designed GUI displays distributed temperature with just a click of the OK button. The 'OK' button first calls the software subroutine to measure the present temperature ($\theta$) of the calibration zone of fiber using DSCU and then performs subsequent steps for distributed temperature calculation. 'Hold plots' button allows the user to keep previous temperature profiles while plotting the current one. The 'Refresh' button can clear the screen, if desired so by the user. Using the 'Save Data' button, temperature profile may be saved for future reference.

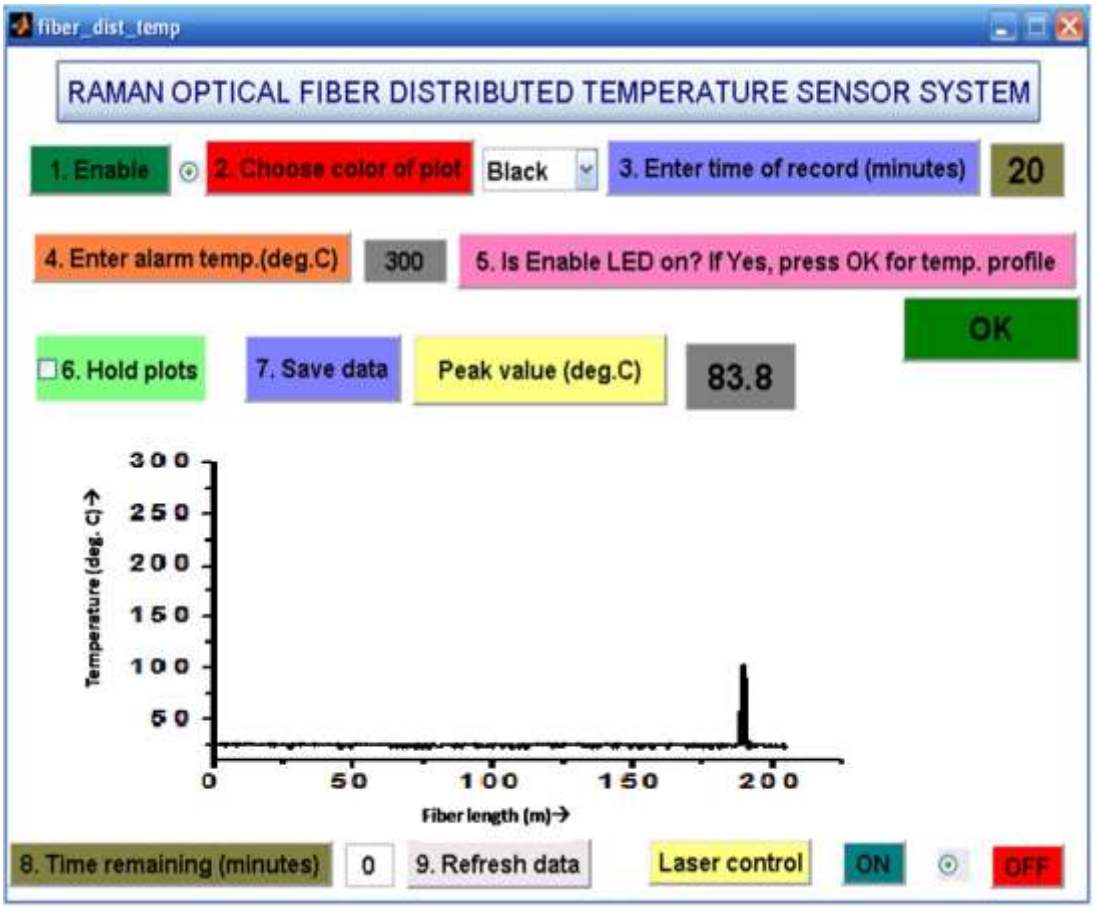


*Fig. 4.12. Graphical user interface (GUI) for the developed protype OFDTS.*

## 4.11 Summary

This Chapter has described the proposed DWT based pre-processing technique for Raman backscattered AS and St signals to reduce the errors in temperature measurement by OFDTS. The proposed technique takes care of the difference in optical attenuation caused by optical fiber for AS and St signals by using their trend and also denoises the AS and St signals while preserving spatial locations of peaks. The present technique is also better than STFT based technique in terms of automation. Unlike STFT based technique, present technique provides denoising of Raman AS and St signals without implementation of any additional algorithm. Temperature measurement over a wide range of 25-295 °C with the maximum error of

±3.5 °C has been demonstrated. Spatial resolution of 1 m was shown for a hot zone having width of 1 m, located at 190 m distance, chosen from a fiber sensing length of ~205 m. Maximum positional error of ±3 cm was observed in detecting the location of the hot zone in the above temperature range. Dynamic measurement of temperature of calibration zone and Raman AS and St signals ensures that distributed temperature is measured correctly even if AS and St signals and also the temperature of the calibration zone change.

# Chapter 5

# Empirical mode decomposition based pre-processing of Raman signals for an OFDTS

## 5.1 Introduction

This Chapter describes the application of empirical mode decomposition (EMD) based signal pre-processing method for Raman AS and St signals for addressing the issues No. 1-4 related to the development of Raman OFDTS. This Chapter also presents the development of an OFDTS using a rugged, low core, standard 62.5/125 µm sized SS covered Mutimode fiber. SS covering on the fiber makes it easier and safer to install the sensing fiber in critical field locations where normal sensing fiber cannot be used. In addition to above, the design of a microcontroller and Raman OFDTS based zone wise temperature alarm system has also been described in this Chapter. The alarm system has been successfully tested for 10 zones in a 100 m long sensing fiber at various temperatures. The above design opens the possibilities for design of an optical fiber based distributed PID temperature controller. In the following section an introduction to EMD is presented first.

EMD, pioneered by N. E. Huang in 1988, is a relatively new technique for analyzing non-stationary signals [28, 80]. Any non-stationary signal can be decomposed by this technique into a finite and often small number of IMFs. This decomposition method is adaptive, and therefore, highly efficient. Since the decomposition is based on the local characteristic time scale of the data, it is applicable to nonlinear and non-stationary processes. The need and suitability of EMD for the present work is also discussed here along with a brief comparison

of earlier transforms used for nonlinear and non-stationary data.

Fourier spectral analysis provides a general method for examining the gross energy-frequency distribution in a signal. Although, the Fourier transform is valid under extremely general conditions there are some crucial restrictions of the Fourier spectral analysis: the system must be linear, and the data must be strictly stationary.

STFT is a technique which is better than Fourier transform. It is essentially a limited time window-width Fourier spectral analysis. By successively sliding the window along the time axis, one can get a time-frequency distribution. Since it relies on the traditional Fourier spectral analysis, one has to assume the data to be piecewise stationary. This assumption is not always justified in non-stationary data. Even if the data are piecewise stationary it cannot be guaranteed that the window size adopted always matches with the stationary time frame. These conflicting requirements make STFT of limited use. When used in OFDTS, above limitation of STFT requires that Raman AS and St signals be inspected manually for selection of the widow size and location. This requirement makes STFT less attractive for development of a fully automated version of an OFDTS.

The wavelet approach is essentially an adjustable window Fourier spectral analysis with the following general definition [28]:

$$W(\tau, a, x) = \frac{1}{\sqrt{a}} \int x(t).\psi\left(\frac{t-\tau}{a}\right) dt \tag{5.1}$$

The physical explanation of Eq. (5.1) is that the parameter $W(\tau,a,x)$ is the energy of scale $a$ at time $t = \tau$. For specific applications, the basic wavelet function, $\psi(.)$, can be modified according to special needs, but the form has to be given well before the analysis. In other words, the wavelet basic function (also called basis function) has to be defined beforehand.

Once the basic wavelet is selected, one will have to use it to analyse all the data. In spite of these limitations, wavelet analysis is still one of the best available non-stationary signal models.

In non-stationary signals, amplitude and frequency both are functions of time. That is why adaptivility of decomposition method is also important for non-stationary data. Adaptibility of a decomposition method takes care of local variations of the data arising due to the underlying physics of the processes. An appropriate way to generate the necessary adaptive basis is to derive the basis from the data itself, which is the main feature of EMD. More information on EMD is appended in Appendix C.

## 5.2 Application of EMD in OFDTS

There are several issues in connection with OFDTS, as described in Section 1.1 which need to be addressed with the help of a digital signal processing technique. Chapter 3 has described the use of STFT for issue No. 1-3 whereas Chapter 4 descibes the application of DWT to address the issue No. 1-4. DWT based technique requires the selection of a basis function in advance which is not mandatory in case of EMD. This is because EMD is a data driven technique. This Chapter attempts to use EMD based signal processing technique for AS and St signals [34]. It describes how various features of EMD technique can be applied to addresse issue No. 1-4 related to OFDTS.

## 5.3 EMD based signal pre-processor for Raman OFDTS

In the present work, a pre-processor based on EMD is proposed for processing of raw AS and

St signals for implementation of OFDTS. The pre-processor processes experimentally obtained AS and St signals before they are used in Eqs. (3.10) and (4.7) to obtain corrected distributed temperature profile. The two parameters *SFDenAS* and *SFDenSt* which have been used in Eq. (4.7) are obtained by EMD based pre-processor. Pre-processor receives unprocessed experimental AS and St signals having different attenuation, removes the attenuation and noise part from both the signals and delivers *SFDenAS* and *SFDenSt* signals. These signals have nearly equalized attenuation and reduced noise. This is achieved with the help of EMD technique by extracting the trends [81, 82] of Raman signals. EMD has been selected to extract the trend because it does not need prior assumption of basis function, knowledge about the signal, prior mathematical assumption of background distribution, selection of suitable background correction points etc.

The technique proposed in this work is better than previously reported techniques [32] in terms of complexity and automation. Also, the present technique does not require any additional filtering or denoising algorithm [30] as this is a built-in feature of EMD technique. This results in reduced complexity of signal processing algorithm. DWT based technique [33] has been described for OFDTS to address the above issues but it requires a prior selection of suitable basis functions for optimum performance [28]. Although, wavelet analysis is essentially an adjustable windowed Fourier spectral analysis [83] with limited length of its basis functions, it has a competitive performance to quantitatively define the time-frequency-energy distribution. Wavelet analysis is able to describe local frequency properties based on predetermined stepping process only. On the other hand, EMD is intuitive, direct, a postriori and adaptive because here the basis functions used for decomposition are based on and derived from data itself [28].

Raman AS and St signals are very weak owing to their low scattering cross sections and two way attenuation in fiber. As mentioned earlier, it is likely that these two important signals are easily affected by noise. Therefore, these signals need to be denoised before they are used in Eqs. (3.10) and (4.7). Conventional Fourier denoising techniques generate spatial inaccuracy in the location of peaks and hence are not suitable for denoising of AS and St signals [30, 83]. The proposed EMD based pre-processor denoises both the AS and St signals and thus allows reduced error in temperature measurement. The above discussion justifies the choice of EMD in the present application.

Dynamic self calibration is also supported by EMD pre-processor and helps compensate the error in temperature measurement caused by the variation in laser power and coupled power. Issue No. 1-4 are well addressed using proposed EMD technique.

### 5.4 Brief overview of empirical mode decomposition

Empirical mode decomposition (EMD) [28] decomposes any non-stationary time domain signal into a finite number of amplitude and frequency modulated (AM-FM) oscillating components. These AM-FM components are also called IMFs and depend on the interpolation of extrema (maxima and minima) of the signal. Each IMF satisfies two basic conditions: (i) the number of extrema and the number of zero-crossings must either be same or differ at most by one in the complete data set, (ii) at any point, the mean value of the envelopes defined by the local maxima and the envelopes defined by the local minima should be zero. The IMFs are the band-limited functions. Thus elimination of selected IMFs allows denoising of the signal. EMD is an intuitive and adaptive signal-dependent decomposition technique. A systematic way to extract the IMFs from the signal is called the sifting process.

The algorithm of sifting process for any time domain signal $s(t)$ can be summarized by the following steps [37]:

(i) Assume $k_1(t) = s(t)$.

(ii) Determine the extrema (both maxima and minima) of $k_1(t)$.

(iii) Find the upper and lower envelopes $e_m(t)$ and $e_l(t)$ respectively, by interpolating the maxima and minima separately.

(iv) Compute the local mean as $n(t) = [e_m(t) + e_l(t)]/2$.

(v) IMF should have zero local mean; subtract $n(t)$ from the original signal as $k_1(t) = k_1(t) - n(t)$.

(vi) Test whether $k_1(t)$ is an IMF or not by checking the two basic conditions as mentioned above.

(vii) Repeat steps (ii) to (vi) described above and stop when an IMF $k_1(t)$ is obtained.

After the first IMF is obtained, put $IMF1(t) = k_1(t)$, which represents the smallest temporal scale in $s(t)$. In order to obtain the remaining IMF components, define the residue $r_1(t)$ of the data by subtracting $IMF1(t)$ from the signal as $r_1(t) = s(t) - IMF1(t)$. The sifting process will be continued until the final residue happens to be a constant, a monotonic function, or a function from which further derivation of the IMFs is not possible. The other basis functions and the residues are calculated as

$$r_1(t) - IMF2(t) = r_2(t), \ldots, r_{M-1}(t) - IMFM(t) = r_M(t) \tag{5.2}$$

where, $r_M(t)$ is the residue obtained at the end of the decomposition.

After the decomposition is over, the signal $s(t)$ can be represented as follows:

$$s(t) = \sum_{v=1}^{M} IMFv(t) + r_M(t) \tag{5.3}$$

where, $IMFv(t)$ represents the $v^{th}$ IMFand $r_M(t)$ represents the trend of the signal.

Due to the adaptive nature of the decomposition and suitability for analysis of non-linear and non-stationary signals without designing sets of basis functions, EMD has been studied for fault diagnosis [84], speech processing [85], human posture control [86] and biomedical applications [87].

### 5.5 Experimental set up

The schematic of the experimental setup implemented for acquiring backscattered Raman AS and St signals is very similar to the setups described in Fig. 4.2. However, the present set up has major changes in signal processing scheme. The DWT based signal processing scheme is replaced by EMD based pre-processor. The experimentally obtained Raman AS and St signals after an averaging of 5000 waveforms are presented in Figs. 5.1(a) and 5.3(a) respectively. The signals are same as depicted in Fig. 3.8. These signals are input for the proposed EMD pre-processor and ouput of the pre-processor is *SFDenAS* and *SFDenSt* respectively. These two parameters are used in Eq. (4.7) and finally Eq. (3.10) is used for determination of distributed temperature profile for complete fiber length.

### 5.6 EMD pre-processor for Raman AS and St signals

Pre-processing of experimental AS and St signals has been carried out using EMD. Following section describes the method of obtaining *SFDenAS* and *SFDenSt* using EMD.

First, the pre-processing of AS signal is described. Various IMFs (*IMF1 to IMF8*) obtained from the application of EMD on AS signal are shown in Fig. 5.1 (b-i). *IMF1* to *IMF8*

represent signal contents from high to low frequency respectively. It can be observed from Fig. 5.1 that the high-frequency IMF (*IMF1*) contains only noise contribution to the original signal. The noise component is removed to obtain the denoised AS signal and is denoted as *dAS*. This step works as an EMD denoiser.

The final residue represents the trend of the AS signal and is shown in Fig. 5.1 (j). It is also removed from AS signal because it represents a contribution which is due to fiber attenuation only. An offset equal to the mean value of 10 samples of *dAS* signal is also obtained. This offset is represented as *OffsetAS*. For the present case, *OffsetAS* is found to be -14.5 mV. Finally, slope free and denoised version of AS profile (*SFDenAS)* is calculated using following expression which acts as an EMD pre-processor for AS signal.

$$SFDenAS(z) = \sum_{k=2}^{8} IMFk(z) + OffsetAS \tag{5.4}$$

where, *IMFk(z)* is the $k^{th}$ IMF of AS signal. Since AS signal is a function of fiber length (*z*), its IMFs are also function of *z*.

The pre-processed AS signal (black colour) is shown in Fig. 5.2 along with the unprocessed AS signal (red colour) for comparison and visualizing improvement. The pre-processed AS signal (*SFDenAS*) is not only denoised but also free from contribution due to optical fiber attenuation. The improvement in peak shape and amplitude after pre-processing can be observed from Fig. 5.2(c). EMD based technique is automatic because it does not involve user's intervention. EMD based pre-processing of AS signal has enabled calculation of the trend from noisy AS signal without any prior knowledge of its baseline function and without assumption of any particular basis function which is mandatory in wavelet based processing [28, 80]. Thus the EMD based OFDTS is more automation friendly than the

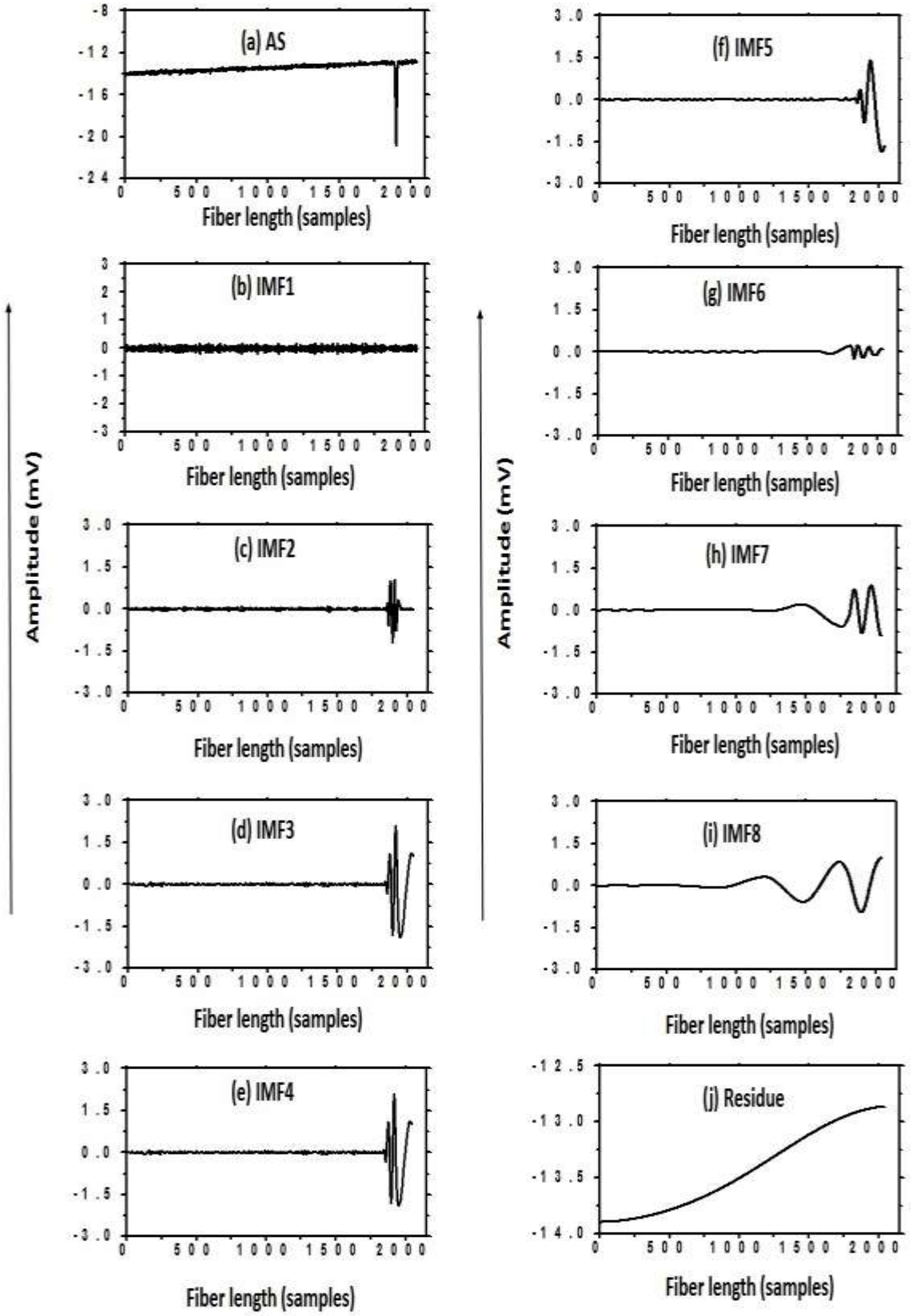


*Fig. 5.1. (a) AS signal, (b-i) various IMFs and (j) residue obtained from the application of EMD on AS signal* (*On horizontal-axis, 10 samples ≡ 10 ns ≡ 1 m*).

wavelet technique. It can also be noted from Fig. 5.2 that EMD based denoising process provides smoothening of AS signal without introducing any undesired shift in the location of the hot zone peak. Thus the EMD technique provides improved spatial accuracy over conventional IIR/FIR based filtering which causes a significant shift in the location of hot zone peaks.

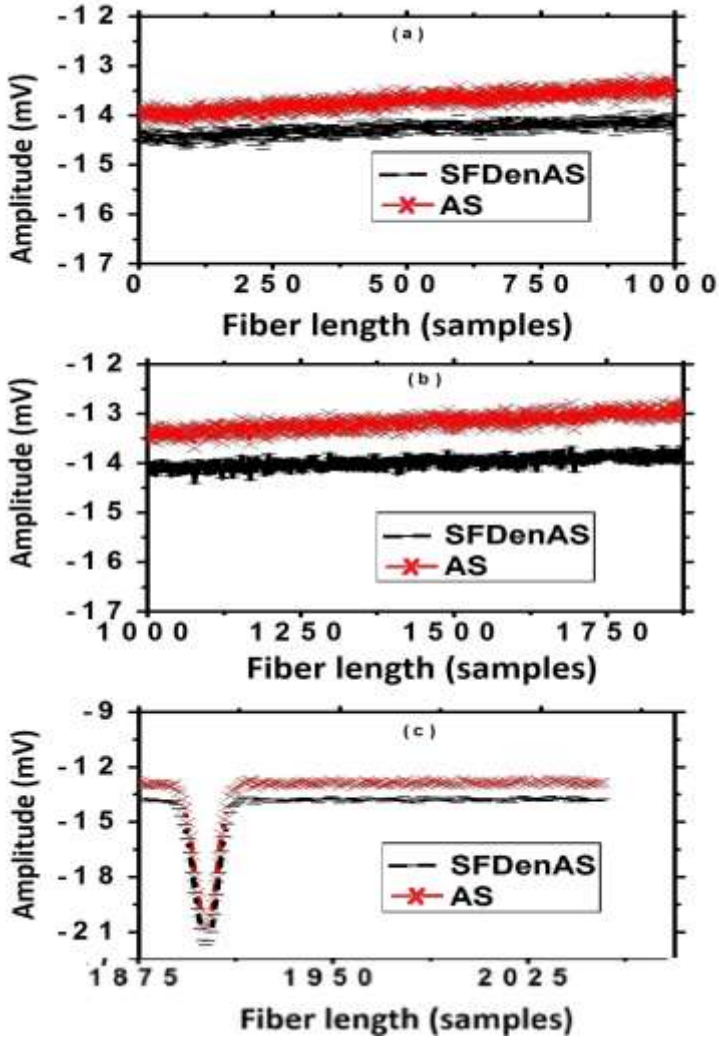


*Fig. 5.2. Unprocessed AS signal and EMD pre-processed AS signal* (*SFDenAS*) *for sample No. (a) 1 to 1000 (b) 1001 to 1875 and (c) 1876 to 2048* (*On horizontal-axis, 10 samples ≡ 10 ns ≡ 1 m*).

The pre-processing of St signal is very similar to one described for AS signal. The EMD based IMFs for St signal are shown in Fig. 5.3. IMFs are sorted from high to low frequency.

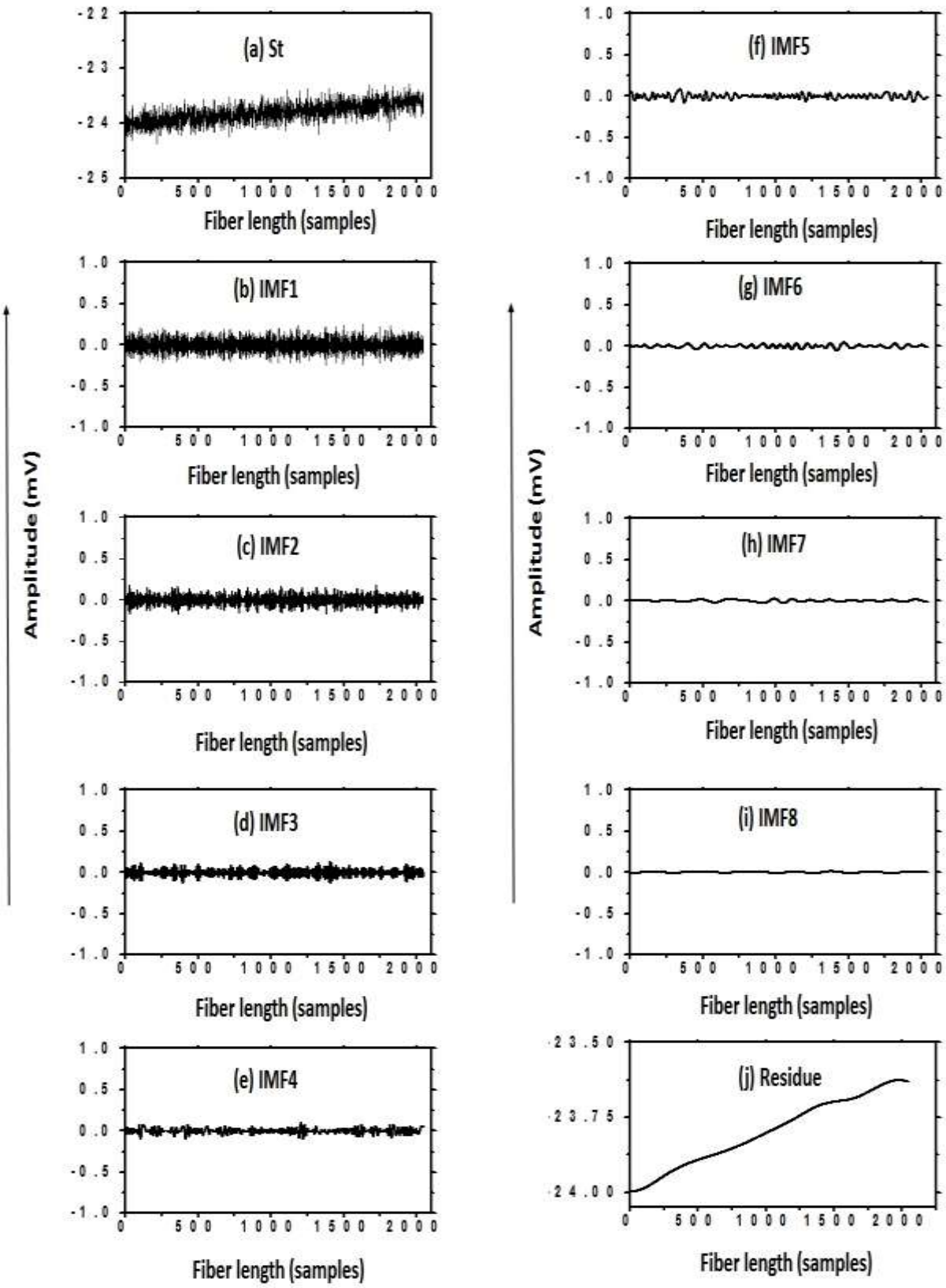


*Fig. 5.3. (a) St signal, (b-i) various IMFs and (j) residue obtained from the application of EMD on St signal* (*On horizontal-axis, 10 samples ≡ 10 ns ≡ 1 m*).

Since *IMF1*to *IMF3* represent high frequency noise component only, these IMFs are removed while reconstructing the signal. The reconstructed St signal is called denoised St (*dSt*) signal. The residue [Fig. 5.3 (j)] represents the trend of St signal. It corresponds to the undesired optical fiber attenuation part in St signal and is also removed. An offset value (*OffsetSt*) equal to mean value of first 10 samples of *dSt* signal is also determined. For the present case,

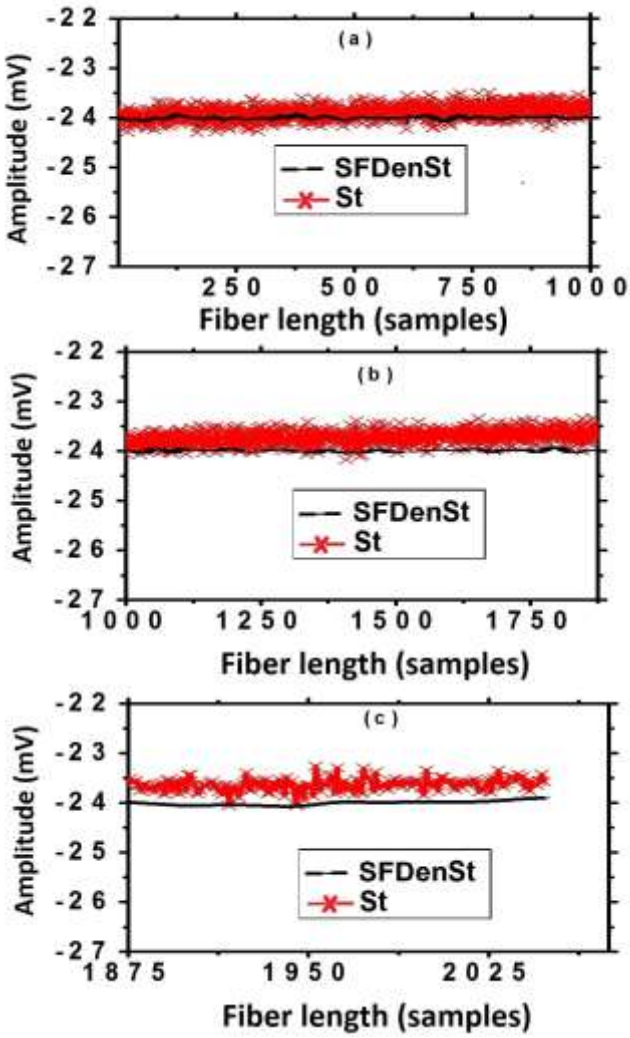


*Fig. 5.4. Unprocessed St signal and EMD pre-processed St signal (SFDenSt) for sample No. (a) 1 to 1000 (b) 1001 to 1875 and (c) 1876 to 2048 (On horizontal-axis, 10 samples ≡ 10 ns ≡ 1 m).*

*OffsetSt* is found to be -24.03 mV. Finally, slope free and denoised version of St signal profile (*SFDenSt*) is reconstructed using above IMFs of unprocessed St with the help of

Eq. (5.5) which acts as the pre-processor for St signal.

$$SFDenSt(z) = \sum_{w=4}^{8} IMFw(z) + OffsetSt \tag{5.5}$$

where, *IMFw(z)* is the $w^{th}$ IMF of St signal. The pre-processed St signal ($St_p$) and its IMFs are function of fiber length ($z$).

The pre-processed St signal (black colour) is shown in Fig. 5.4 along with the unprocessed St signal (red colour) for comparison. It can be observed from Fig. 5.4 that the pre-processed St signal (*SFDenSt*) is not only denoised but also free from the optical fiber attenuation part.

## 5.7 Results

### 5.7.1 Results of distributed temperature measurement with EMD pre-processing technique

The distributed temperature profile for complete fiber length can be obtained using the profiles of pre-processed AS signal (*SFDenAS*) and St signal (*SFDenSt*) in Eqs. (4.7) and (3.10). *SFDenAS* and *SFDenSt* are obtained using the proposed EMD pre-processor as described in Section 5.6. The temperature ($\theta$) of the calibration zone is measured with the help of DSCU and was found to be 24.5 °C. The parameter $R_\theta$ is the ratio (AS/St) value for the calibration zone which was at temperature $\theta$ while conducting the experiment. The parameter $R_\theta$ can be calculated from the ratio of amplitudes of *SFDenAS and SFDenSt* signals for first one meter calibration section of the fiber and is found to be 0.603. Now, values of all the parameters in Eq. (3.10) are known and the corrected distributed temperature profile ($T$) for the whole of the fiber can be obtained. The corrected distributed temperature profile (black color) for complete fiber length of 204.8 m, obtained with EMD pre-processed Raman signals is shown in Fig. 5.5. The distributed temperature profile (red colour) obtained with

unprocessed signals is also shown in Fig. 5.5 for comparison and a significant improvement is evident.

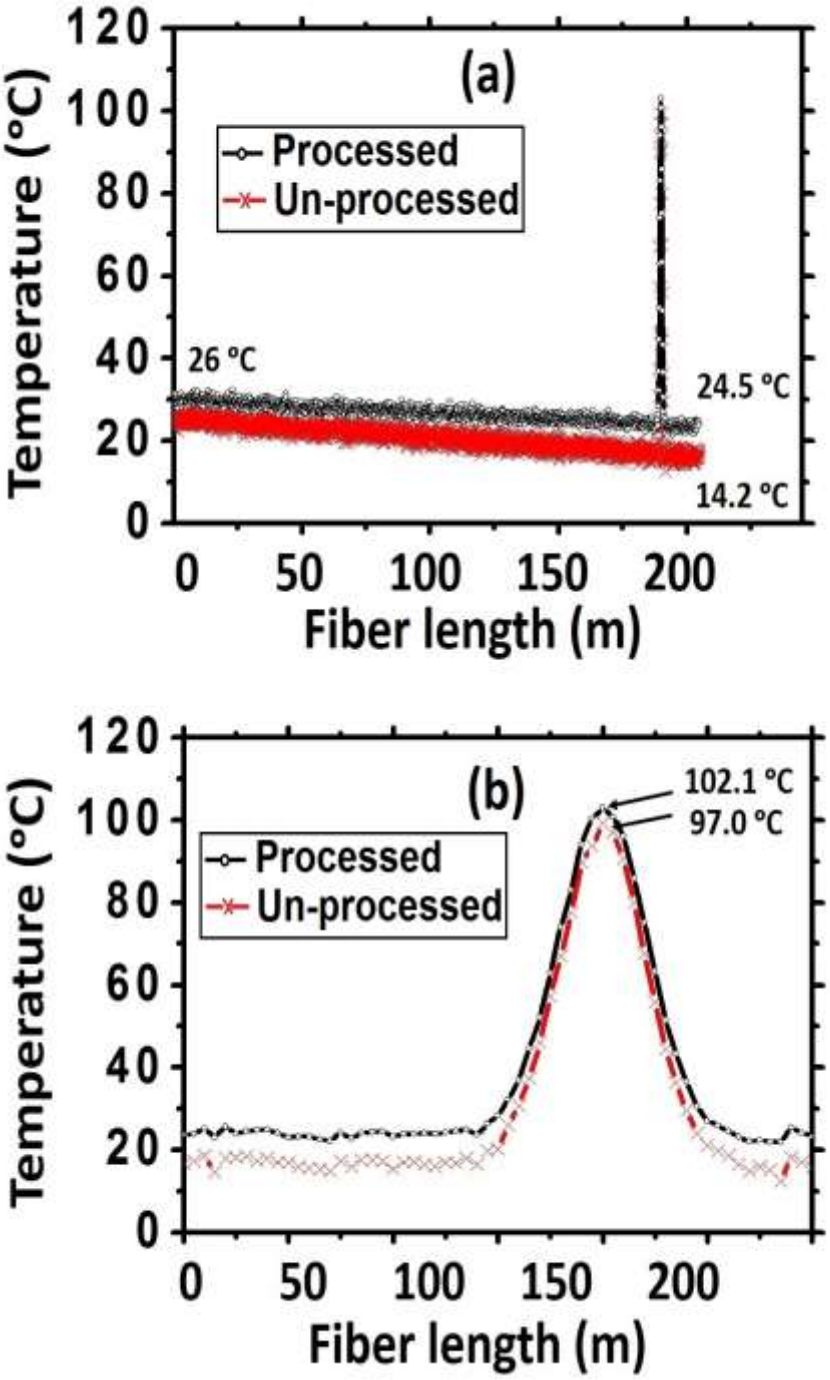


*Fig. 5.5. Distributed temperature profile for (a) whole fiber length obtained with unprocessed Raman signals (black colour) and EMD pre-processed Raman signals (red colour) (b) zoomed view at hot zone.*

It can be observed from Fig. 5.5(a) that in the corrected distributed temperature profile, the measured temperature of the far end of the fiber (kept at a room temperature of 25 °C) is measured with a significantly lower error of -2% compared to the error of -43.2% obtained with unprocessed Raman signals. Similarly, the temperature of the hot zone (kept at 105 °C) is measured as 102.1 °C with a reduced error of -2.7% which is much less than the temperature error of -7.6% obtained with unprocessed signals. The peak to peak variation in corrected distributed temperature profile has also improved to 7.6 °C from 10.8 °C in the profile obtained with unprocessed signals. However, DWT based signal processing provided comparatively less peak-to-peak variation of as 3.6 °C in measurement of room temperature along fiber length. These measurement results have been summarized in Table 5.1.

**Table 5.1**

Comparison of error in temperature measurement at various zones with unprocessed and EMD pre-processed Raman signals.

| Zone (Location) | Reference temperature | Measured temperature | |
|---|---|---|---|
| | | Unprocessed | Processed |
| Start of fiber (Location: 0 m) | 24.5 °C | 24.0 °C | 26.0 °C |
| | Error | -0.5 °C (- 2.04%) | -1.5 °C (- 6.1%) |
| Hot zone (Location: 190 m) | 105 °C | 97.0 °C | 102.1 °C |
| | Error | -8.0 °C (- 7.6%) | -2.9 °C (- 2.7%) |
| End of fiber (Location: 205 m) | 25 °C | 14.2 °C | 24.5 °C |
| | Error | -10.8 °C (- 43.2%) | -0.5 °C (- 2%) |

The reference temperatures at different locations for fiber were measured by thermocouple

based thermometers (model: Digirad71, make: Radix, India) placed in the close vicinity of the fiber. The error in temperature profile obtained using unprocessed signals will be quite high for longer fibers (say few km). In such cases, EMD pre-processor will be more useful and provides reduced temperature measurement error.

The total time required in obtaining the final distributed temperature profile is the sum of averaging time (100 s), EMD based pre-processing time (50 s) and additional time (5 s) taken in computing and printing the final distributed temperature profile on PC screen attached with an Intel Pentium-4 (1.9 GHz) processor based PC that has 1 GB RAM and Windows 2000 operating system. Thus the total time required in updating the distributed temperature profile is ~155 s. A direct comparison of SNR values observed in the unprocessed (red colour) and pre-processed (black colour) signals can be made by considering a fiber zone (0-188 m) which is kept at a reference temperature of 24.5 °C. SNR in unprocessed and processed signals is found to be 14.22 dB and 24.05 dB respectively. Clearly, SNR gets improved after EMD based processing. If the same level of improvement in SNR, which allows better temperature accuracy, is to be achieved without EMD based pre-processing additional averaging of AS and St signals would have to be carried out. It was observed that number of averages required is 15,000 which would require an averaging time of ~300 s instead of 100 s in present case. Thus, EMD based processing makes it possible to have lower processing time and yields better accuracy in temperature measurement. However, it is observed that the processing time taken by EMD technique is ~1.4 times higher than DWT based technique.

The measured spatial location of hot zone is 190 m and the width of the hot zone, as given by the full width half maxima (FWHM) of the peak, is 1 m. These measured parameters conform to the values set initially in the experiment. It can thus be concluded that the EMD based pre-

processing does not introduce any additional spatial error in the measurement of the location of hot zones. The spatial resolution is given by the 10% - 90% rise time of the hot zone peak and is measured to be 1 m. With dynamic measurement of AS and St signals for calibration zone on every fresh measurement of temperature profile, it is possible to compensate the changes in AS and St signals caused by the variation in laser power and coupled power. Moreover, since calibration zone's temperature is also measured by DSCU on every update of the distributed temperature profile it is not mandatory to keep the calibration zone at a constant temperature. The maximum error in temperature measurement was observed to be ±5.5 °C in the whole temperature range of 25-295 °C with spatial error of ± 3 cm.

### 5.7.2 Results of distributed temperature measurement with EMD pre-processing technique applied for 62.5/125 µm sized SS covered sensing fiber

In above experiment, the size of the sensing fiber was 200/220 µm. In addition to above experiment, an OFDTS using a rugged, low core, standard 62.5/125 µm sized SS covered Mutimode fiber of 90 m length was also developed. A hot zone of 1 m length was created at 70 m distance from laser end of fiber. The hot zone was heated upto various temperature values in the range of 25-105 °C.

There are numerous advantages of using low core, standard 62.5/125 µm SS covered fiber in OFDTS. Normal sensing fibers which do not have a SS covering are susceptible to even small mechanical shocks because of their fragile nature. On the other hand, SS covering supports ruggedness and also provides protection to fiber against rodents. Also, SS covering makes it easy and safe to install the sensing fiber in critical field locations where normal sensing fibers cannot be used. Moreover, various fiber components (e.g. coupler, splicer etc.)

can be made available more easily and commonly for 62.5/125 μm size. However, better coupling optics has to be designed for such a low core size fiber as compared to the optics used for 200/220 μm sized fiber. Also, amplitude of AS and St signals obtained for 62.5/125 μm fiber is much lower compared to AS and St signals for 200/220 μm sized fiber. Fig. 5.6 shows the photograph of 62.5/125 μm SS covered fiber along with DSCU unit.

Fig. 5.7 shows the averaged and amplified AS and St signals obtained for 62.5/125 μm fiber with a 1 m long hot zone at 70 m. Fig. 5.8 represents various IMFs obtained with application of EMD on AS signal.

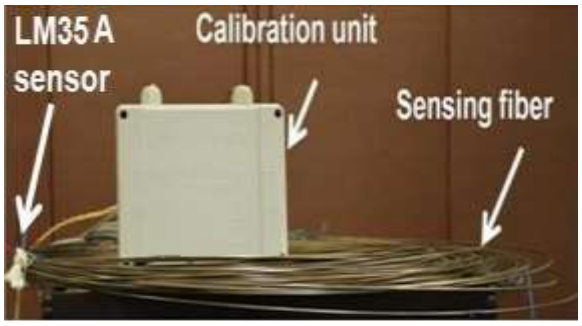


*Fig. 5.6. Photograph of the dynamic self-calibration unit (DSCU) and SS covered 62.5/125 μm sized sensing fiber.*

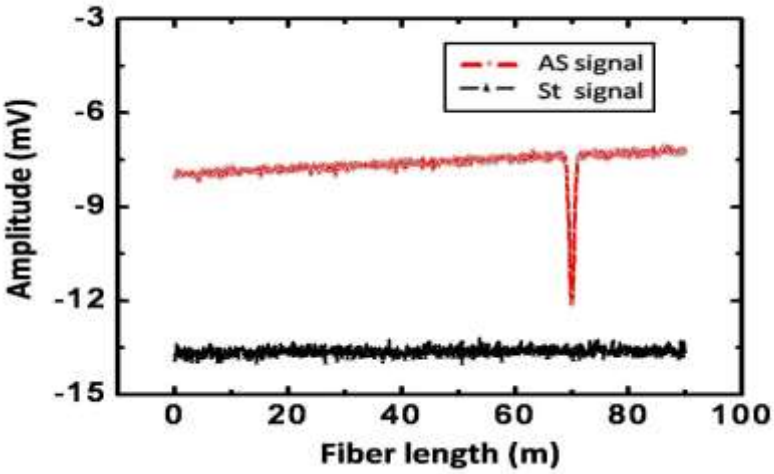


*Fig. 5.7. AS (upper curve) and St (lower curve) signals obtained for 62.5/125 μm fiber with 1 m long hot zone at 70 m.*

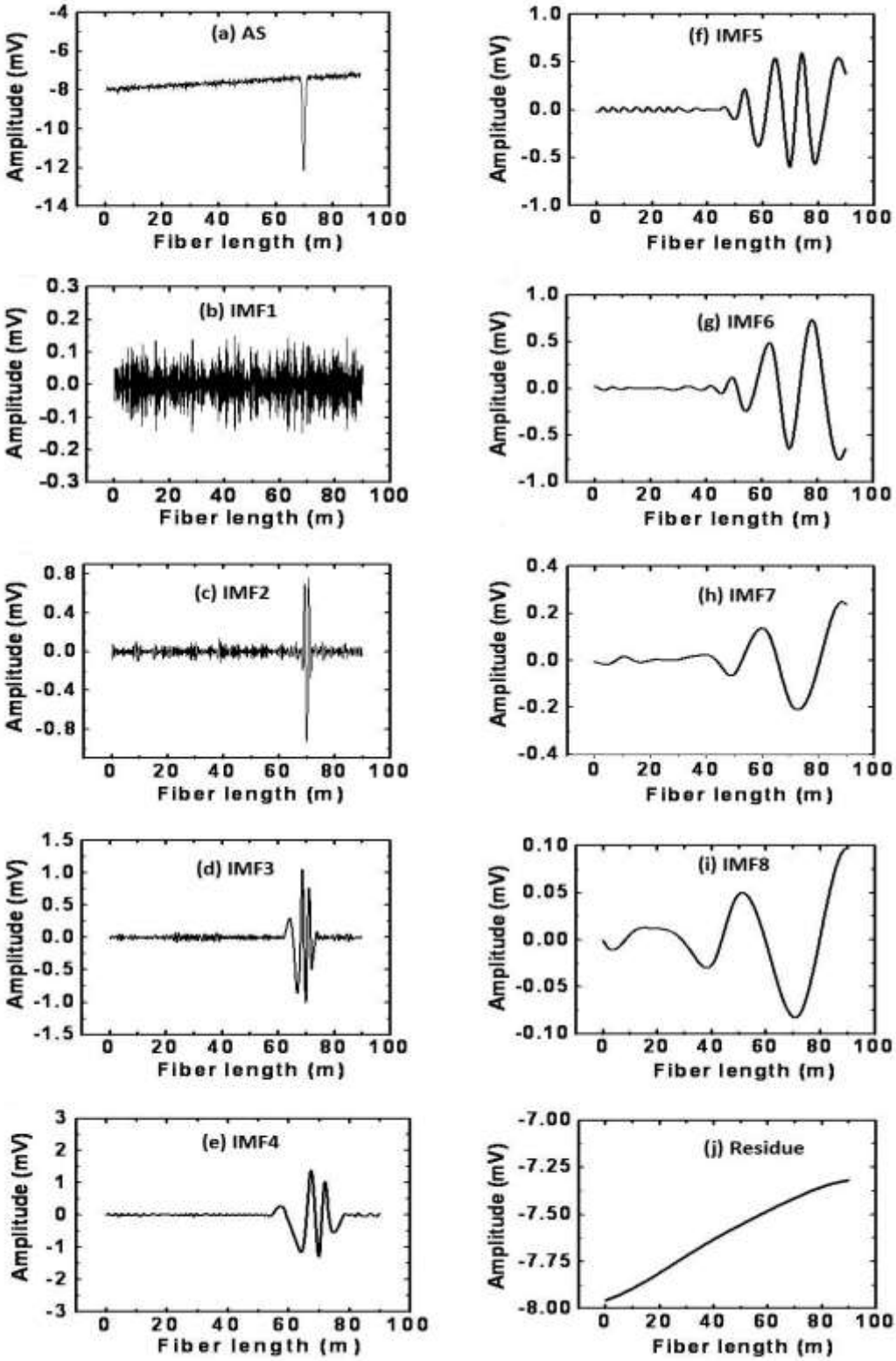


*Fig. 5.8. (a) AS signal, (b-i) various IMFs and (j) residue obtained from the application of EMD on AS signal for 62.5/125 μm fiber.*

The AS signal was pre-processed by EMD pre-processor described by Eq. (5.4). The pre-processed AS signal (solid red circles) (represented by *SFDenAS*) is shown in Fig. 5.9 along with the unprocessed AS signal (hollow black circles) for comparison. The improvement in peak shape and amplitude after preprocessing can be observed from the inset of Fig. 5.9.

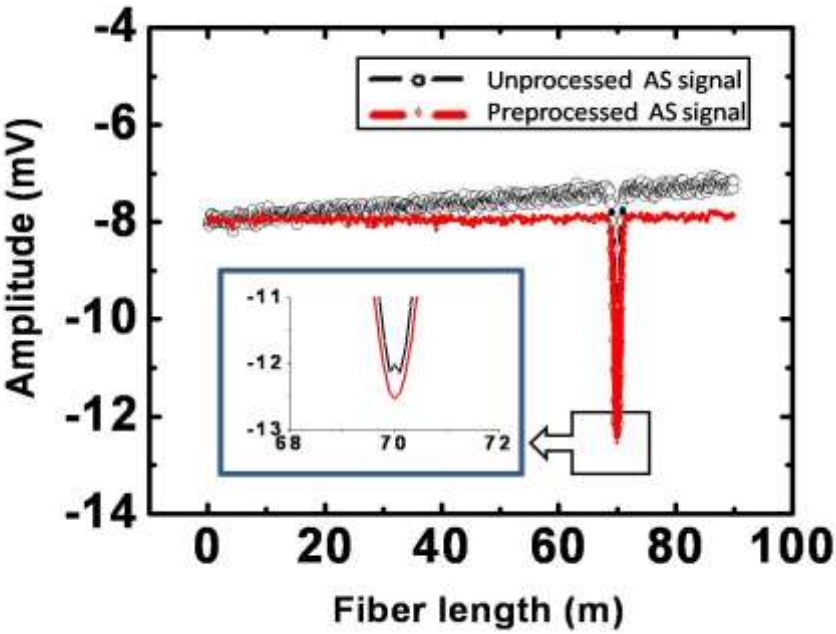


*Fig. 5.9. Unprocessed AS signal and pre-processed AS signal* (*SFDenAS*) *for 62.5/125 μm fiber. Inset shows the improvement in amplitude of hot zone peak after pre-processing.*

The EMD based IMFs for St signal are shown in Fig. 5.10. The EMD based pre-processing of St signal was also carried out as per the pre-processor descried by Eq. (5.5). Fig. 5.11 shows the unprocessed St signal and pre-processed St signal (*SFDenSt*). The corrected distributed temperature profile (solid red circles) for complete fiber length of 90 m, obtained with pre-processed Raman signals is shown in Fig. 5.12. The distributed temperature profile (hollow black circles) obtained with unprocessed signals is also shown in Fig. 5.12 for comparison and a significant improvement can be observed.

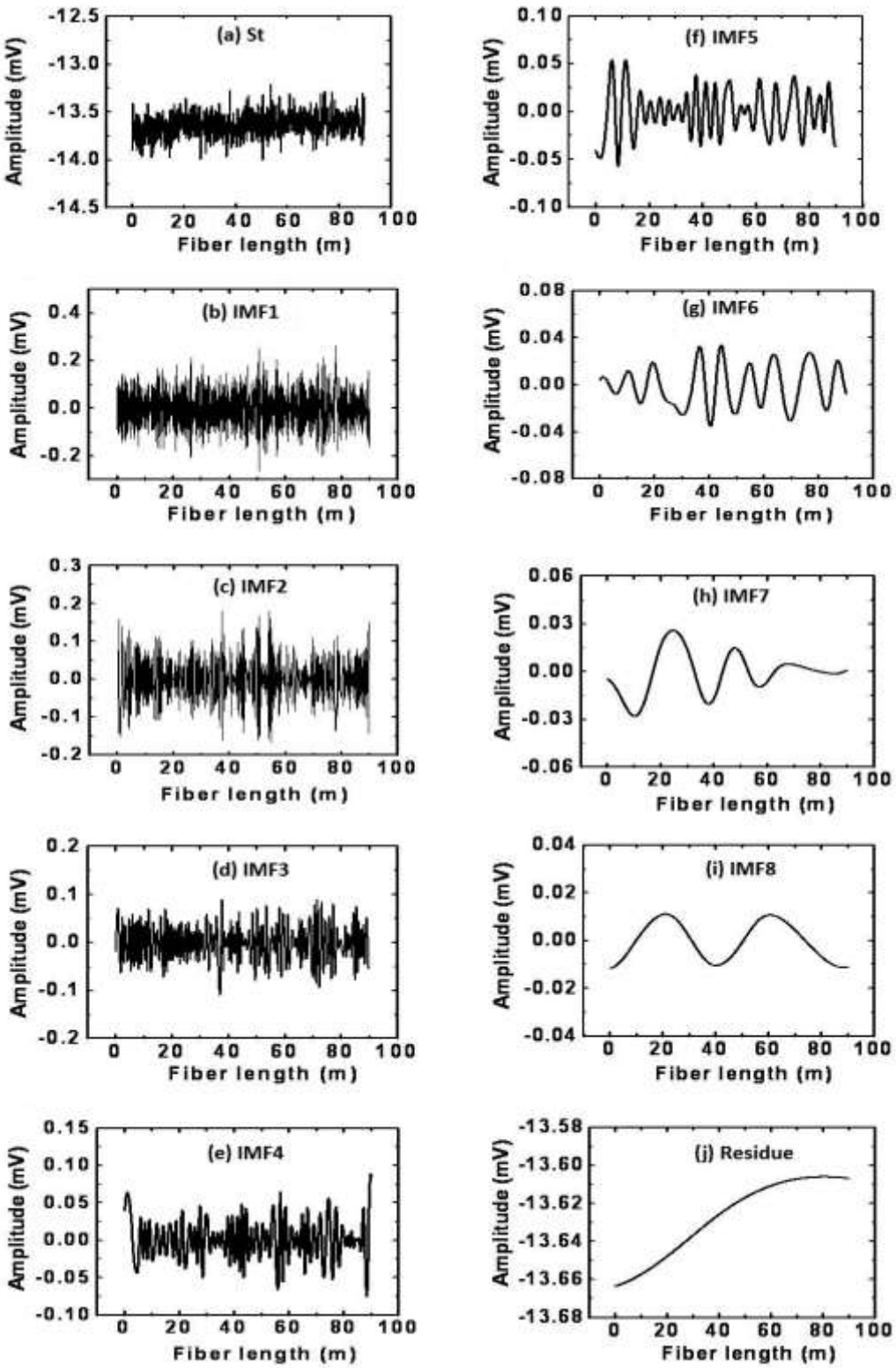


*Fig. 5.10. (a) St signal, (b-i) various IMFs and (j) residue obtained from the application of EMD on St signal for 62.5/125 μm fiber.*

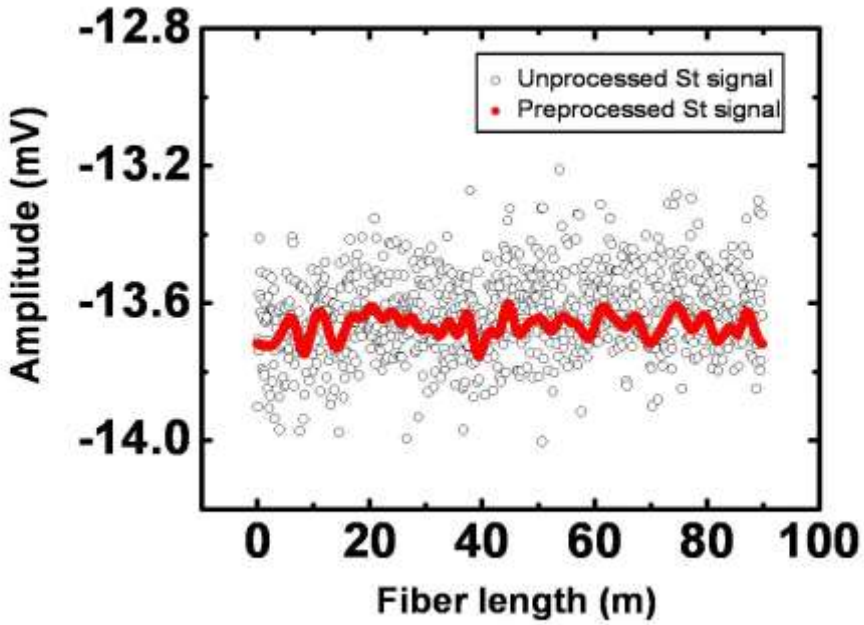


*Fig. 5.11. The unprocessed St signal and pre-processed St signal (SFDenSt) for 62.5/125 μm fiber.*

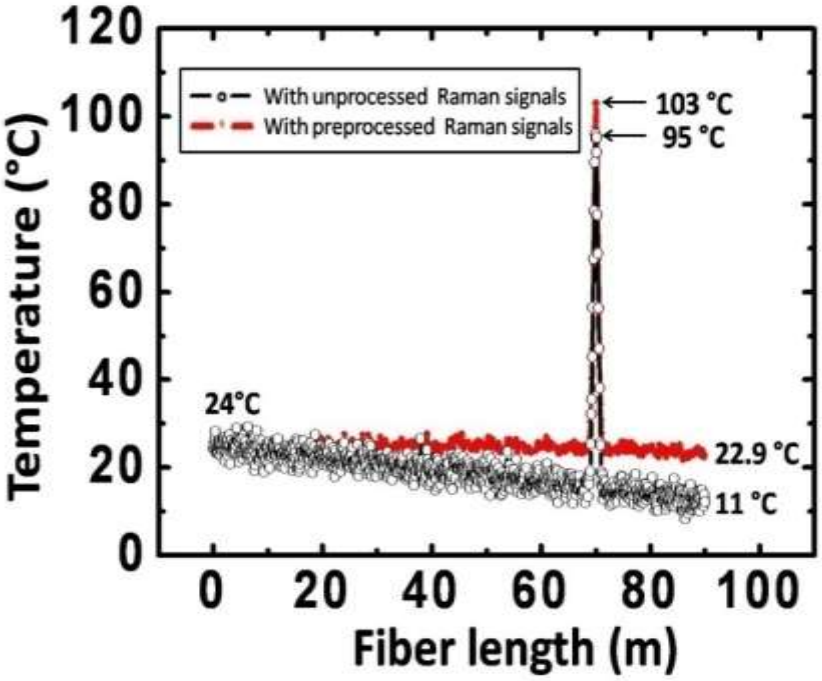


*Fig. 5.12. Distributed temperature profile for whole fiber length obtained with unprocessed Raman signals (black color) and pre-processed Raman signals (red color) for 62.5/125 μm fiber.*

**Table 5.2**

Comparison of measured temperature values using unprocessed and EMD pre-processed Raman signals at various locations in case of 62.5/125 μm fiber.

| Zone (Location, m) | Reference temperature | Measured temperature | |
|---|---|---|---|
| | | Unprocessed | Pre-processed |
| Start of the fiber (Location: 0 m) | 26 °C | 24 °C | 24.8 °C |
| | Error | -2 °C (-7.6%) | -1.2°C (- 4.6%) |
| Hot zone (Location: 70 m) | 105 °C | 95 °C | 103 °C |
| | Error | -10 °C (- 9.5%) | -2 °C (- 1.9%) |
| Between hot zone & end of the fiber (Location: 87 m) | 25 °C | 8.2 °C | 23 °C |
| | Error | -16.8 °C (- 67.2%) | -2 °C (- 8%) |
| End of the fiber (Location: 90 m) | 24.5 °C | 11 °C | 22.9 °C |
| | Error | -13.5 °C (- 55.1%) | -1.6 °C (- 6.5%) |

The temperature of the hot zone was set experimentally at different values in the range of 25-105 °C and the measurement using OFDTS was carried out at these reference temperature values. Fig. 5.13 presents the measured temperature profiles of the hot zone for above temperature range. The maximum error in temperature measurement was found to be ±2.5 °C in the whole temperature range. The location of hot zone was measured to be 70 m for the above temperature range which is same as set originally in the experiment. Also, the width of hot zone is correctly measured to be 1 m. Thus the developed OFDTS has successfully measured the temperature, location and width of the hot zone and also the temperature profile along the whole length of the fiber with above mentioned accuracy.

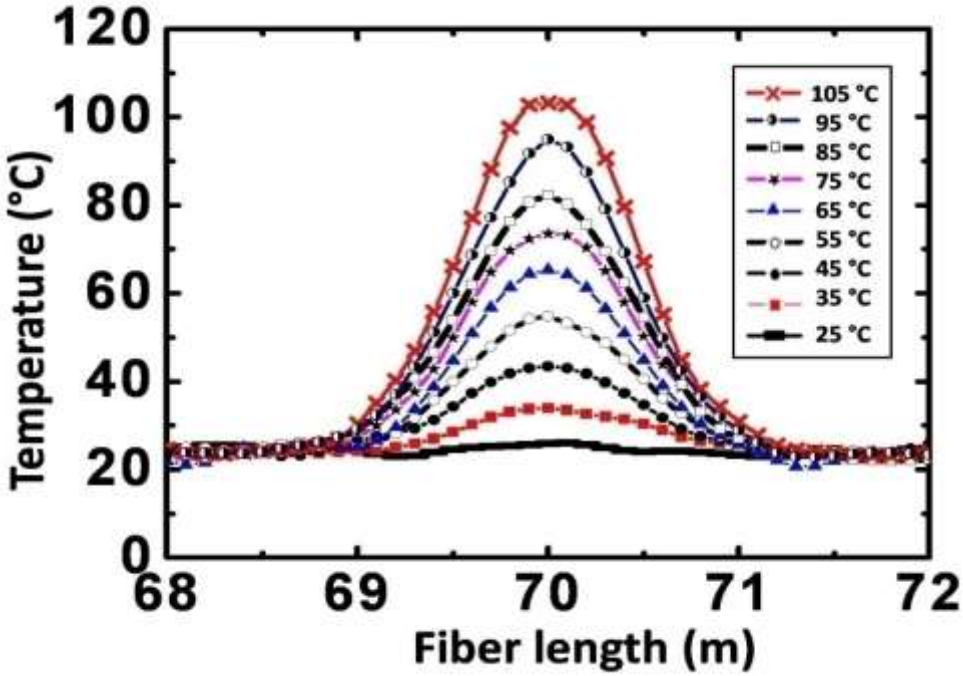


*Fig. 5.13. Measured distributed temperature profile at hot zone for different temperature values in case of 62.5/125 μm fiber.*

**5.8 Raman OFDTS based distributed zone wise temperature alarm system**

As described earlier, OFDTS can be used for temperature measurement over long gas pipe lines, high voltage electrical cables, coolant loops of FBTRs [12-15, 17 and 55] etc. It can also be employed for air-conditioning management in server rooms and for fire detection in tunnels, mines and buildings etc [6, 8, 88-90]. In many applications such as mentioned above, zone wise temperature profile with different temperature range limits and alarm for breaching these limits is required in control room for proper operation and safety of the system. This section describes a zone-specific fiber based alarm system that has been designed and developed to generate audio-visual warnings if temperature of any zone crosses the threshold limit. The system has been designed around a microcontroller [91, 92], relay system and

developed prototype OFDTS. The temperature profile data from the OFDTS that employs 200/220 μm, Multimode fiber is used as input to PC. After analysis of distributed temperature data in the PC, a message is sent to microcontroller via serial port, for generating warning alarms in the control room. The alarm system has been successfully tested for 10 zones, in a 100 m long sensing fiber in the temperature range of 25-300 °C.

### 5.8.1 Block diagram of OFDTS based alarm system using microcontroller

Fig. 5.14 depicts the block diagram of the developed system. It mainly consists of an in-house developed OFDTS and microcontroller based alarm system. The OFDTS part is marked by a dashed block in Fig. 5.14. The OFDTS used in present work has already been described in Section 4.7. Additional blocks like microcontroller (89V51RD2) [91], relay driver ICs (ULN2003) and alarm indicator array (which are shown outside the dashed block) have also been interfaced to main PC of OFDTS.

Once the temperature profile of the optical fiber is available on PC, it is analyzed zone-wise along the fiber length and suitable signals are sent to the alarm system to generate audio visual alarms. The alarm system has been designed around two units of microcontroller (89V51RD2) μC2 and μC3 (termed as μCs). An array of 10 visual indicators and two audio alarms is suitably interfaced to output ports of μCs. Audio visual alarms are interfaced through relay drivers (ULN2003) which can drive the alarms through relays. The alarm system is interfaced to PC through its serial ports (COM2, 3) using RS232 standard.

Temperature profiles of various zones, their allowed temperature range limits and the corresponding indications are designed to be available continuously on PC monitor. The

sensing fiber is mapped by an array of 10 visual indicators which is mounted on a display

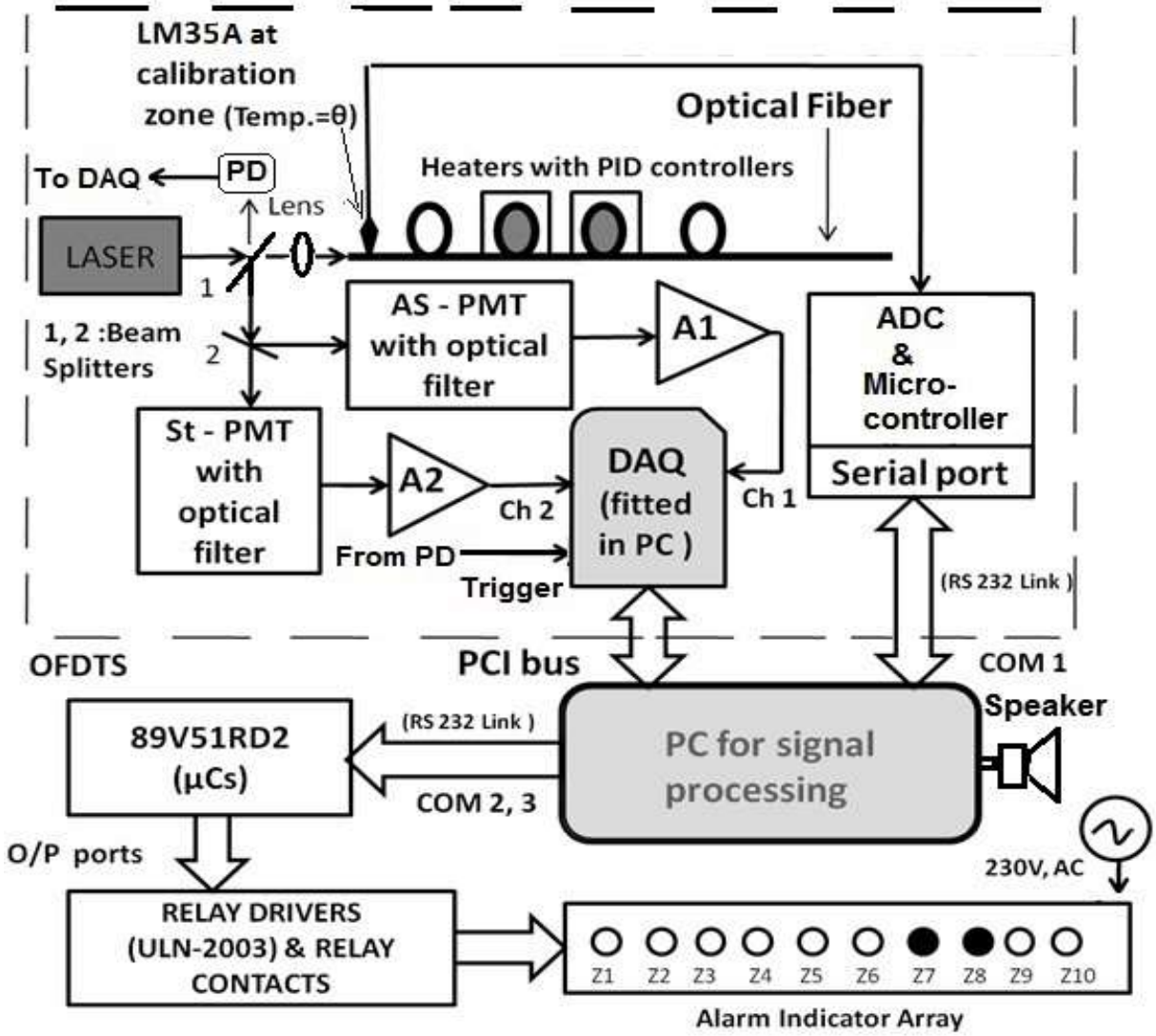


*Fig.5.14. Block diagram of microcontroller and OFDTS based distributed zone-wise alarm system.*

panel to facilitate the visibility of status of each zone from the whole laboratory area. Visual indicators are supported by audio alarms on speaker attached to PC. Fiber length from 0 to 5 m includes the calibration zone of 1 m length and remaining fiber length is divided in 10 zones. However, the length of various fiber zones can be flexibly adjusted from GUI available on PC screen. For conducting experiment, two hot zones, termed as Zone-7 and

Zone-8, located at 70 m and 78 m respectively are created with the help of electrical heaters. The developed alarm system is tested on these hot zones.

### 5.8.2 Data processing and analysis

The developed OFDTS measures distributed temperature and makes it available in the main 'PC for signal processing'. The alarm system is interfaced to PC via RS232 link. Fig. 5.15 presents the flow chart for the developed system. DAQ card is initialized by the user by selecting various parameters like triggering mode, coupling mode, sampling rate and memory depth etc. The triggering mode is kept in 'external' which allows synchronization of DAQ card with laser as described in Section 3.5.2. Sampling rate selection permits the number of samples for AS and St signals that can be allowed by the selected memory depth of DAQ card. The selected memory depth is 2000 samples and the sampling rate selected in the present case is 1 GSamples/s which results in 1000 samples for 100 m long fiber. This satisfies the relation expressed in Eq. (3.8).

The total time ($t_s$) for which temperature monitoring is to be carried out is also required to be entered by the user. Temperature limit ($T_a$) of various zones is adjustable and can be set by the user. Next, the temperature ($\theta$) of the calibration zone is obtained by PC from the temperature sensing 'IC LM35A, ADC and microcontroller' based temperature sensor system (also called DSCU). AS and St signals are obtained on PC from amplifier outputs by sampling through DAQ cards and are used for determination of temperature profile of complete fiber length using Eq. (3.10). Once temperature profile for full fiber length is determined, it is divided into various zones along the fiber length. For each zone, maximum

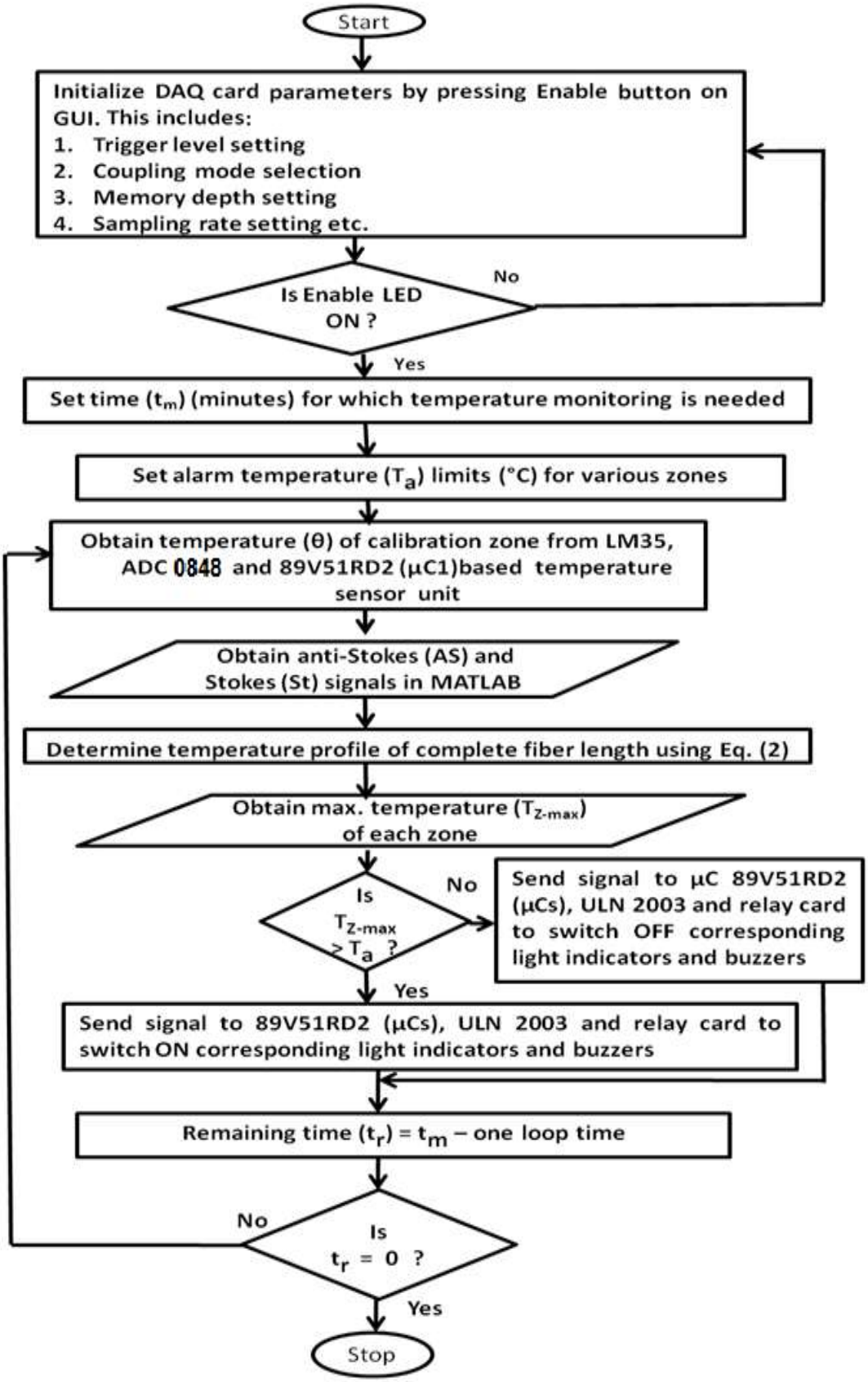


*Fig.5.15. Flow chart for the developed alarm system.*

value of measured temperature ($T_{Z\text{-}max}$) is compared with the user defined alarm temperature limit ($T_a$) for that zone. If, within a zone, $T_{Z\text{-}max} > T_a$, PC sends a predefined ASCII character to μCs. Next, μCs identify these characters and activate the relevant bits of their output ports to drive relays (on relay card) corresponding to audio visual alarms of that zone. In case, $T_{Z\text{-}max}$ comes within the limit of $T_a$ after the alarm is sounded for that zone, the alarm gets reset. The time taken in calculating temperature profile and activation/deactivation of indicators is calculated in advance. This is termed as 'one loop time' and is subtracted from total measurement time ($t_m$) to calculate the remaining time ($t_r$). If $t_r$ becomes zero, program stops else it continues to calculate the temperature profile and also the process to raise the alarms. A user friendly GUI developed in MATLAB for alarma system is shown in Fig. 5.16. It is used to set alarm temperatures for various zones and monitor the temperature profiles of complete fiber length.

### 5.8.3 Testing of alarm system

In the present work, microcontroller (89V51RD2) and Raman OFDTS based zone wise temperature alarm system has been developed and tested for a length of 100 m. Fig. 5.17 presents the photograph of display panel for temperature alarm system. A user friendly GUI (Fig. 5.16) supports the automation of the system. As can be seen from the snapshot of GUI, the alarm temperature limits ($T_a$) of Zone-7 and Zone-8 were set to 50 °C and 100 °C respectively (indicated by dotted lines) whereas the measured peak temperatures ($T_{Z\text{-}max}$) of these zones were found to be 74.1 °C and 298.2 °C respectively. Temperature peaks were detected by the system and audio visual alarms were raised immediately as measured temperature values crossed the alarm temperature limits for these zones. The glowing indicators Z-7 and Z-8 in Fig. 5.17 are visible under this condition. A hooting sound is also

created on speaker attached to PC by playing an audio file under above condition. The system was rigorously tested for 10 different zones in a 100 m long sensing fiber and its performance was found to be satisfactory.

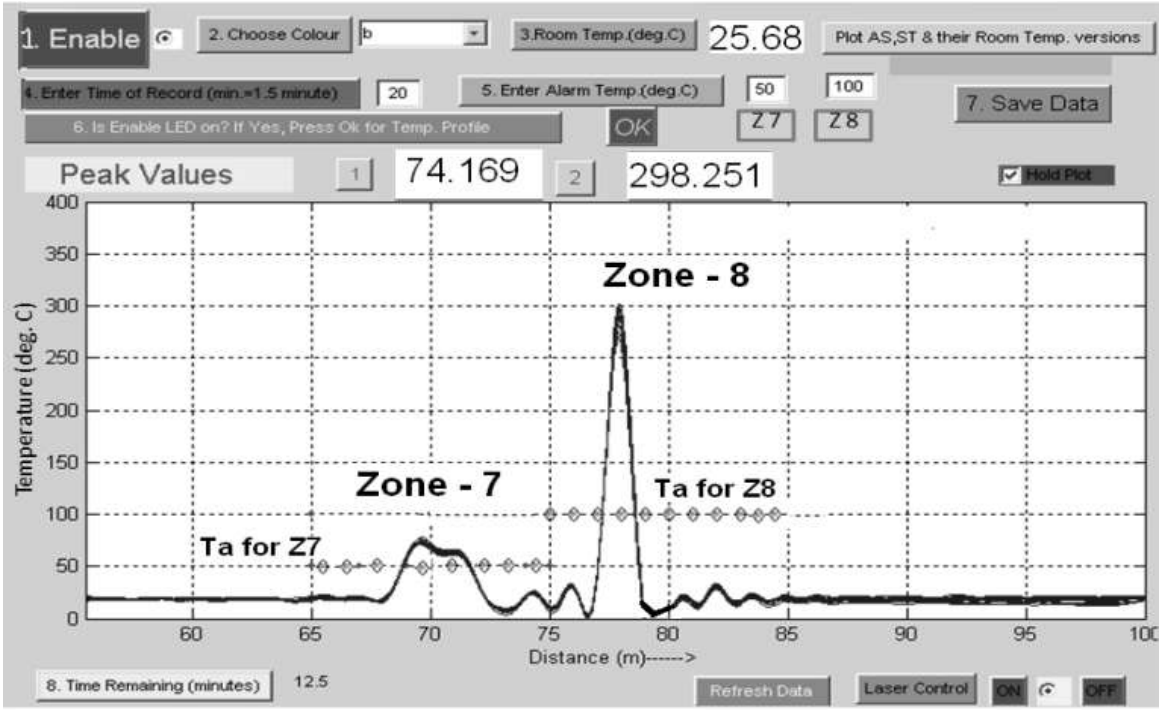


*Fig. 5.16. Snapshot of GUI for OFDTS based alarm system.*

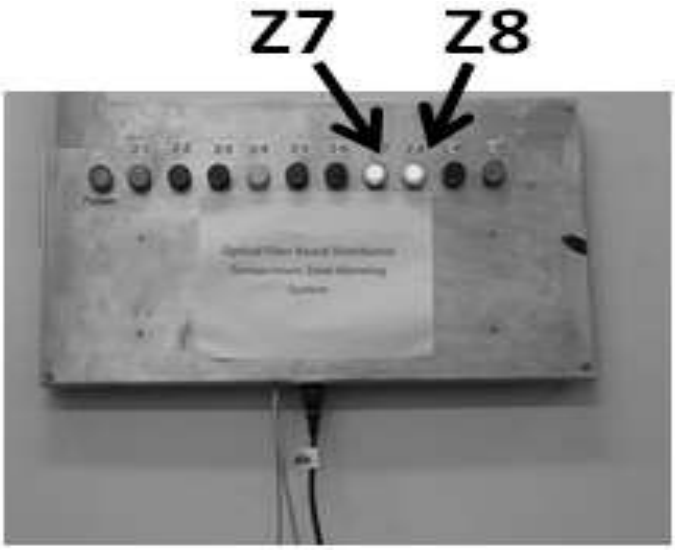


*Fig. 5.17. Photograph of display panel for temperature alarm system.*

## 5.9 Summary

The concept of EMD has been discussed in this Chapter. It has been shown that the proposed EMD based technique is a promising method to address the various issues described in Section 1.1. It has also resulted in reduction in measurement errors in distributed temperature profile, especially at far off locations. The EMD based pre-processor for Raman AS and St signals provided denoising of these signals, in addition to compensation for wavelength dependent attenuation and thus achieving better SNR and lower temperature measurement errors. Contrary to other decomposition methods, EMD is empirical, intuitive, direct, adaptive and without pre-determined basis functions. These features allow determination of trends for AS and St signals without involvement of the user and thus making the technique more automation friendly. The dynamic self calibration is also supported by EMD pre-processor thus relaxing the requirements on variation in Raman signals caused by the changes in laser power and its coupling to the sensing fiber. The proposed EMD based pre-processor has alo been implemented for measurement of temperature profiles using a rugged 62.5/125 µm standard sized SS covered sensing fiber which makes the developed OFDTS suitable for field applications. It may be noted that inspite of the different amplitude levels of AS and St signals, EMD pre-processor works well for both 62.5/125 µm and 200/220 µm sensing fiber.

This Chapter has also demonstrated that distributed temperature data of OFDTS can be used to generate audio-visual alarms in a control room if temperature of any particular zone crosses the temperature limit set by the user. The audio-visual alarms can be generated with the help of microcontroller and relay based circuitry after analyzing the temperature data in PC. The microcontroller generates logic level signals to activate/deactivate the relays. The

work can be extended to switch ON/OFF the heaters and in turn control the distributed temperature by using logic and relays. In future, a ‘distributed P-I-D temperature controller’ can also be designed to control the temperature of various zones by using suitable heating and cooling arrangements. In a conventional approach of distributed temperature control several point sensors (like RTDs, thermocouple etc.) are to be used for measuring the present value and P-I-D controllers produce the control signal to control the power to heaters. Unlike the conventional point sensor based approach for distributed temperature control, OFDTS-PID based scheme will require just a single fiber as sensing element for the whole sensing length.

# Chapter 6

# EMD based study of bend induced error in a Raman OFDTS

## 6.1 Introduction

As outlined in Section 1.1 there are several major issues (issue No. 1-5) in connection with Raman OFDTS which can be addressed with the help of digital signal processing. The issues No. 1-4 were properly addressed in Chapter 3-5. However, issue No. 5 remains unaddressed in these Chapters. In the present Chapter, focus has been made on resolution of the issue No. 5 which is related to the error in distributed temperature profile caused by bend in sensing fiber. As described in Chapter 3-5, calibration of an OFDTS is performed using temperature of the reference (calibration) loop located at the start of the sensing fiber. Also, OFDTS measures correct distributed temperature profile if sensing fiber is free from any discontinuity. In such cases, AS and St signals have uniform decay within the fiber due to fiber attenuation only. However, in real applications, as the time passes, the fiber loss may get affected if the sensing fiber undergoes perturbations such as bends, tensions and compressions which cause discontinuity in AS and St signals [31]. If OFDTS is still calibrated by using the same calibration loop, measured temperature profile of the fiber zone that exists after the bend will be highly erroneous. Therefore, detection of the bend, its location and temperature error caused by that bend alongwith compensation of that error is of utmost importance. In practice, it is difficult for the user to visually identify the presence and location of the bend from AS and St signals directly. This Chapter presents EMD based automatic and dynamic technique for detection of bend and its location using area of analytic form of IMFs. Once the analytic form [23] of IMFs calculated for St signal is available, it may be utilized as a feature [93-95] for automatic detection of bend. Further, the proper

selection of the second calibration loop after the detected bend makes it possible to use rest of the fiber for obtaining correct temperature profile.

### 6.2 Analysis of bend induced error in a Raman OFDTS

As mentioned in Section 3.6 that for a Raman OFDTS system, temperature ($\theta$) and ratio ($R_\theta$) of a small reference (calibration) loop are used to measure the distributed temperature profile ($T$) of rest of the fiber. Parameter $R_\theta$ is the ratio value (AS signal value/St signal value) for the calibration loop. Eq. (3.10) is used for estimation of $T$ using above mentioned parameters. The distributed temperature profile is determined using Eq. (3.10) with the assumption that sensing fiber is free from any discontinuity. However, a bend in sensing fiber may result in erroneous distributed temperature profile. Therefore, detection and localization of bend is extremely important to obtain correct distributed temperature profile over whole fiber length.

In the suggested methodology, it is proposed that first, the presence of bend should be detected, second the location of the bend should be identified and then an additional DSCU should be suitably installed to obtain an error free distributed temperature profile of the fiber zone existing after the bend.

As discussed in Section 2.6, several methods have been suggested for detection of bend in previous years. These methods include the use of Rayleigh [96, 97] in OTDR mode, costly Brillouin optical time domain analyser (BOTDA) [56, 57], loop back arrangement [40, 55] and reflected AS signal from the mirror located at the far fiber end [31]. Each method has its own merits and limitations.

Raman AS and St signals also exhibit signatures of bend but a manual and visual inspection is required to identify these signatures. Visual inspection requires involvement of an attentive, careful and experienced human operator. Moreover, the step change caused by the fiber bend in the amplitudes of AS and St signals may be small compared to the dynamic range covered by these signal levels and thus may not be easily observed by the operator. In such a situation, the fiber bend may be easily missed by the operator. On the other hand, even a small step change in AS and St signals may result in a large error in distributed temperature profile. In order to eliminate the involvement of human operator, make OFDTS more rugged and automation friendly, presence of bend in sensing fiber and its location should be detected automatically and dynamically.

Compared with above mentioned techniques which work in optical domain, the innovative contribution of the present work is that it discusses an advanced digital signal processing technique for St signal that first detects the presence of bend in fiber, estimates its location and then alerts the user. Later, the temperature error is compensated by employing an additional DSCU. Fourier transform based frequency-domain analysis method may be used for gaining insight into the hidden discontinuity which is caused by fiber bend in St signal. However, location of frequency components cannot be estimated using conventional Fourier transform. As a result, it will not determine the location of bend in AS or St signals which are non-stationary in nature since Fourier transform is suitable for analysis of stationary signals only. STFT is also a commonly used method for obtaining time and frequency information of non-stationary signals. However, the requirement on selecting a proper window type, window size and a trade-off between time and frequency resolution limit its scope. DWT can also be used to obtain time-frequency information simultaneously. However, proper selection of wavelet basis has to be made beforehand. A new technique for analysis of nonlinear and non-

stationary signals has been proposed recently to study non-stationary signals [93-95] and is based on EMD [26].

The present Chapter describes the analysis of St signal that is based on the Hilbert–Huang transform (HHT) [37]. In this analysis, first the IMFs are extracted by using EMD and then the Hilbert transform of each IMF is computed to obtain corresponding analytic IMFs. Plots of the obtained analytic IMFs in the complex plane exhibit a circular form and each IMF has its own frequency of rotation [93-95, and 98].

A newly suggested parameter called the area of the circle in the complex plane of IMF has been utilized for discrimination between normal and epileptic seizure electroencephalogram (EEG) signals [93-95] by Pachori *et al.* which are typical non-stationary signals. In the present work, the area parameter of the trace of analytic form of IMFs calculated for St signals has been used as a feature to automatically detect the presence of bend in sensing fiber. The main advantage of using IMFs of St signal for discrimination is the fact that these IMFs respond to bend only and remain unaffected with change in temperature of hot zones, laser power and/or laser-fiber coupling. It is also proposed that an additional DSCU is placed immediately after the bend to obtain the error free temperature profile of the fiber section which is located after the bend. The dynamic self calibration makes the distributed temperature measurement independent from the changes in the temperature of calibration loop, variations in AS and St signal levels caused by the variation in laser power and/or laser-fiber coupling. A new methodology has also been proposed to reduce the temperature measurement error caused by bend. To test the effectiveness of the proposed methodology, the temperature of the hot zone located after the discontinuity was measured and compared with the reference value. It is shown that before applying the proposed methodology, the

error was as high as -24 ºC in the range of 21-100 ºC. However, after applying the proposed methodology the reduction in error was achieved and the error was within ±3.5 ºC.

### 6.2.1 Experimental set up, data set and problem description

This section describes the experimental set up, data set and problem in hand.

#### 6.2.1.1 Experimental set up

The basic form of the experimental set up is similar to the earlier versions described in Section 3.5.2. However, there are some major differences between the new and earlier setup. The block diagram of new setup has been outlined in Fig. 6.1.

A pulsed laser (wavelength = 1064 nm, pulse energy =100 μJ, pulse width = 10 ns, pulse repetition rate = 1 kHz) is used as the pump source. The laser is coupled to a 100 m long, 100/125 μm sized Polyamide coated Multimode optical fiber using coupling optics. As described in Section 3.5.2, AS and St signals after amplification are digitized by a PCI bus based DAQ system. The samples are accessed by the PC which are used for EMD based signal pre-processing and to display final distributed temperature profile.

The setup also makes use of precision integrated-temperature-sensor-circuit LM35A and ADC and microcontroller based temperature sensor as described in Sections 3.5.2. This unit has been termed as dynamic self-calibration unit (DSCU) 1 and sends the most recent value of temperature ($\theta_1$) of the calibration loop (zone)-1 to main PC. The calibration loop-1 is 1 m long part of the sensing fiber itself and is located at the very start of the sensing fiber. In order

to test the performance of the proposed methodology, two hot zones in the sensing fiber are created. These hot zones use P-I-D controlled electrical heaters described in Section 3.5.2. Hot zone-1 is located at 21 m whereas hot zone-2 is located at 91 m. Hot zone-1 and 2 have lengths of 1.5 m and 1 m respectively. The reference temperature of both the hot zones is 80 °C. Initial measurement is taken with normal condition of the fiber in which no bend in the fiber was present. This situation is referred to as 'normal fiber condition'. Later, a bend in

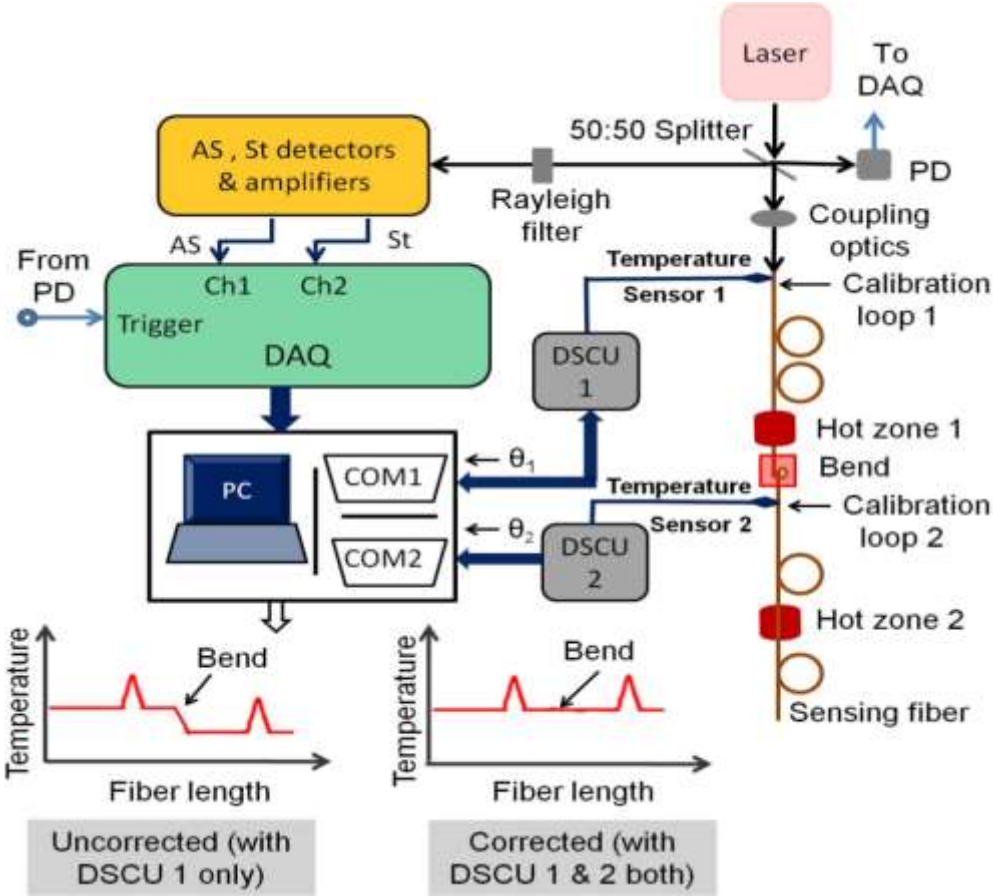


*Fig. 6.1. Schematic diagram of the experiment for bend detection.*

the fiber is deliberately created at the location of 65 m by winding by winding 2 rounds of fiber on a spool of 10 mm radius. This situation is referred to as 'bent fiber condition'. The

bend in the fiber makes the present experimental setup different from the setup described in previous Chapters. The bend in fiber causes error in temperature profile of the fiber especially in the zone that exists after the bend. The bent situation is created to cross-verify the bend detection capability of proposed methodology.

#### 6.2.1.2 Data set and problem description

A data set of 100 signals was prepared by repeating the experiment for 100 times. Every time, AS and St signals were averaged for 5000 times. We now have 100 signal data set of St signals for both the normal and bent fiber conditions. Under normal conditions when the fiber did not have any bend, the AS and St signals were free from any discontinuity. Fig. 6.2 presents AS and St signals for normal fiber conditions. With DAQ's sampling rate of 1GSample/s, the relation 10 samples ≡ 10 ns ≡ 1 m can be used to convert number of samples into fiber length.

In normal condition, the distributed temperature (Fig. 6.3) can be estimated with the help of Eq. (3.10) using the temperature $\theta_1$ of calibration loop-1. It is observed that the room temperature (21 °C) at the start of the fiber and temperature (80 °C) of hot zone-1 and 2 are measured with small error of ± 3 °C. However, when a bend is created in the fiber at 65 m location, AS and St signals witness discontinuity at sample number 650 (Fig. 6.4). The distributed temperature profile corresponding to bent fiber condition is shown in Fig. 6.5 which reveals that the temperature profile after the bend location is highly erroneous. The temperature (80 °C) of hot zone-2 is incorrectly measured as 56 °C. Similarly, the temperature (21.5 °C) of the rest of the fiber existing after the bend is erroneously measured as 6 °C.

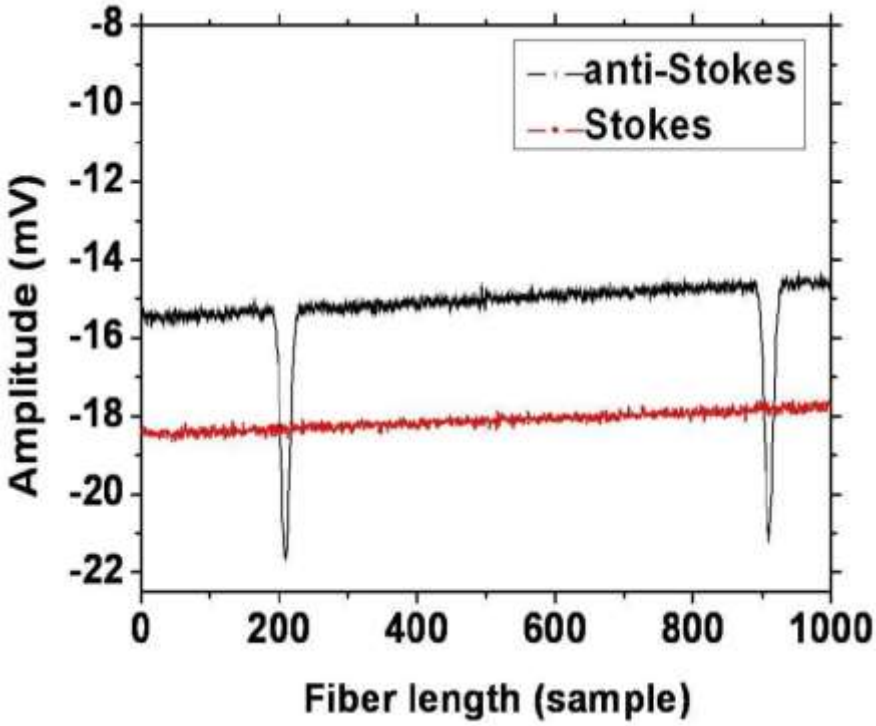


*Fig. 6.2. AS and St signals for normal fiber condition* (*On horizontal-axis, 10 samples ≡ 10 ns ≡ 1 m*).

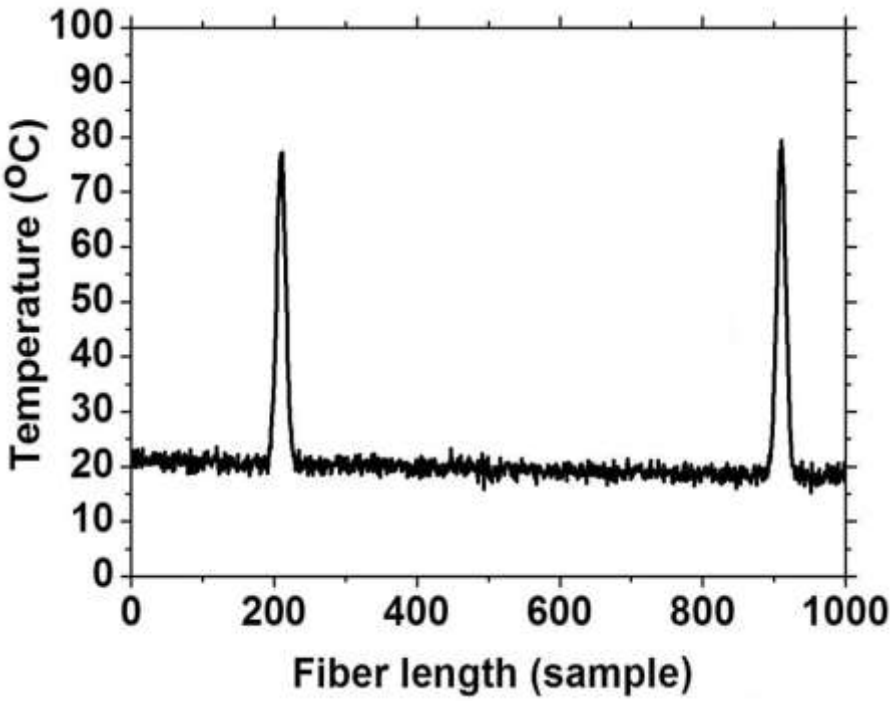


*Fig. 6.3. Distributed temperature profile for normal fiber condition* (*On horizontal-axis, 10 samples ≡ 10 ns ≡ 1 m*).

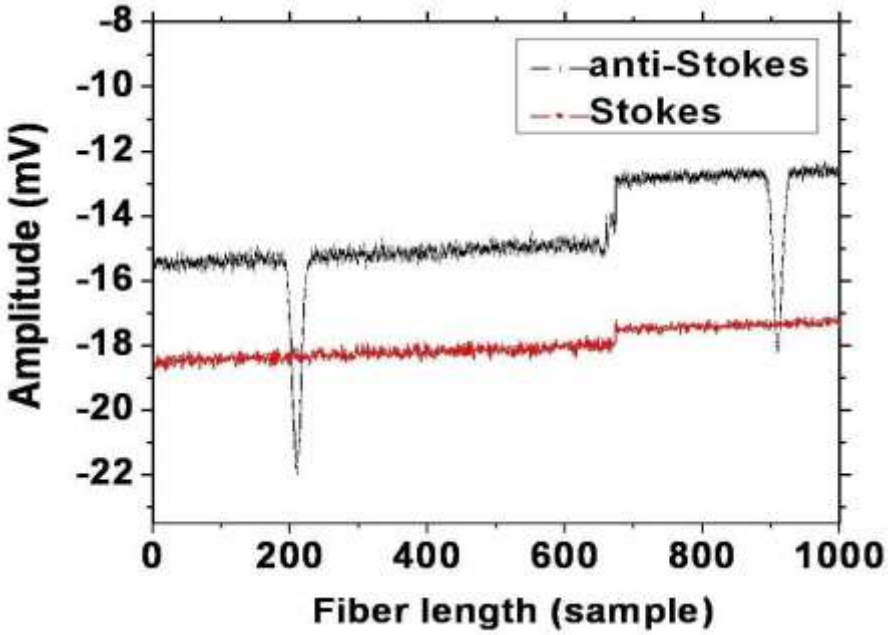


*Fig. 6.4. AS and St signals for the bent fiber condition* (*On horizontal-axis, 10 samples ≡ 10 ns ≡ 1 m*).

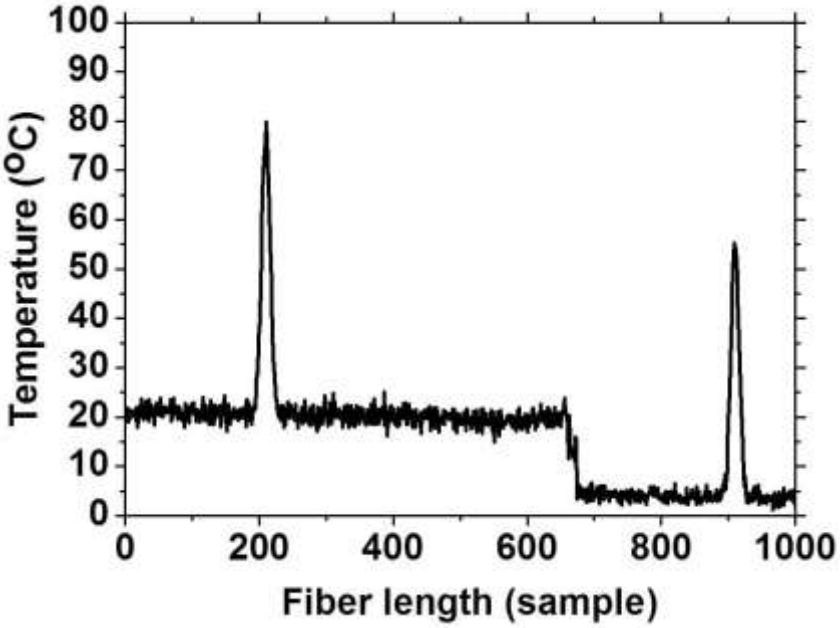


*Fig. 6.5. Distributed temperature profile for the bent fiber condition* (*On horizontal-axis, 10 samples ≡ 10 ns ≡ 1 m*).

### 6.2.2 Analytic signal representation of IMFs

As described in Section 5.4, EMD allows decomposition of any nonlinear and non-stationary time domain signal into a finite number of AM-FM oscillating components which are known as IMFs. The IMFs can be extracted from the signal using the so-called sifting process. A time domain signal *s(t)* can be represented as a sum of various IMFs and final residue in accordance with Eq. (5.3).

In digital signal processing, the analytic signal representation of a real signal *w(t)* can be found with the help of Hilbert transform [28, 37]. Hilbert transform *u(t)* of signal *w(t)* is defined as:

$$u(t) = w(t) * \frac{1}{\pi t} \tag{6.1}$$

The analytic signal *z(t)* of real time signal *w(t)* can be written as:

$$z(t) = w(t) + j\,u(t) \tag{6.2}$$

In exponential form, analytic signal is written as:

$$z(t) = I(t)e^{j\varphi(t)} \tag{6.3}$$

where, *I(t)* is the amplitude of analytic signal and is given by:

$$I(t) = |z(t)| = \sqrt{w^2(t) + u^2(t)} \tag{6.4}$$

and instantaneous phase *φ(t)* is given as:

$$\varphi(t) = arctan\left[\frac{u(t)}{w(t)}\right] \tag{6.5}$$

The instantaneous frequency, $f_i(t)$ can be found from instantaneous phase as:

$$f_i(t) = \frac{1}{2\pi}\frac{d\varphi(t)}{dt} \tag{6.6}$$

In the present work, it is proposed to apply the Hilbert transform on various IMFs obtained

by EMD process. This can be achieved by using various IMFs in place of *w(t)*. It is possible to reveal a meaningful feature [28] of the signal from the instantaneous frequency for following reasons: (a) it is well localized in the time-frequency domain, (b) IMFs are mono-components and locally symmetric functions.

For a discrete version of an IMF which is given by $I[n]\cos(\varphi[n])$, the analytic signal can be represented by:

$$z[n] = I[n]e^{j\varphi[n]} \tag{6.7}$$

Eq. (6.7) can be expanded as

$$z[n] = I[n]\cos(\varphi[n]) + jI[n]\sin(\varphi[n]) \tag{6.8}$$

### 6.2.3 Area of analytic signal as a feature for bend detection

EMD technique is applied on St signals which were obtained corresponding to normal fiber and bent fiber conditions. The first four IMFs (*IMF1-IMF4*) for normal fiber and bent fiber conditions are presented in Fig. 6.6 and 6.7 respectively.

Analytic signals for first four IMFs of St signal are obtained corresponding to normal fiber and bent fiber conditions according to the method described in Section 6.2.2. The obtained analytic signals are used to plot the traces in complex planes for above eight IMFs and are shown in Figs. 6.8 and 6.9 respectively. These traces are obtained by plotting imaginary part of the analytic signal *z[n]* (i.e. *u[n]*) against the real part of *z[n]* (i.e. *w[n]*). It may be noted from Figs. 6.8 and 6.9 that the form of the traces corresponding to IMFs is like rotating curves. The rotating curves for IMFs have a unique center which makes it possible to calculate the area of these curves [93-95]. The following two conditions are satisfied by

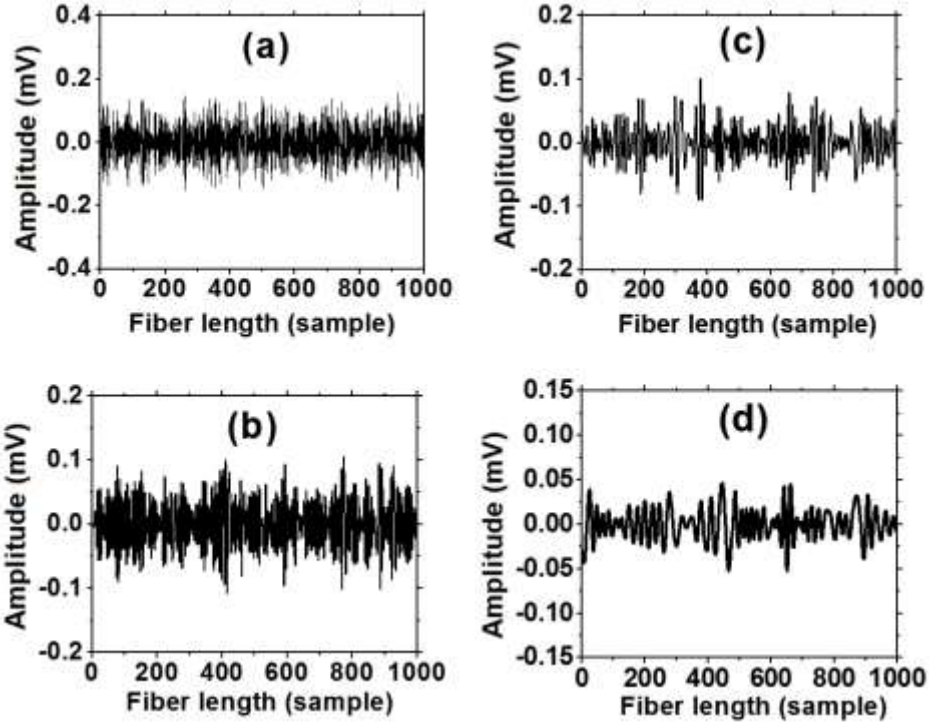


*Fig. 6.6. IMFs of St signal (normal fiber condition): (a) IMF1 (b) IMF2 (c) IMF3 (d) IMF4* (*On horizontal-axis, 10 samples ≡ 10 ns ≡ 1 m*).

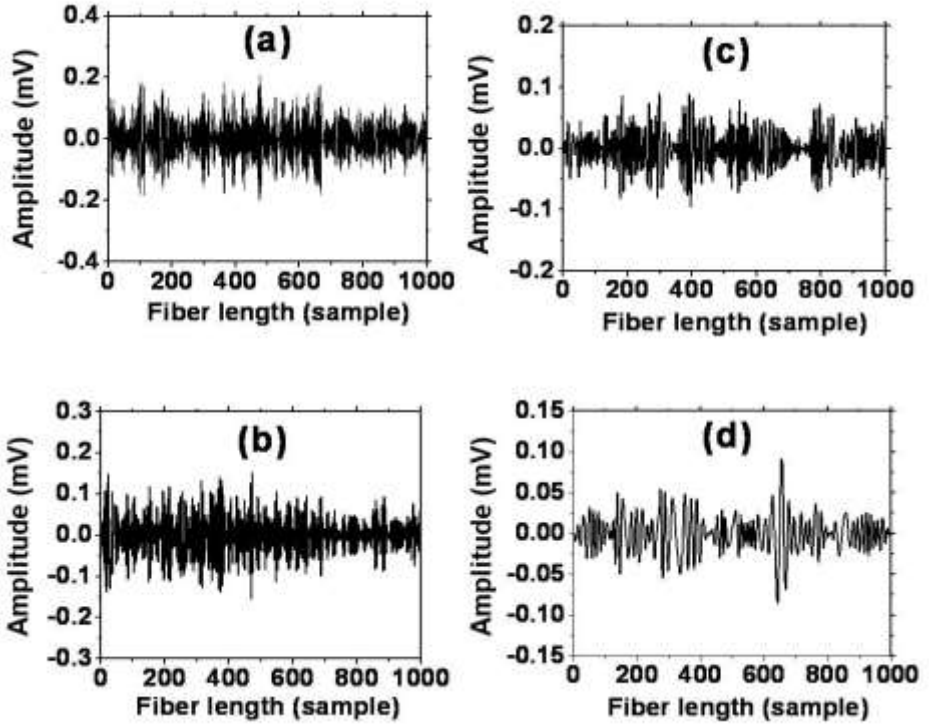


*Fig. 6.7. IMFs of St signal (bent fiber condition): (a) IMF1 (b) IMF2 (c) IMF3 (d) IMF4* (*On horizontal-axis, 10 samples ≡ 10 ns ≡ 1 m*).

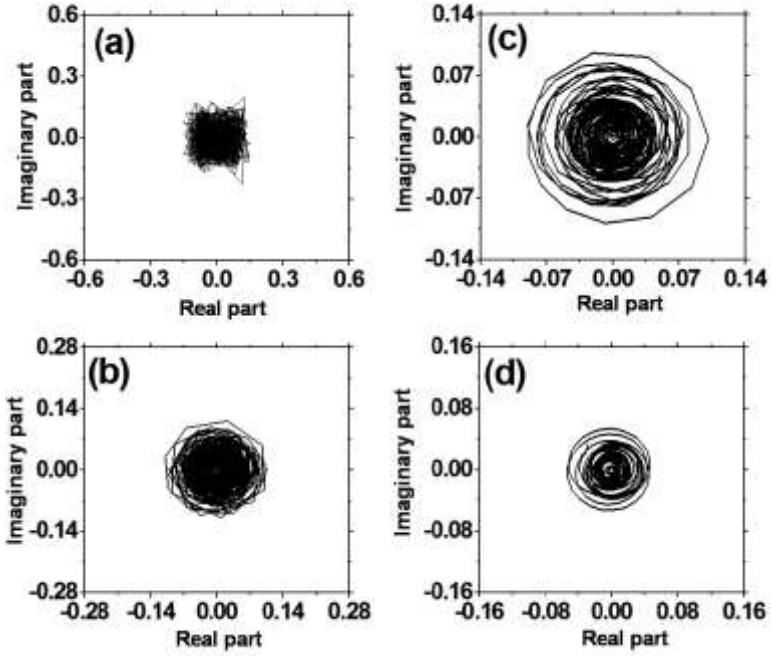


*Fig. 6.8. Complex plane traces for IMFs of St signal (normal fiber condition): (a) IMF1 (b) IMF2 (c) IMF3 (d) IMF4.*

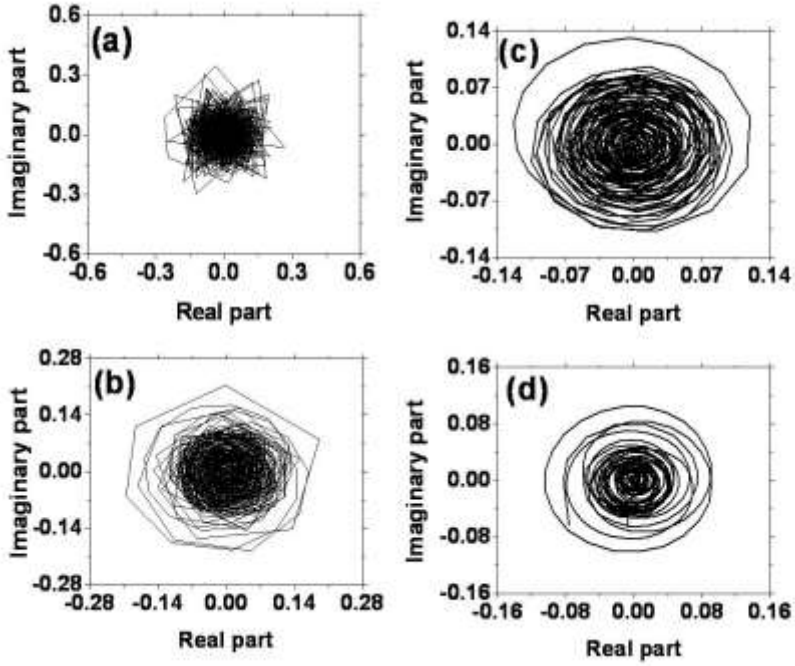


*Fig. 6.9. Complex plane traces for IMFs of St signal (bent fiber condition): (a) IMF1 (b) IMF2 (c) IMF3 (d) IMF4.*

these rotating curves: (a) the plot has a direction of rotation and (b) the rotation in the plot has unique center. Present work shows that the area measurement of rotating curves of analytic

form of IMFs in complex plane can be utilized for discrimination between normal fiber and bent fiber conditions. In other words, area measure can act as a visual indicator to detect the presence of a bend in fiber. Once bend is detected, its location can also be estimated from IMFs.

Central tendency measure (CTM) [99] has been used in literature to measure the degree of variability of various non-stationary processes like EEG signals [94], center of pressure signals [86] and vibration signals generated from a gear fault [84]. CTM presents visual information contained in plots. Earlier, CTM has also been used to determine the radius of the circle of analytic signal representation of IMFs for non-stationary signals in complex plane [93-95].

In order to calculate the CTM, a circular region of radius is selected around the origin. Then the number of points falling within that radius is divided by the total number of points to yield the CTM. In case, *N* is the total number of points and *r* is the radius of the central area then, the CTM for analytic signal *z[n]* can be expressed using following relation [94].

$$CTM = \frac{\sum_{k=1}^{N} \Delta(d_k)}{N} \tag{6.9}$$

where,

$$\Delta(d_k) = \begin{cases} 1 \; if \; |z| < r \\ 0 \; otherwise \end{cases} \tag{6.10}$$

In Eq. (6.10), $\Delta(d_k)$ is a function of $|z|$ which is expressed as:

$$|z| = \left(\{w[n]\}^2 + \{u[n]\}^2\right)^{0.5} \tag{6.11}$$

In the present work, area parameters are calculated using the radii of the circles shown in Fig.

6.8 and Fig. 6.9. In each case, $|z|$ was estimated first, then radius value was gradually increased and corresponding CTM (%) for each value was calculated using Eq. (6.9). Radius value, for which CTM value is found to be 95%, has been chosen to calculate area parameter. The 95% value of CTM means that the area parameter has enclosed 95% samples of the signal which makes it a reliable and significant parameter.

A data set containing total 100 versions of St signals corresponding to normal fiber and bent fiber situations (can be termed as 'classes' more appropriately) were recorded to check the class discriminating ability of area parameter. Table 6.1 summarizes the area parameters (minimum, median, maximum) for data set corresponding to each class using various IMFs (*IMF1-IMF4*). It may be observed from Table 6.1 that the computed area has smaller values for normal fiber compared to bent fiber. The bent fiber condition might have more area because of the sudden transition in time domain St signal which results in increased

**Table 6.1**

Data set of area (a.u.) parameter for analytic signal representation of IMFs, in (minimum, median, maximum) format, calculated for St signal.

| Fiber Condi-tion | Area (a.u.) Parameter using | | | |
|---|---|---|---|---|
| | IMF1 (min., med., max.) | IMF2 (min., med., max.) | IMF3 (min., med., max.) | IMF4 (min., med., max.) |
| Normal | (64.6, 71.8, 79.7) $\times 10^{-3}$ | (19.6, 25.5, 33.3) $\times 10^{-3}$ | (8.7, 13.7, 18.9) $\times 10^{-3}$ | (4.7, 6.4, 9.3) $\times 10^{-3}$ |
| Bend | (123, 138.6, 145) $\times 10^{-3}$ | (39.7, 47.9, 56.7) $\times 10^{-3}$ | (16.8, 24.7, 38.3) $\times 10^{-3}$ | (9.5, 17.8, 27.5) $\times 10^{-3}$ |

maximum value of IMFs. The reason for above observation can be explained by the following physical link between bent fiber condition and area parameter. When a fiber undergoes a bend, it offers more loss for transmitting photons compared to a normal fiber because a bent fiber has lesser critical angle compared to normal fiber. The reduced critical angle causes leakage of photons transmitting through the bent fiber [4]. The leakage of photons in a bent fiber causes increased loss to St signals and thus a discontinuity in time-domain St signal is observed. The discontinuity in time-domain St signal results in increased maximum values of IMFs, analytic IMFs and finally in increased area parameter. The increased area parameter indicates that a bend has been detected. Also, the increased value in IMF is indicated by a peak which is localized at the location of bend and helps identify the location of bend. Further, Kruskal-Wallis statistical test (KWST) [100] has been used to test the class discriminating ability of area as feature. KWST is a non-parametric one-way analysis of variance (ANOVA) method and has been used in MATLAB platform to obtain box plots of area parameter for two classes viz. normal fiber (N) and bent fiber (B) conditions. The class discriminating ability of a parameter is characterized by the probability $p$ obtained from KWST. The area parameter values are said to be significantly different for two classes and can be utilized for discrimination if $p < 0.01$. The box plots of area parameter calculated for two classes (viz. normal and bent) using IMF1-IMF4 are depicted in Fig. 6.10.

It is observed that for different IMFs (IMF1-IMF4), $p <<< 0.01$. However, since IMF4 witnesses the signature (i.e. peak) of the bend most clearly [Fig. 6.7(d)] around sample number 655 (i.e. at 65.5 m location); it is selected for area parameter calculation. Therefore, in final algorithm IMF4 will be used for detection of bend in fiber. Rest of the IMFs i.e. IMF5-IMF8 do not show the signature of bend (i.e. peak) at correct sample number. For example, IMF5 has a peak at 668 sample number indicating the incorrect location of bend at 66.8 m. Similarly, IMF6, IMF7 and IMF8 indicate the incorrect bend location at 71.2 m,

72.5 m and 88.0 m respectively. That is why among all IMFs, IMF4 has been chosen for bend detection. Residue (RM) of bent St signal is the lowest frequency part of the signal and does not witness any signature of bend and hence was not considered for detection of bend.

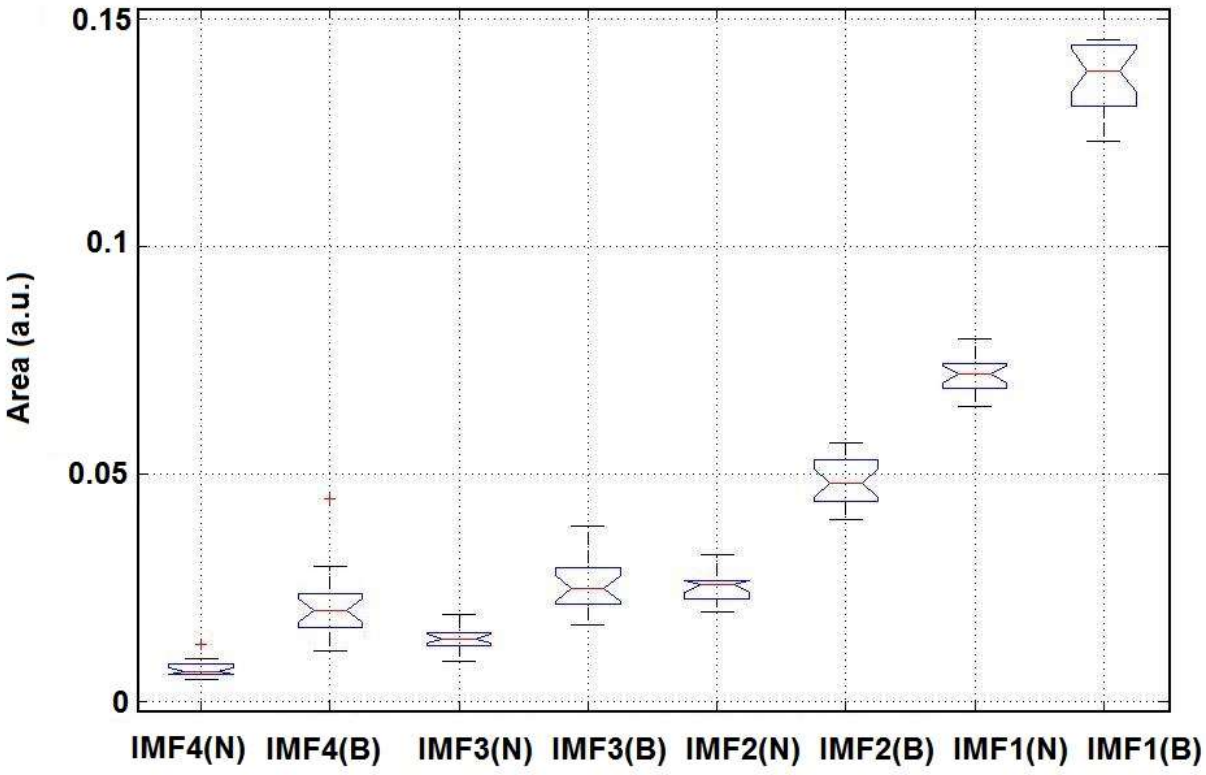


*Fig. 6.10. Comparison of box plots for area parameter of IMF1-IMF4 for normal fiber (N) and bent fiber (B) conditions.*

### 6.2.4 Proposed methodology

The proposed methodology consists of four stages. In first stage, presence of bend in St signal is detected. In second stage, the location of bend is estimated. Third stage involves the selection of new calibration zone and installation of second DSCU (i.e. DSCU 2). Finally, in fourth stage the correct distributed temperature profile of the whole fiber length including the sensing fiber that exists after the bend is obtained.

*(a) First stage:*

First of all, a data set of area parameter corresponding to normal fiber and bent fiber condition is prepared by recording the St signal for 100 times which are represented by $I_{normal}$ and $I_{bent}$ respectively. In the present study, $I_{normal}$ and $I_{bent}$ represent area parameters in the range of 0.0047-0.0093 and 0.0095-0.0275 using IMF4. On every measurement of complete distributed temperature profile (*TP*), the St signal is measured and analyzed during two consecutive measurements. In case, during two consecutive measurements, the later one corresponds to bent fiber (denoted as $St_{bent}$) and the previous one corresponds to normal fiber (denoted as $St_{normal}$) then two St signals can be automatically discriminated using following proposed algorithm:

(i) Obtain 4th IMF (represented as $IMF_{normal}$) of $St_{normal}$ *signal.*

(ii) Obtain Hilbert transform ($u_n$) of $IMF_{normal}$.

(iii) Obtain analytic signal, $z_n[n]$ corresponding to $IMF_{normal}$.

(iv) Plot and calculate area ($A_{normal}$) of the rotating curves of $z_n[n]$.

(v) Now repeat step (i)-(iv) for $St_{bend}$ signal and calculate area ($A_{bent}$).

(vi) Test following conditions using $A_{bent}$ and $A_{normal}$.

Check whether $A_{bend} > A_{normal}$, $A_{bend} \in I_{bend}$ and $A_{normal} \in I_{normal}$ are true. If results of all these conditions are found true, a bend is said to be present. Raise the warning message for the user that a bend has occurred and the measured temperature profile (*TP*) is incorrect. On the other hand, if above conditions are false, no bend is said to be detected and temperature profile for the complete fiber length (*TP*) can be easily calculated using Eq. (3.10) with the help of temperature ($\theta_1$), ratio value $R_{\theta 1}(=AS/St)$ for calibration loop 1 (1 m long) and ratio $R_T$ $(=AS/St)$ profile for complete fiber length from 0-100 m. There is no need to follow second, third and fourth stage.

*(b) Second stage:*

If a bend is detected, the temperature profile for the complete fiber length (*TP*) would be incorrect. In such a case temperature profile of fiber zones existing before and after the bend location should be calculated separately. If the temperature profile for the fiber length upto the location of the bend is represented by $TP_1$ and the temperature profile for the fiber zone existing after the fiber is represented by $TP_2$ then correct *TP* can be obtained by concatenating the profiles $TP_1$ and $TP_2$. In the presence of a bend, $TP_1$ and $TP_2$ are to be calculated separately using Eq. (3.10) after slope minimization of AS and St signals [34]. For calculation of $TP_1$, temperature ($\theta_1$), ratio value $R_{\theta 1}(=AS/St)$ for calibration loop 1 (1 m long) and $R_T$ (=*AS/St*) for fiber length from 0-65 m (in case bend is deteted at 65 m) will be used in Eq. (3.10). However, for calculation of $TP_2$, temperature $\theta_2$ obtained from DSCU 2, ratio value $R_{\theta 2}$ (=*AS/St)* for calibration loop 2 (which is 1 m long) and $R_T$ (=*AS/St*) for rest of the fiber length (e.g. 65-100 m) will be used in Eq. (3.10). Once, the presence of bend is detected, it is necessary to find the location of the bend. The location of the bend is estimated using following proposed algorithm:

(i) Obtain 4th IMF ($IMF_{normal}$) of $St_{normal}$ *signal.*

(ii) Obtain 4th IMF ($IMF_{bend}$) of $St_{bent}$ signal.

(iii) Calculate the difference IMF ($IMF_d$) given by $IMF_d = IMF_{bent} - IMF_{normal}$.

(iv) Find out the location, $R_{max}$ (*in sample No.)* where maximum value of $IMF_d$ occurs.

(v) Convert $R_{max}$ to fiber length, *L (m) u*sing following expression

$$L = \frac{c.R_{max}}{2nS} \tag{6.11}$$

where, *c* is the speed of light in vauum (=3 ×$10^8$ m/s ), *n* (=1.5) is the refractive index of the fiber core and *S* is the sampling rate (=1GSamples/s) of the DAQ system.

(vi) Estimate correct temperature profile $TP_1$ using $\theta_1$ with the help of Eq. (3.10) for further use and discard $TP_2$.

*(c) Third stage:*

It involves the proper choice of the location of an additional new calibration loop. The new calibration loop can be chosen at ($L+3.5$) m with a loop length of 1 m. The temperature profile of the section (~3.5 m) around bend remains ambiguous due to the transition in AS and St signals at bend position. For this reason, the new calibration loop may be been chosen at ($L+3.5$) m. The tip of temperature senor of new dynamic self calibration unit (DSCU 2) is located at new calibration loop to obtain $\theta_2$. Once the location of additional new calibration zone is determined it remains fixed for further usage.

*(d) Fourth stage:*

It follows following algorithm:

(i) Obtain the value of $\theta_2$, ratio value ($R_{\theta 2}$) for calibration loop 2 and $R_T$ (=$AS/St$) for fiber length from ($L+3.5$)-100 m. Use Eq. (3.10) to obtain the correct distributed temperature profile $TP_2$ separately.

(ii) Concatenate $TP_1$ and $TP_2$ to obtain correct distributed temperature profile ($TP$) for complete fiber length.

MATLAB software has been used for above processing including the estimation of IMFs from EMD and analytic signal representation.

### 6.2.5 Results and discussion: Distributed temperature profile with and without proposed technique

For the present experiment, the values of $A_{normal}$ and $A_{bent}$ are found to be $7.1\times10^{-3}$ and $20.3\times10^{-3}$ respectively which indicate that a bend in the fiber is present. The circles with increased radii in Fig. 6.9 act as visual indicator for bent fiber condition. The value of $\theta_2$ was measured to be 21.5 °C with DSCU 2. The location of bend ($R_{max}$) was found to be sample number 655 which when converted into $L$ (m) using Eq. (6.11) indicates that bend has occurred at 65.5 m. The detected location of bend is approximately same as the known location of bend (65 m). The location of calibration loop 2 was chosen at 69 m. Fig. 6.11 presents the corrected distributed temperature profile (upper curve, red colour) of complete fiber length for bent condition, obtained by the proposed methodology. The incorrect temperature profile (earlier shown in Fig. 6.5) which was obtained without using proposed methodology is also shown (lower curve, black colour) in Fig. 6.11 for comparison.

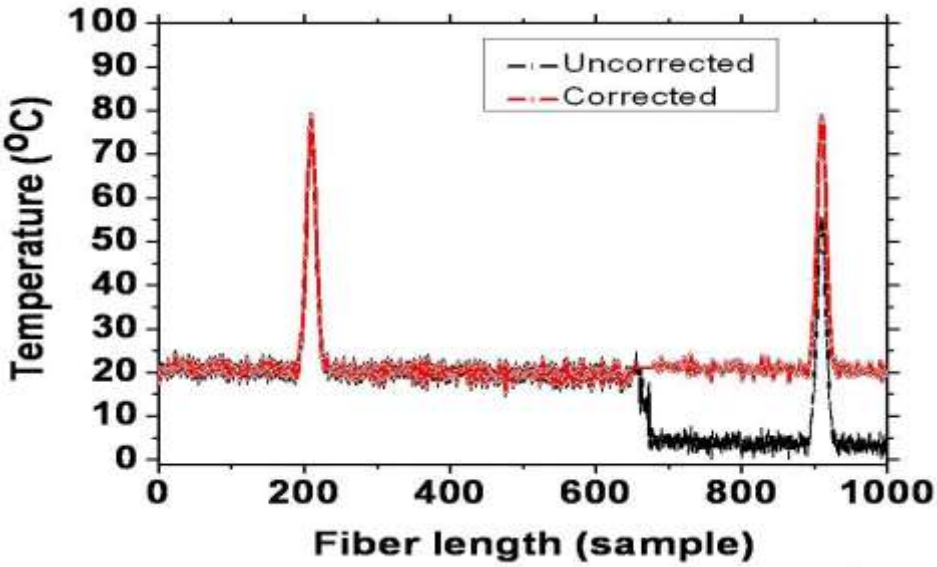


*Fig. 6.11. The distributed temperature profile for bent fiber condition. Upper (red colour) curve shows the corrected profile obtained with proposed methodology whereas lower (black colour) curve shows the uncorrected profile* (*On horizontal-axis, 10 samples ≡ 10 ns ≡ 1 m*).

Table 6.2 summarizes the results of temperature measurement. In the corrected temperature profile, the reference temperature (80 °C) of the hot zone 2 is measured to be 77.7 °C with an error of -2.3 °C (-2.8%). The temperature of rest of the fiber that exists after the bend (at 65 m) is measured with maximum error of ±3 °C. On the other hand, without using the proposed methodology, the measured temperature values of hot zone-2 and rest of the fiber existing after the bend were measured with a large error of -24 °C (-30%) and -17 °C (-77.2%) respectively. It is clear that the proposed methodology effectively reduces the error in

**Table 6.2**

Comparison of error in measured temperature values with and without proposed methodology in a sensing fiber of 100/125 μm size having a bend at 65 m location.

| Zone (Location, m) | Reference temperature | Measured temperature | |
|---|---|---|---|
| | | Without proposed methodology | With proposed methodology |
| Start of the fiber (Location: 0 m) | 21 °C | 23 °C | 23.5 °C |
| | Error | 2 °C (-9.5%) | 2.5°C (- 11.9%) |
| Hot zone 1 (Location: 21 m) | 80 °C | 77 °C | 78 °C |
| | Error | -3 °C (- 3.7%) | -2 °C (- 2.5%) |
| Hot zone 2 (Location: 91 m) | 80 °C | 56 °C | 77.7 °C |
| | Error | -24 °C (- 30%) | -2.3 °C (- 2.8%) |
| Between hot zone 2 & bend (Location: 70 m) | 21.5 °C | 6 °C | 23 °C |
| | Error | -15.5 °C (- 72%) | 1.5 °C (6.9%) |
| End of the fiber (Location: 100 m) | 22 °C | 5 °C | 20 °C |
| | Error | -17 °C (- 77.2%) | -2 °C (- 9%) |

temperature measurement for the fiber zone existing after the bend. However, the temperature profile in the close vicinity of the bend location is still ambiguous. This is because some fiber length is sacrificed around the bend because of the transition and associated noise in AS and St signal levels for which temperature estimation is difficult. The proposed methodology was verified for different temperatures of hot zone 2 in the range of 21-100 ºC. Also, the laser power was varied by ±20% to cause variation in AS and St signal levels. The proposed methodology was able to detect the presence of bend and correct the error in temperature profile measurement even with such variations in laser power.

DWT of a non-stationary signal also decomposes it into several approximation and detail components. The improved version of DWT called complex dual tree DWT (ℂWT) [101] is implemented as two separate two-channel filter banks. The lowpass (scaling) and highpass (wavelet) filters of one tree must generate a scaling function and wavelet that are approximate Hilbert transforms of the scaling function and wavelet generated by the lowpass and highpass filters of the other tree. Therefore, the complex-valued scaling function and wavelet formed from the two trees are approximately analytic. On the basis of above discussion, there appears a possibility of using these components in lieu of IMFs for detecting bend in sensing fiber.

However, EMD based IMFs are always monocomponents of AM-FM nature whereas DWT based components need not be of above nature all the time. The AM-FM nature of IMF and the two conditions [28] of being IMF make sure that circular pattern of analytical form of an IMF in complex plane has a circular symmetry and unique centre. This property in turn makes it possible to calculate the area parameter of that IMF. On the other hand, in case of DWT and ℂWT based decomposition it is not guaranteed that components will definitely be of AM-FM nature and follow the conditions of an IMF. Therefore, DWT is not very

attractive for finding the area parameter in complex plane and has not been used as a feature for detection of bend.

Similarly, STFT also can not be used for automatic detection of bend from a St signal. This is because in STFT, a window has to be manually chosen by the operator of OFDTS in such a manner that discontinuity in St signal caused by bend appears well within the window. Fourier transform of that window where bend condition appears will have different frequency component compared to normal fiber condition and will help discriminate the bend condition from normal one. However, STFT requires a careful, vigilent and experienced operator for identifying bend from St signal and therefore, is not very attractive for bend detection in an automated version OFDTS. Moreover, STFT is one sort of Fourier transform which will convert St signal into frequency domain and loses the time information. The time information is related to spatial location of bend through OTDR relation given by Eq. (3.8). Therefore, STFT will not be able to yield the correct location of bend. It will only indicate that the location of bend in within the width of window. Thus STFT will only gauge the gross location of bend. For above mentioned reasons, STFT is not a viable option for bend detection in OFDTS.

### 6.3 Summary

In this Chapter, a technique based on area parameter of analytic version of IMFs corresponding to St signal has been proposed to detect the presence of bend in sensing fiber. The area parameter serves as a feature and also acts as a visual indicator to alert the operator in real time against any temperature measurement error caused by the bend. Such an error if not detected automatically could easily be missed by a human operator and may result in

false temperature alarms. The area parameter provided statistically significant difference between normal and bent fiber conditions. Installation of second DSCU has made it possible to correct the errors in temperature profile measurement for the fiber section existing after the bend.

In future, the nature of fiber loss whether it is due to bend, tension, compression or poor splice can be classified using a more sophisticated classifier like artificial neural network and support vector machine etc. It would be of interest to compare the various classification techniques in order to obtain the better classification accuracy. More features are required to be extracted for this purpose and is a subject matter of future studies. Study related to a new parameter that corresponds to instantaneous (i.e. at each sample) value of area of analytic form of IMF for St signal may be carried out. Such a parameter should alone be sufficient to detect both the ‘presence’ and ‘location’ of bend in the sensing fiber.

# Chapter 7

# Conclusion and scope for future work

## 7.1 Conclusion

Apart from their application in communication, the optical fibers have opened a completely new and vibrant field of distributed sensing technology. In this thesis, non-stationary signal processing models to address various issues encountered in the development of Raman scattering based OFDTS have been extensively investigated. The various issues dealt in the thesis are dynamic self calibration, fiber attenuation difference for AS and St signals, their denoising without causing any spatial inaccuracy in location of hot zone information and automatic detection of bend induced error. The various non-stationary signal models which have been used are based on STFT, DWT and EMD. Out of these the EMD based model is most automation friendly as no basis function needs to be assumed. On the other hand, DWT based processing provides better denoising of Raman AS and St signals. STFT based processing model is the simplest one. However, STFT based technique does not support efficient denoising of AS and St signals and also is least automation friendly. The processing time taken by EMD technique is ~1.47 times of wavelet based technique. Also, it is observed that the error in temperature measurement by EMD technique is ± 5.5 °C compared to ± 3.5 °C in wavelet based technique over temperature range of 25-300 °C for the OFDTS developed in the present experiment.

A prototype OFDTS using optical fibers of various core/clad size, signal processing techniques and data acquisition methods was developed for laboratory as well as field applications. The developed OFDTS was demonstrated with a maximum temperature

accuracy of ± 3.5 °C over temperature range of 25-300 °C with processing time of 110 s using wavelet based technique. Spatial resolution of 1 m was obtained over the fiber length of 220 m. Better accuracy and less processing time can be achieved with better DAQ system. An improvement in spatial resolution can be obtained by using a laser source of smaller pulse width. A fiber sensor based distributed zone-specific temperature alarm system for generating audio-visual alarms in control room was also designed and developed using OFDTS, microcontroller and relay based circuitry. The design of alarm system opens the possibilities of a new optical fiber based distributed P-I-D temperature controller.

The thesis has also presented an EMD based novel technique for automatic and dynamic detection of the error caused by presence of a bend in the sensing fiber of an OFDTS. Presence of the bend is estimated by using the area parameter of analytic form of IMFs extracted from St signal. Area parameter is utilized as a feature for discrimination between normal fiber and bend fiber conditions. Also, a method to compensate the error was evolved by employing second calibration loop after the detected bend that allows correct distributed temperature profile even with the existence of bend.

## 7.2 Scope for future work

Based on the achievement of present work, it would be interesting to extend it in the several new directions. Following studies as listed below are envisaged.

1. One of the major issues in the development of OFDTS is its temperature resolution which is governed by SNR of backscattered Raman AS and St signals. Wavelet based image processing is being used to obtain significant improvement in SNR of backscattered signals

[53]. EMD based image processing of Raman backscattered AS and St signals can also be proved to be of great importance in improving the temperature resolution of OFDTS.

2. There has been a lot of interest in enhancing spatial resolution of OFDTS. Spatial resolution of OFDTS primarily depends on pulse width of laser source and refractive index of the sensing fiber's core. However, use of pulse width lesser than a finite time duration results in undesired non-linear effect like stimulated Raman scattering. Changing the refractive index of the fiber core has been reported very recently but is a difficult to apply solution [66]. In literature, several studies have been reported that allow better spatial resolution without any reduction in pulse width of laser source. Such techniques include use of new algebraic algorithms [102] and deconvolution theories [50-52]. Empirical mode decomposition technique introduced in this thesis in conjunction with deconvolution theory can be exploited for spatial resolution enhancement of the developed OFDTS without opting low pulse width lasers.

3. Any undesired fiber event like fiber bend, break in fiber, point of high reflectance due to splice or connector loss causes error in distributed temperature profile obtained from OFDTS. The nature of fiber event, whether it is due to bend, tension, compression or poor splice can be classified by employing more sophisticated classifiers like artificial neural network and support vector machine. Such information would help rectify the cause of error in a faster manner. More features from AS and St signals would be required for comparing classification accuracy of various classifiers.

4. A new parameter called 'instantaneous area' may be drived from St signal which alone would be sufficient to detect both the 'presence' and 'location' of bend in the sensing fiber.

# Appendix A

# Short term Fourier transform

Since Fourier transform does not work for non-stationary signals, it is possible to assume that some portion of a non-stationary signal is stationary and apply conventional Fourier transform. If the region where the signal can be assumed to be stationary is too small, then a narrow window is used, narrow enough that the portion of the signal seen from these windows are indeed stationary. This approach of researchers ended up with a revised version of the Fourier transform and is known as short term Fourier transform (STFT) [22-24].

## A.1 Fundamental concepts and an overview of the short term Fourier transform

There is only a minor difference between STFT and Fourier transform. In STFT, the signal is divided into several small segments, where these segments of the signal can be assumed to be stationary. For this purpose, a window function *'w'* is chosen. The width of this window must be equal to the segment of the signal where its stationarity is valid. The window function, having width $T$, is first located to the very beginning of the signal. That is, the window function is located at $t = 0$. At this time instant ($t=0$), the window function will overlap with the first $T/2$ seconds. The window function and the signal are then multiplied. By doing this, only the first $T/2$ seconds of the signal is being chosen, with the appropriate weighting of the window. If the window is a rectangle, with amplitude 1, then the product will be equal to the signal. Then this product is assumed to be just another signal for which Fourier transform is to be computed. The result of this transformation is the Fourier transform of the first $T/2$ seconds of the signal. If this portion of the signal is stationary, as it is assumed, then there will be no problem and the obtained result will be a true frequency representation of the first

*T/2* seconds of the signal.

The next step would be shifting this window (for $t_1$) to a new location, multiplying with the signal, and taking the Fourier transform of the product. This procedure is followed until the end of the signal is reached by shifting the window with $t_1$ seconds intervals.

The following definition of the STFT summarizes all the above explanations in one line:

$$STFT_x^w(t',w) = \int [x(t).w(t-t')].e^{-j\omega t}dt \qquad \text{(A.1)}$$

In Eq. (A.1), *x(t)* is the signal itself and *w(t)* is the window function. As seen from the expression, the STFT of the signal is nothing but the Fourier transform of the signal multiplied by a window function. For every *t'* and $\omega$ a new STFT coefficient is computed. Fig. A.1 explains the procedure of STFT in more detail.

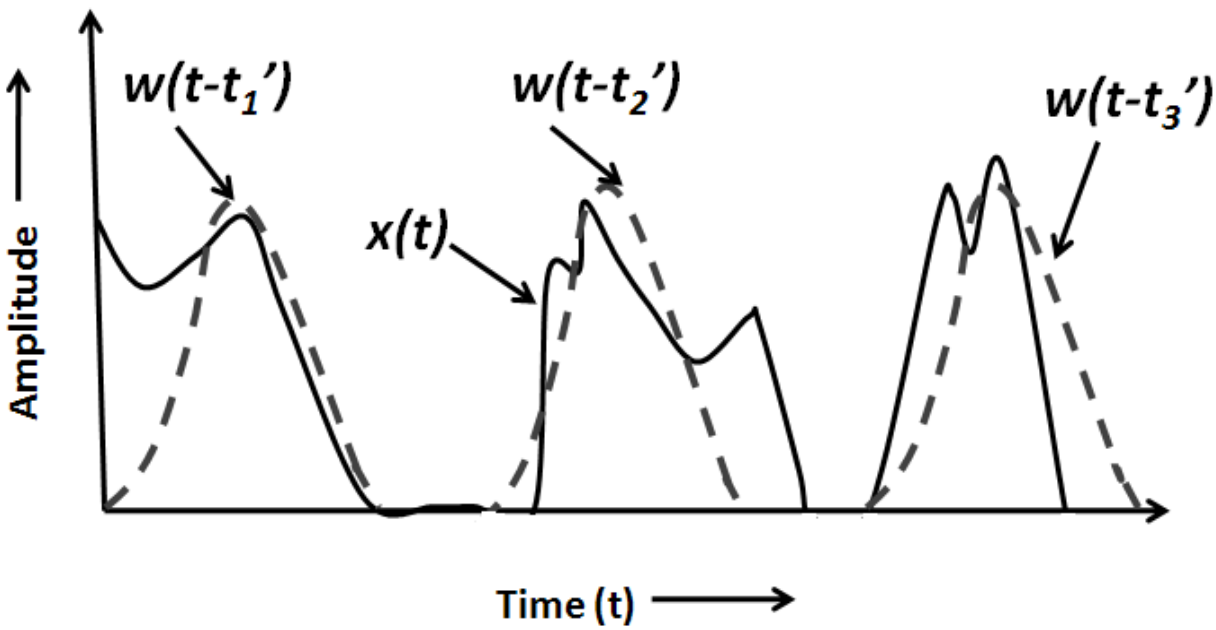


*Fig. A.1. STFT process as windowing Fourier transform [22].*

The Gaussian-like functions *(w)* are the windowing functions. The first window shows the window located at $t = t_1'$, the second one shows $t = t_2'$, and the third one shows the window located at $t = t_3'$. These will correspond to three different Fourier transforms at three different times. Therefore, a true time-frequency representation of the signal may be obtained. STFT is a function of time and frequency (unlike Fourier transform, which is a function of frequency only), the transform would be two dimensional.

### A.2 Short term Fourier transform and spectrogram

To study the properties of the signal at time *t*, it is necessary to emphasize the signal at that time and suppress the signal at other times. This is achieved by multiplying the signal by a window function, *h(t)*, centered at *t*, to produce a modified signal,

$$s_t(\tau) = s(\tau)h(\tau - t) \tag{A.2}$$

The modified signal is a function of two time factors, the fixed time *t* and the running time $\tau$. The window function is chosen to leave the signal more or less unaltered around the time *t* but to suppress the signal for times distant from the time of interest. That is,

$$s_t(\tau) = \begin{cases} s(\tau) & for\ \tau\ near\ t \\ 0 & for\ \tau\ far\ from\ t \end{cases} \tag{A.3}$$

The term 'window' comes from the idea that only a small piece of the signal is being checked. Since the modified signal emphasizes the signal around the time *t*, the Fourier transform will reflect the distribution of frequency around that time and is given as,

$$S_t(\omega) = \int s_t(\tau) . e^{-j\omega\tau} d\tau \tag{A.4}$$

$$= \int s(\tau)h(\tau - t) . e^{-j\omega\tau} d\tau \tag{A.5}$$

The energy density spectrum at time *t* is, therefore

$$P_{SP}(t,\omega) = |S_t(\omega)|^2 = \left|\int s(\tau)h(\tau - t)\,.e^{-j\omega\tau}d\tau\right|^2 \quad \text{(A.6)}$$

For each different time, a different spectrum is obtained and totality of these spectra is the time-frequency distribution, $P_{SP}$. It goes under many names, depending on the field, the most common phraseology being 'spectrogram'.

Since here interest is to analyze the signal around the time *t*, a window function that is peaked around *t*, was chosen. Hence the modified signal is short and its Fourier transform, given by Eq. (A.5) is called short-term Fourier transform.

For example, the spectrogram of the signal, *s(t)* (plotted in Fig. A.2)

$$s(t) = e^{j\,2\pi f t}e^{-\frac{at^2}{2}} \text{ for } f = 10 \text{ Hz and } a = 1 \quad \text{(A.7)}$$

is as shown in Fig. A.3.

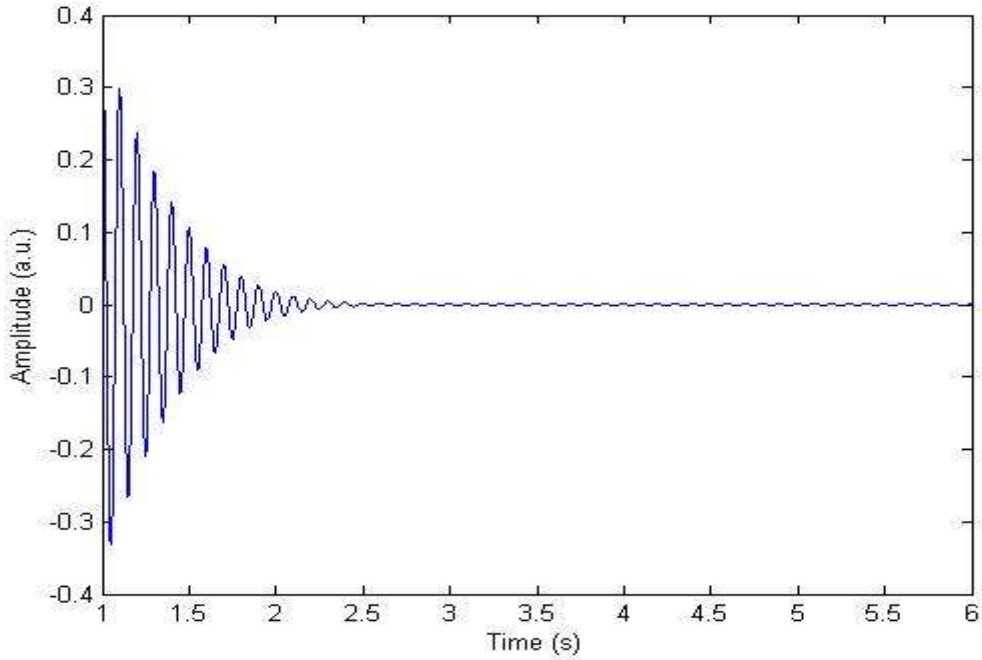


*Fig. A.2. Signal s(t) expressed by Eq.(A.7).*

Following MATLAB program was used to draw spectrogram.

```
%% MATLAB program for drawing Spectrogram
t= 1:0.001:6;
s= [exp (j*2*pi*10*t).*exp (-1.*t.*t)];
plot (t, s)
figure; spectrogram(s,128,120,128,1e3);
%where arguments are in following order
%spectrogram(x, window, noverlap, nfft, sampling frequency);
%% End of MATLAB program %%
```

Spectrogram in Fig. A.3 is with rectangular windows of size 128 points.

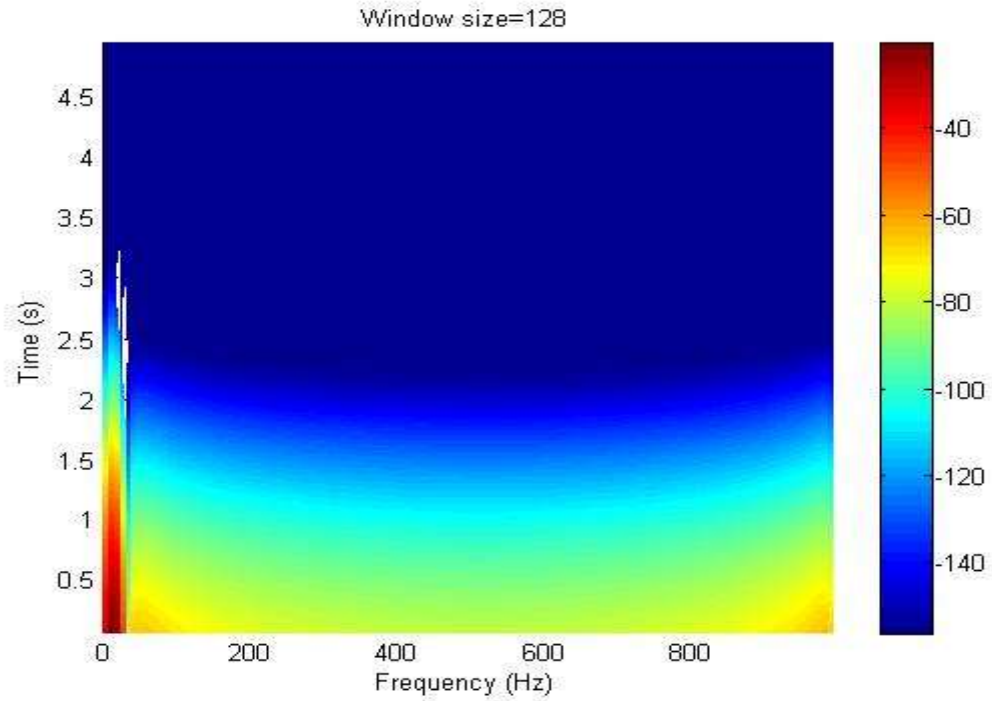


*Fig. A.3. Spectrogram of s(t) with window size 128.*

Similarly, with window size of 256 and 512 spectrograms as shown in Fig. A.4 and Fig. A.5 respectively are obtained.

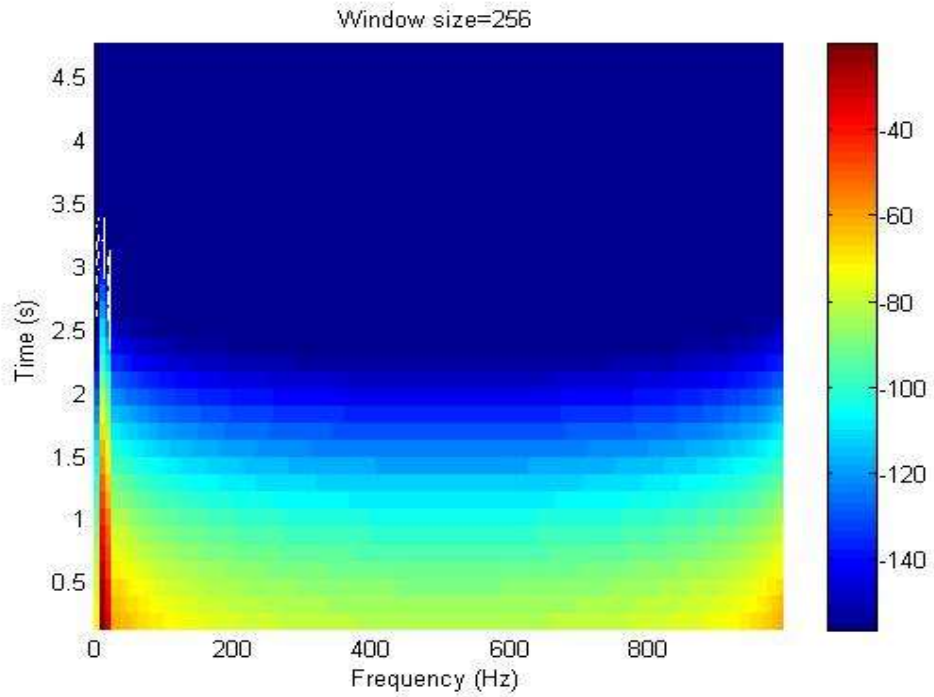


*Fig. A.4. Spectrogram of s(t) with window size 256.*

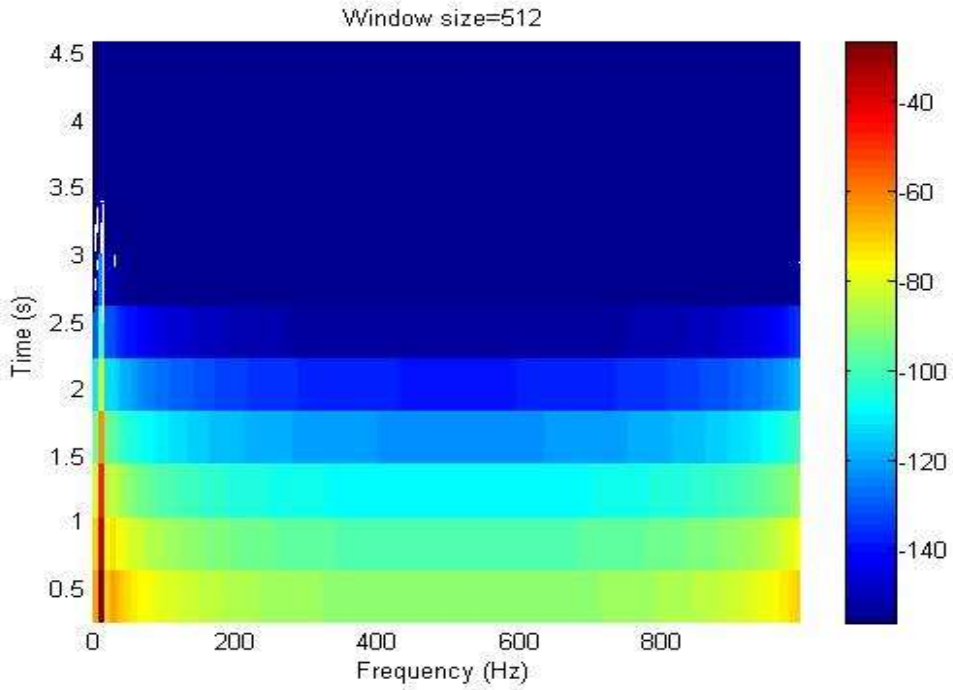


*Fig. A.5. Spectrogram of s(t) with window size 512.*

From comparison of above three figures, it is clear that as window size increases, time localization becomes poor but frequency localization improves.

### A.3 Limitations of short term Fourier transform

The problem with STFT is the fact which finds its roots in the Heisenberg uncertainty principle. This principle was originally applied to the momentum and location of moving particles and can also be applied to time-frequency information of a signal. The principle states that one cannot know the exact time-frequency representation of a signal, i.e., one cannot know what spectral components exist at what instances of times. What one can know only the time intervals in which certain band of frequencies exist and is a resolution problem.

The problem with the STFT has something to do with the width of the window function used. In Fourier transform there is no resolution problem in the frequency domain, i.e., it is possible to know exactly what frequencies exist; similarly there is no time resolution problem in the time domain, since the value of the signal at every instant of time is known. Conversely, the time resolution in Fourier transform, and the frequency resolution in the time domain are zero, since there is no information about these parameters. Poorer frequency resolution means it is difficult to know the exact frequency components that exist in the signal, but it is possible to only know a band of frequencies that exist.

In Fourier transform, the kernel function, allows to obtain perfect frequency resolution, because the kernel itself is a window of infinite length. In STFT, window is of finite length and does not allow having perfect frequency resolution. On the other hand making the length of the window in the STFT infinite, just like as it is in the FT, to get perfect frequency resolution, results in loss of all the time information. This basically ends up with Fourier

transform instead of STFT. In brief in signal processing following dilemma is faced.

With use of a window of infinite length, the obtained Fourier transform gives a perfect frequency resolution, but no time information. Furthermore, in order to obtain the stationarity, it is required to have a short enough window, in which the signal is stationary. The narrower the window, the better the time resolution, and better the assumption of stationarity, but poorer the frequency resolution:

In brief: Narrow window $\Longrightarrow$ Good time resolution, poor frequency resolution.

Wide window $\Longrightarrow$ Good frequency resolution, poor time resolution.

The short term Fourier transform is nothing but windowed Fourier transform assuming signal under consideration to be stationary. The main limitation of the short term Fourier transform is the fixed resolution in time-frequency domain that can be modulated with new technique called wavelet transform.

# Appendix B

# Continuous wavelet transform

The aperiodic, noisy, intermittent, transient signals are the type of signals for which wavelet transforms are particularly useful. Wavelets have special ability to examine signals simultaneously in both time and frequency. This has resulted in the development of a variety of wavelet based methods for signal manipulation and interrogation. Current applications of wavelet include climate analysis, financial time series analysis, heart monitoring, condition monitoring of rotating machinery, seismic signal denoising, denoising of astronomical images, crack surface characterization, characterization of turbulent intermittency, audio and video compression, compression of medical and thumb impression records, fast solution of partial differential equations, computer graphics and so on. All of these applications require wavelet transform.

Many a times, a particular spectral component occurring at any instant can be of particular interest. In these cases it may be very beneficial to know the time intervals these particular spectral components occur. For example, in EEGs, the latency of an event-related potential is of particular interest (Event-related potential is the response of the brain to a specific stimulus like flash-light, the latency of this response is the amount of time elapsed between the onset of the stimulus and the response.). Wavelet transform is capable of providing the time and frequency information simultaneously with flexible resolution rather than being fixed as in case of short time Fourier transform (STFT).

## B.1 Fundamental concepts and overview

The analysis of an analytical signal which has frequencies up to 1000 Hz, can be obtained in the way described here. In the first stage it is divided up in to two parts by passing the signal from a high-pass and a low pass filter which results in two different versions of the same signal: portion of the signal corresponding to 0-500 Hz (low-pass portion), and 500-1000 Hz (high-pass portion) Then, either portion (usually low pass portion) or both, is taken and the same thing is done again. This operation is called decomposition**.** Assuming that the low pass portion is taken, three sets of data are obtained, each corresponding to the same signal at frequencies 0-250 Hz, 250-500 Hz, 500-1000 Hz. Then low pass portion is taken again and it is passed through low and high pass filters yielding four sets of signals corresponding to 0-125 Hz, 125-250 Hz, 250-500 Hz and 500-1000 Hz. If this procedure is continued until the signal is decomposed to a pre-defined certain level. Then a bunch of signals is obtained which actually represents the same signal, but all corresponding to different frequency bands. One can know which signal corresponds to which frequency band, and if all of them are put together and is plotted on a 3-D graph, with time in one axis, frequency in the second and amplitude in the third axis, it will show which frequencies exist at which time.

Higher frequencies are better resolved in time, and lower frequencies are better resolved in frequency. This means that, a certain high frequency component can be located better in time (with less relative error) than a low frequency component. On the contrary, a low frequency component can be located better in frequency compared to high frequency component.

## B.2 Wavelet transform- a first level introduction

Wavelet means ‘small wave’. So wavelet analysis is about analyzing signal with short duration finite energy functions. Wavelets transform the signal under investigation into another representation which presents the signal in a more useful form. This transformation of the signal is called wavelet transform. Unlike Fourier transform, wavelet transform has variety of wavelets which are used for signal analysis [103, 104].

The continuous wavelet transform was developed as an alternative approach to the short time Fourier transforms to overcome the resolution problem. The wavelet analysis is done in a way similar to the STFT analysis, in the sense that the signal is multiplied with a function (here it is wavelet), similar to the window function in the STFT, and the transform is computed separately for different segments of the time-domain signal. However, there are two main differences between the STFT and the CWT:

1. In CWT, the Fourier transforms of the windowed signals are not taken, and therefore single peak will be seen corresponding to a sinusoid, i.e., negative frequencies are not computed.

2. In CWT, the width of the window is changed as the transform is computed for every single spectral component, which is probably the most significant characteristic of the wavelet transform.

The wavelets are manipulated in two ways [103]. The first one is translation wherein the central position of the wavelet along the time axis is changed. The second is scaling wherein the wavelets are stretched or compressed along the time axis. Figs. B.1 and B.2 show the

translated and scaled versions of wavelets.

Fig. B.3 displays a schematic of the wavelet transform which basically quantifies the local matching of the wavelet with the signal. If the wavelet matches the shape of the signal well at

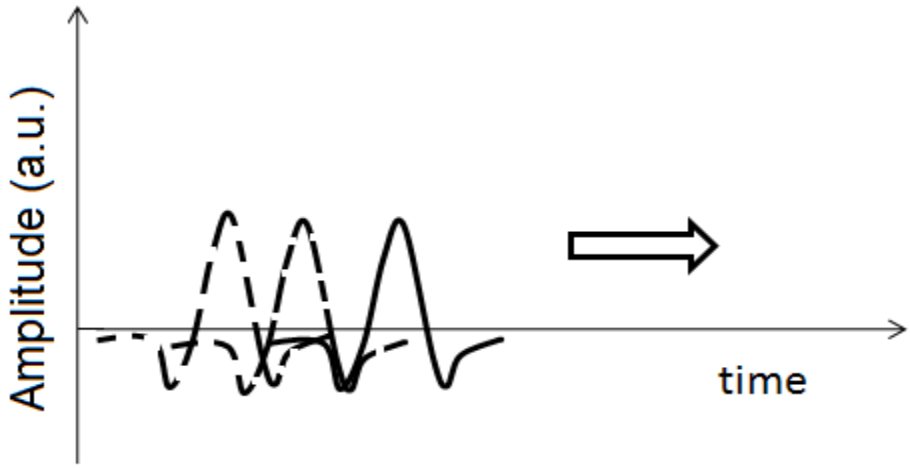


*Fig. B.1. Translation of wavelets [103].*

a specific scale and location, as it happens to do in the top plot of the Fig. B.3, then a large transform value is obtained. If, however, the wavelet and signal do not correlate well, a low value of transform is obtained. The transform value is then plotted in the two-dimensional transform plane shown at the bottom of the Fig. B.3 (indicated by a dot). The transform is computed at various locations of the signal and for various scales of the wavelet, thus filling up the transform plane. If the process is done in a smooth and continuous fashion (i.e. if scale and position are varied very smoothly) then the transform is called continuous wavelet transform. If the scale and position are changed in discrete steps, the transform is called discrete wavelet transform.

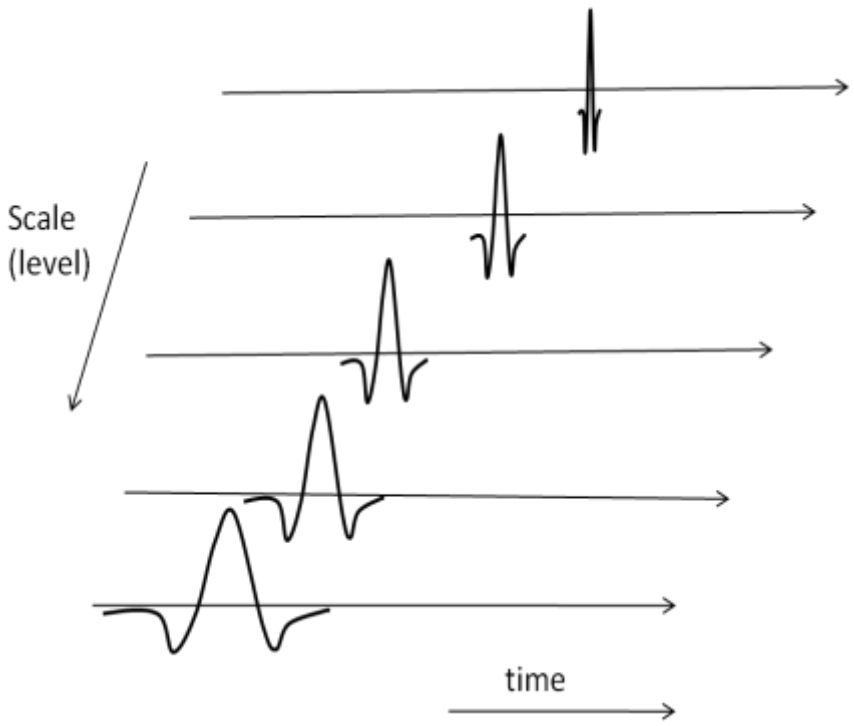


*Fig. B.2. Change in scale (also called level) of wavelets [103].*

Plotting the wavelet transform allows a picture to be built up of correlation between wavelet- at various scales, locations and the signal. Commercial software packages use various colours and its gradations to show the spectrum values on the two-dimensional plot. It may be noted that in case of Fourier transform, spectrum is one-dimensional array of values whereas in wavelet transform, a two-dimensional array of values is obtained. Also, the wavelet spectrum depends on the type of wavelet function used for analysis.

Mathematically, a wavelet is denoted as [103]:

$$\psi_{a,b}(t) = \frac{1}{\sqrt{|a|}}\psi\left(\frac{t-b}{a}\right) \tag{B.1}$$

where, *b* is location parameter and *a* is scaling parameter. For the function to be a wavelet, it should be time limited. For a given scaling parameter *a* wavelet is translated by varying the parameter *b*.

The wavelet transform is defines as [103],

$$W_{(a,b)} = \int f(t) \frac{1}{\sqrt{|a|}} \psi\left(\frac{t-b}{a}\right) dt \tag{B.2}$$

According to Eq. (B.2), for every *(a, b)*, a wavelet transform coefficient is obtained representing how much the scaled wavelet is similar to the function at location $t = b/a$.

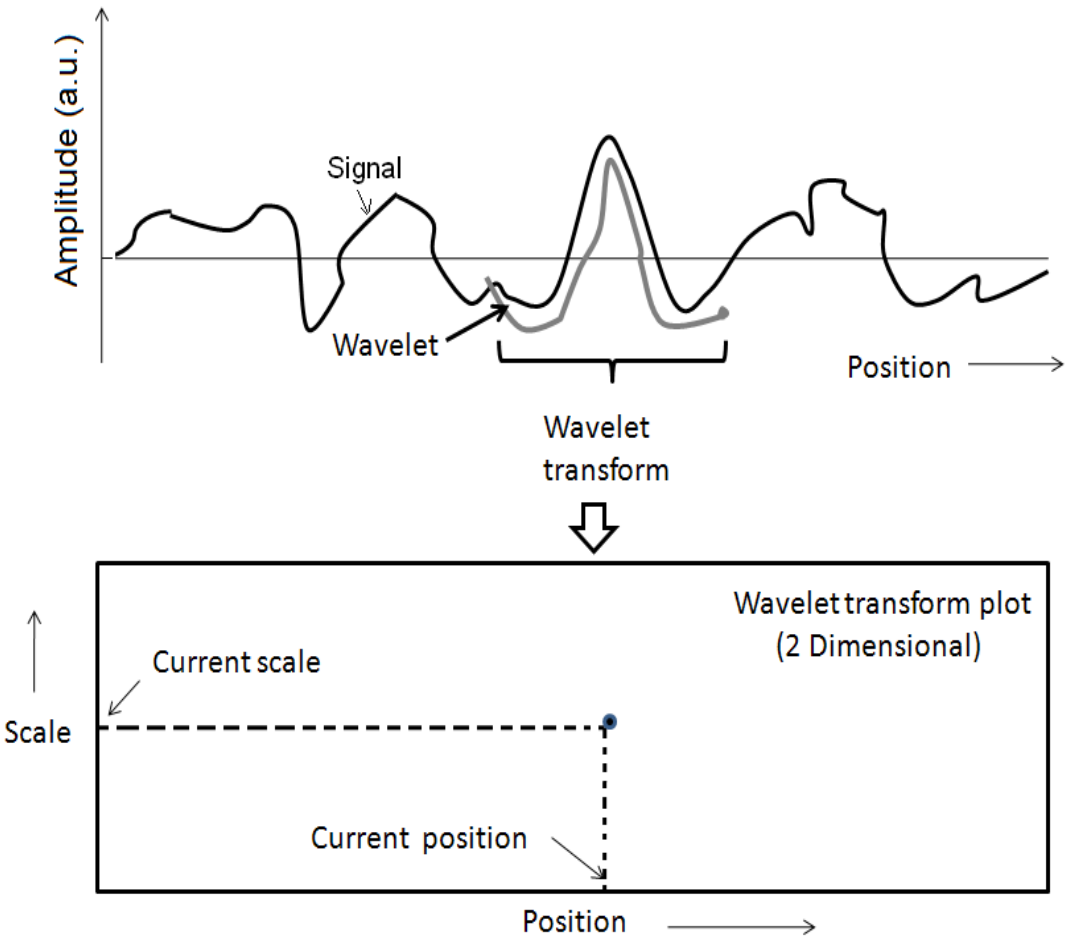


*Fig. B.3. The signal, wavelet and its wavelet transform [103].*

It is interesting to note here that *ψ(t)* is the transforming function, and it is called the mother wavelet. The term mother wavelet gets its name due to two important properties of the wavelet analysis as explained below:

The term wavelet means a small wave. The smallness refers to the condition that this (window) function is of finite length (compactly supported). The wave refers to the condition that this function is oscillatory. The term mother implies that the functions with different region of support that are used in the transformation process are derived from one main function, or the mother wavelet. In other words, the mother wavelet is a prototype for generating the other window functions.

For a signal *y(t)* defined as below, CWT plot could be obtained as below

$$y(t) = f1(t) + f2(t) + f3(t) \tag{B.3}$$

where,

$$f1(t) = \begin{cases} \sin(\,0.06\,\pi t) & 0 \leq t \leq 150 \\ 0 & otherwise \end{cases} \tag{B.4}$$

$$f2(t) = \begin{cases} \sin(\,0.04\,\pi t) & 150 \leq t \leq 300 \\ 0 & otherwise \end{cases} \tag{B.5}$$

and

$$f3(t) = \begin{cases} \sin(0.02\,\pi t) & 300 \le t \le 450 \\ 0 & otherwise \end{cases} \tag{B.6}$$

The function y(t) and its CWT can be plotted using following MATLAB program and are shown in Fig. B.4 and Fig. B.5 respectively.

```
%% MATLAB program for plotting CWT
t1=0:1:150;
t2=150:1:300;
t3=300:1:450;
f1=sin(2*pi*0.03*t1);
f2=sin(2*pi*0.02*t2);
f3=sin(2*pi*0.01*t3);
y=[f1 f2 f3];
plot(y)
figure;COEFS = cwt(y,1:200,'dB4','plot');
%% End of MATLAB program
```

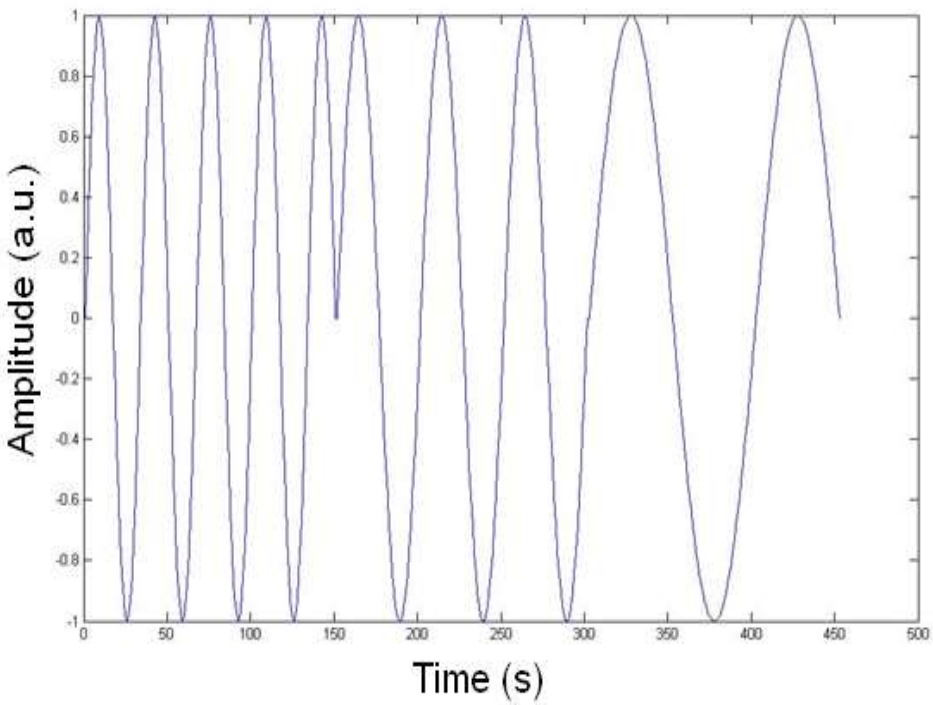


*Fig. B.4. Signal y(t) as a sum of three frequencies.*

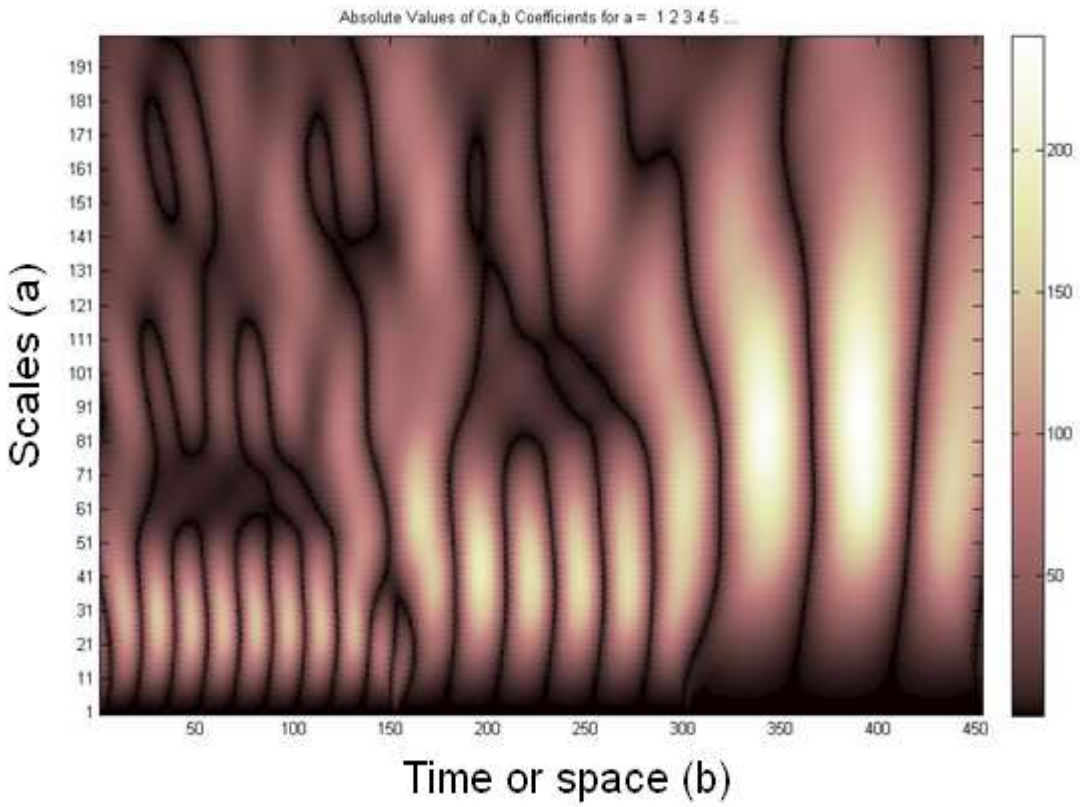


*Fig. B.5. CWT of the signal y(t).*

As seen in Fig. B.4, *y(t)* is sum of three truncated sine waves or tones of three different frequencies occurring over three different time periods. The CWT coefficients for this signal obtained through the 'sym2' wavelet function are depicted in Fig. B.5. Peaks occur in this figure for lower scales *(a = ~31)* in the range of $0 \leq b \leq 150$. This is the reflection of the fact that *y(t)* has highest frequency component (0.03 Hz). The next peak is observed at some higher scale (*a = ~47*) in the range of $150 \leq b \leq 300$. In this region, frequency is a bit lower (= 0.02 Hz). The third peak is observed at the highest level of scale (a = 90) for the period of in the range of $300 \leq b \leq 450$ which is because the frequency in this part of the signal is lowest (0.01 Hz).

## B.3 Time frequency tiles

In this section, a closer look at the resolution properties of the wavelet transform is examined.

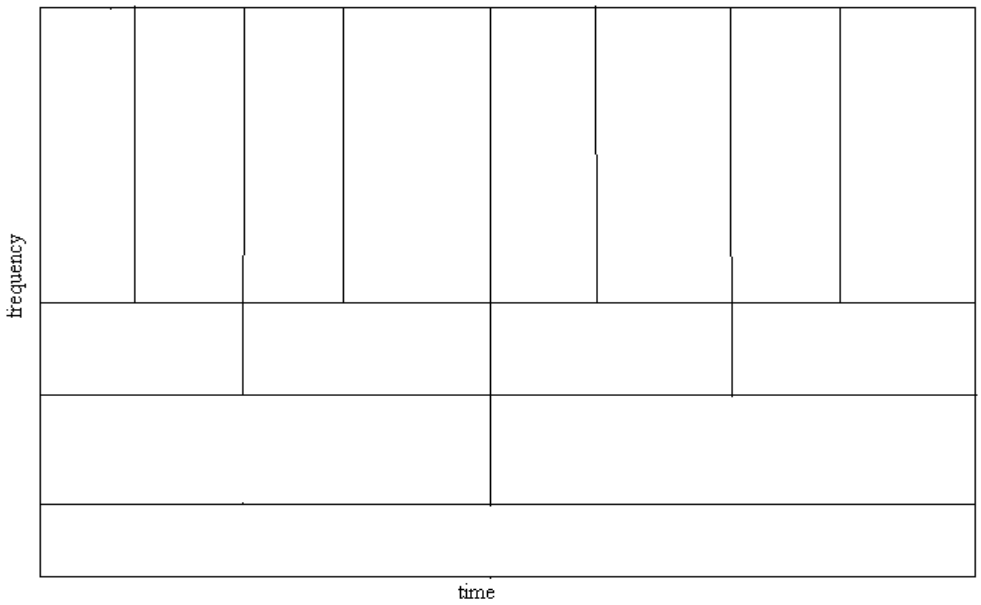


*Fig. B.6. Time frequency tiles [22].*

It may be noted that the resolution problem was the main reason for having switched from short term Fourier transform to wavelet trasnform. The illustration in Fig. B.6 is commonly used to explain how time and frequency resolutions should be interpreted. Every box in Fig. B.6 corresponds to a value of the wavelet transform in the time-frequency plane. It may be observed that boxes have a certain non-zero area, which implies that the value of a particular point in the time-frequency plane can not be known. All the points in the time-frequency plane that falls into a box are represented by one value of the wavelet trasnform. First thing to notice is that although the widths and heights of the boxes change, the area is constant. That is each box represents an equal portion of the time-frequency plane, but giving different proportions to time and frequency. At low frequencies, the height of the boxes are shorter

(which corresponds to better frequency resolutions, since there is less ambiguity regarding the value of the exact frequency), but their widths are longer (which correspond to poor time resolution, since there is more ambiguity regarding the value of the exact time). At higher frequencies the width of the boxes decreases, i.e., the time resolution gets better, and the heights of the boxes increase, i.e., the frequency resolution gets poorer. It is worthwhile to note how the partition looks like in the case of STFT. In STFT the time and frequency resolutions are determined by the width of the analysis window, which is selected once for the entire analysis, i.e., both time and frequency resolutions are constant. Therefore the time-frequency plane will consist of squares in the STFT case.

### B.4 Various wavelets

One-dimensional analysis is based on one scaling function $\varphi$ and one wavelet $\psi$. Fig. B.7 shows $\varphi$ and $\psi$ for each wavelet. All the functions decay quickly to zero. The Haar wavelet is the only noncontinuous function with three points of discontinuity (0, 0.5, 1). The 'coif2' wavelet exhibits some angular points; db6 and sym6 are quite smooth. The Morlet and Mexican hat wavelets are symmetrical.

### B.5 Continuous versus discrete wavelet transform

Continuous wavelet transform is a function of two parameters and, therefore, contains a high amount of extra (redundant) information when analyzing a function. Instead of continuously varying the parameters, the analysis of the signal with a small number of scales with varying number of translation at each scale is carried out. This is what is known as discrete wavelet transform. Although discrete wavelet transform may be derived without referring to

continuous wavelet transform, it may also be viewed as a “discretization” of the continuous wavelet transform through sampling specific wavelet coefficients. A critical sampling of continuous wavelet transform is given below.

$$W_{(a,b)} = \int f(t) \frac{1}{\sqrt{|a|}} \psi\left(\frac{t-b}{a}\right) dt \tag{B.7}$$

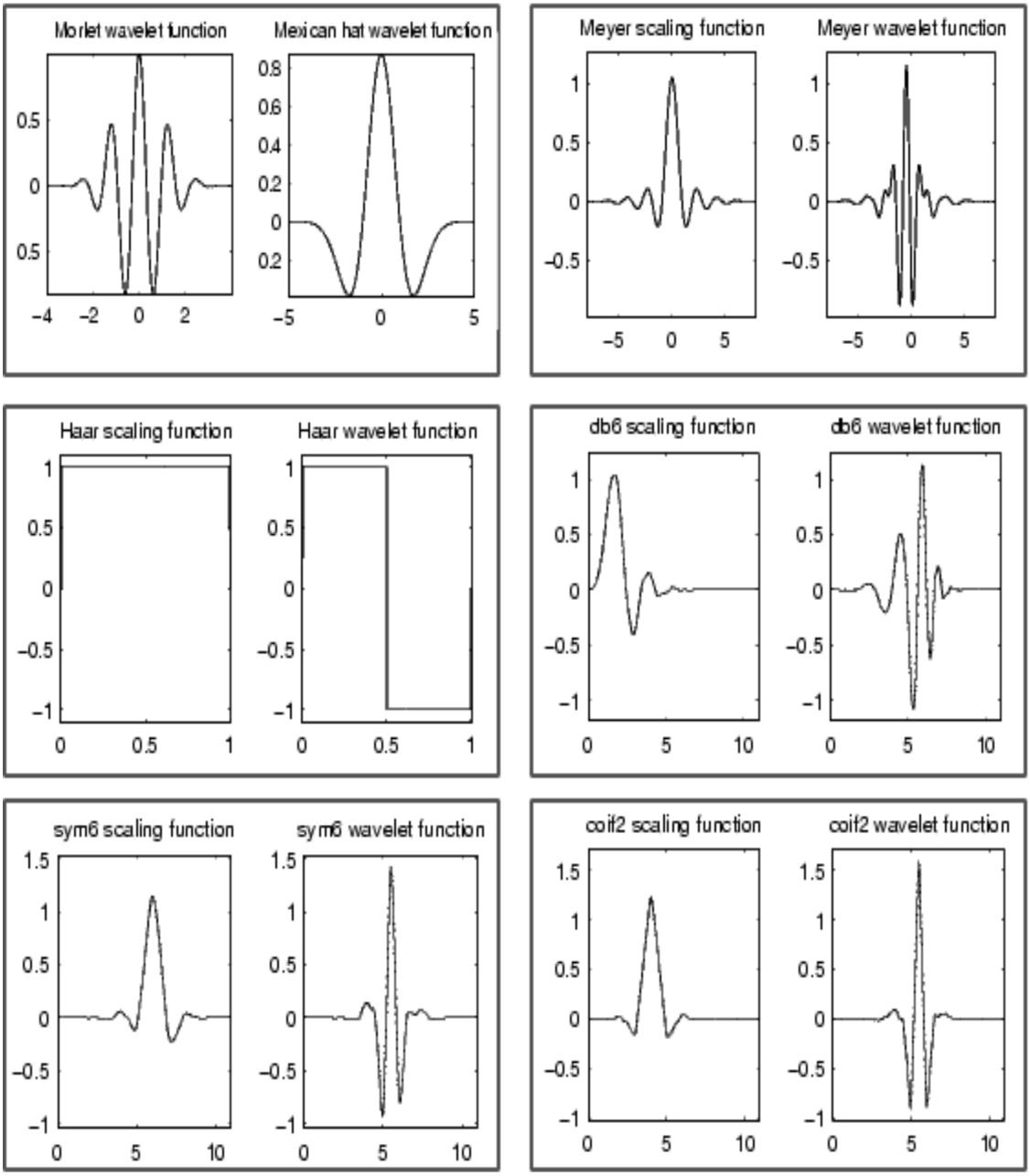


*Fig. B.7. Various wavelets (On horizontal axis is time and on vertical axis is amplitude) [103, 104].*

may be obtained via $a = 2^{-j}$ and $b = k2^{-j}$, where $j$ and $k$ are integers representing the set of discrete translations and discrete dilations. Upon this substitution, the term

$$\int f(t)\frac{1}{\sqrt{|a|}}\psi\left(\frac{t-b}{a}\right)dt$$

becomes

$$\int f(t)\,2^{j/2}\psi\left(2^{j}t-k\right)dt$$

which is a function of $j$ and $k$.

A critical sampling defines the resolution of discrete wavelet transform in both time and frequency. The term critical sampling is used to denote the minimum number of coefficients sampled from continuous wavelet transform to ensure that all the information present in the original function is retained by the wavelet coefficients. In continuous wavelet transform, wavelet coefficients are found for every *(a, b)* combination whereas in discrete wavelet transform, wavelet coefficients are found only at very few points denoted by the dots and the wavelets that follow these values are given by

$$\psi_{j,k}(t) = 2^{j/2}\psi\left(2^{j}t-k\right) \tag{B.8}$$

These wavelets for all integers $j$ and $k$ produce an orthogonal basis. It is interesting to note that $\psi_{0,0}(t) = \psi(t)$ is called as mother wavelet. Other wavelets are produced by translation and dilation of the mother wavelet.

# Appendix C

# Empirical mode decomposition

Empirical mode decomposition (EMD) is a new method for analyzing nonlinear and non-stationary data. It was pioneered by N. E. Huang in 1988 [28]. The key part of the technique is the ‘empirical mode decomposition’ method with which any complicated data set can be decomposed into a finite and often small number of `intrinsic mode functions' that have Hilbert transforms. This decomposition method is adaptive, and, therefore, highly efficient. Since the decomposition is based on the local characteristic time scale of the data, it is applicable to nonlinear and non-stationary processes.

## C.1 Evolution of empirical mode decomposition

The empirical mode decomposition (EMD) method generates a collection of intrinsic mode functions (IMFs). The decomposition is based on the direct extraction of the energy associated with various intrinsic time scales, the most important parameters of the system. Expressed in IMFs, they have Hilbert transforms, from which the instantaneous frequencies can be calculated. Thus, localization of any event on the time as well as the frequency axis is possible. The decomposition can also be viewed as an expansion of the data in terms of the IMFs. Then, these IMFs, based on and derived from the data, can serve as the basis of that expansion which can be linear or nonlinear as dictated by the data, and it is complete and almost orthogonal. Most important of all, it is adaptive. Also, locality and adaptivity are the necessary conditions for the basis for expanding nonlinear and non-stationary time series; orthogonality is not a necessary criterion for basis selection for a nonlinear system. The principle of this basis construction is based on the physical time scales that characterize the

oscillations of the phenomena. The local energy and the instantaneous frequency derived from the IMFs through the Hilbert transform can give a full energy - frequency - time distribution of the data. Such a representation is designated as the Hilbert spectrum and it is ideal for nonlinear and non-stationary data analysis. The first step is to pre-process the data by the empirical mode decomposition method with which the data can be decomposed into a number of intrinsic mode function components. Thus, the data is expanded into a number of bases derived from the data. The second step is to apply the Hilbert transform to the decomposed IMFs and construct the energy-frequency-time distribution, designated as the Hilbert spectrum, from which the time localities of events will be preserved. In other words, the instantaneous frequency and energy are needed rather than the global frequency and energy defined by the Fourier spectral analysis.

The notion of the instantaneous energy or the instantaneous envelope of the signal is well accepted; the notion of the instantaneous frequency, on the other hand, has been highly controversial. Existing opinions range from editing it out of existence to accepting it but only for special mono-component signals. There are two basic difficulties with accepting the idea of an instantaneous frequency as follows. The first one arises from the deeply entrenched influence of the Fourier spectral analysis. In the traditional Fourier analysis, the frequency is defined for the sine or cosine function spanning the whole data length with constant amplitude. As an extension of this definition, the instantaneous frequencies also have to relate to either a sine or a cosine function. Thus, at least one full oscillation of a sine or a cosine wave is needed to define the local frequency value. According to this logic, nothing shorter than a full wave will do. Such a definition would not make sense for non-stationary data for which the frequency has to change values from time to time. The second difficulty arises from the non-unique way in defining the instantaneous frequency. Nevertheless, this

difficulty is no longer serious since the introduction of the means to make the data analytical through. The instantaneous frequency is defined as differentiation of instantaneous phase $\theta(t)$ with respect to time.

This leads to introduce the term, 'mono-component function'. In principle, some limitations on the data are necessary, for the instantaneous frequency given in above equation is a single value function of time. At any given time, there is only one frequency value; therefore, it can only represent one component, hence `mono-component'. Unfortunately, no clear definition of the `mono-component' signal was given to judge whether a function is or is not `mono-component'. For lack of a precise definition, `narrow band' was adopted as a limitation on the data for the instantaneous frequency to make sense.

It is interesting to know the difference between global frequency and instantenous frequency. Global frequency $(<\omega>)$ is given by the average frequency derived by weighting by the Fourier power spectrum, $|S(\omega)|^2$ whereas for instantaneous frequency , first Hilbert transform $[Y(t)]$ of signal $X(t)$ is calculated and then a new term $Z(t)$ is introduced which is represented as

$$Z(t) = X(t) + i\,Y(t) = a(t)e^{i\theta(t)} \qquad \text{(C.1)}$$

$Z(t)$ has the same positive frequency spectrum as $X(t)$, but zero negative frequency spectrum. The physical interpretation of above two equation is that: $Y(t)$ is the best local fit (since the $1/t$ emphasizes local properties) of a trig function to $X(t)$ and polar coordinate description for $Z(t)$ allows the phase $\theta(t)$ to be defined from which instantaneous frequency $(\omega_i)$ can be calculated.

## C.2 The empirical mode decomposition as a filter bank

From the previous introduction, it can be seen that, the frequency-splitting principle of EMD is the same as wavelet transform. Both decompose the signal into two components, high frequency part and low frequency part, then, iterate on the latter, until all the information of different frequency band are extracted. Although the principle is similar, the frequency-splitting characteristics differ.

Wavelet transform is pre-determined frequency band decomposition, in other words, each frequency band is pre-determined, every resolution level is a band-pass filtering; EMD is different, EMD decomposes the data adaptively, the first IMF is high-pass filtering, residual is low-pass filtering, and others are all band-pass filtering. Furthermore, the entire frequency band is unknown, depending on the physical construction of the signal. To illustrate the filtering ability which is an inherent function of empirical mode decomposition's sifting process, a set of wind data collected in a laboratory wind-wave tunnel with a high-frequency response Pitot tube located 10 cm above the mean water level has been analyzed (Fig. 8.1 and 8.2). The data are quite complicated with many local extrema but no zero crossings, for the time series represents all positive numbers. If IMFs from C5 to C9 are combined, it is possible to get a filtered data which is free from high pass frequencies.

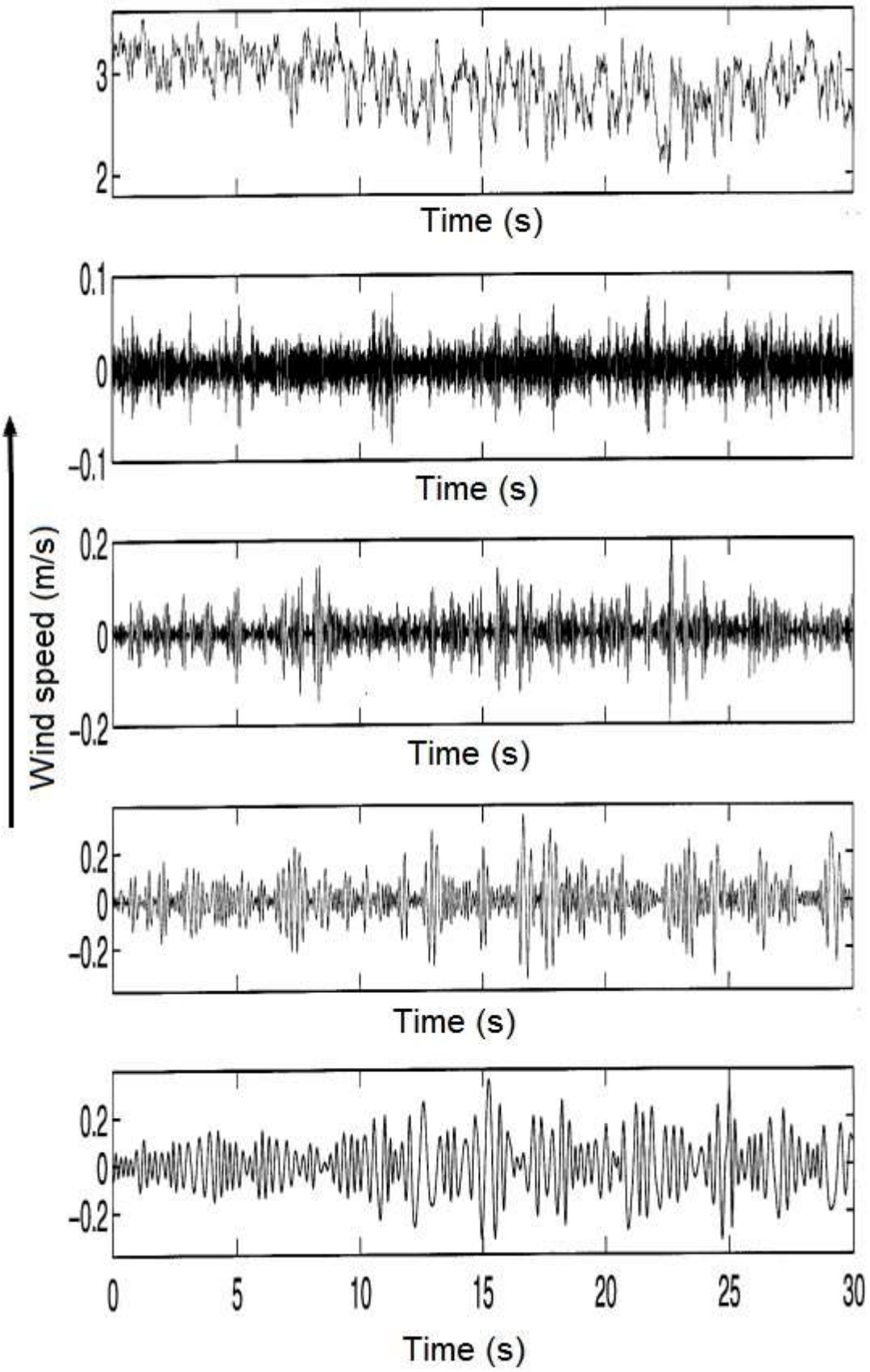


*Fig. C.1. The resulting EMD components from the wind data: the original data and the components C1-C4 appearing top to bottom [28].*

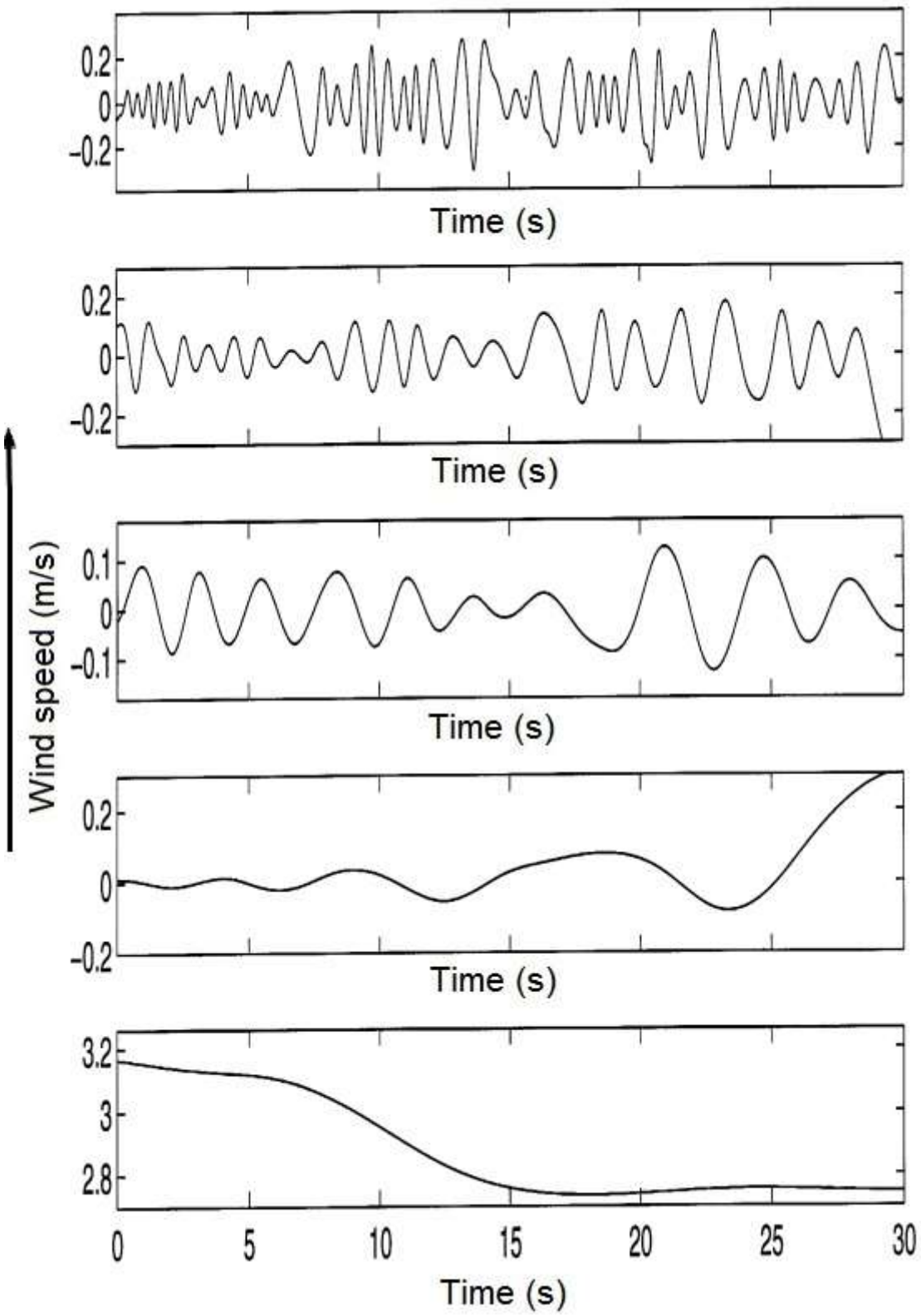


*Fig. C.2. The resulting EMD components from the wind data: components C5-C9 appearing top to bottom. The last component is the trend [28].*

# Appendix D

# PMT based detectors and DSCU

Schematic diagram of PMT based detectors [105, 106] and circuit diagram of DSCU [92] are presented in Fig. D.1 and D.2 respectively. Two number of PMT detector circuits were prepared using PMT R5108 [105]. One is used for AS signal detection whereas another is utilized for St signal detection. In Fig. D.1 power supply C4900 [106] is a high voltage dc-dc converter that converts +12 dc into –1.2 kV dc voltage. The high voltage is applied to PMT R5108 for dc biasing between Cathode (K) and Anode Plate (P). The signal ouput from PMT is fed to electrical amplifier (EA1/EA2) of SR445A (Fig. 3.5).

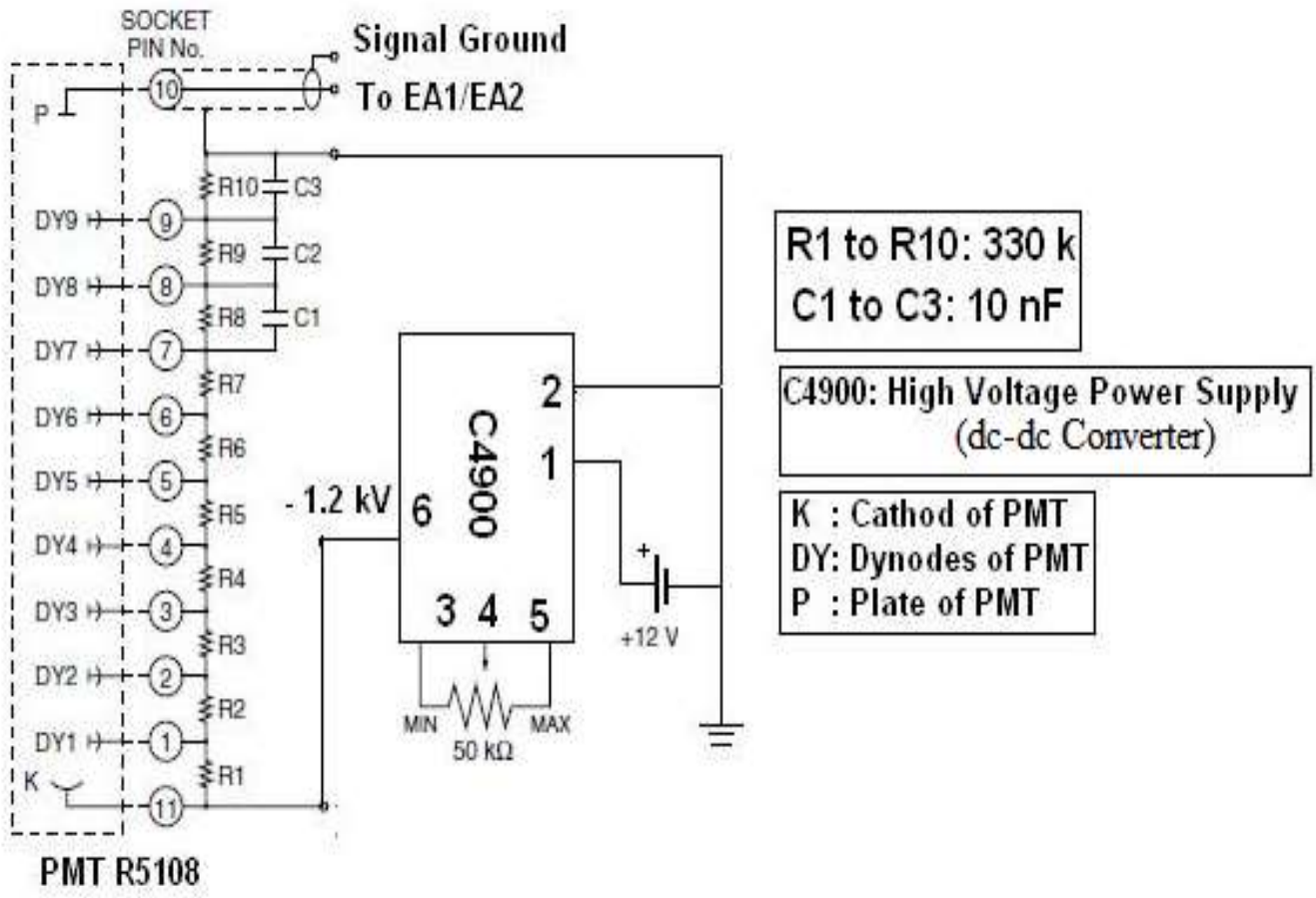


*Fig. D.1. Schematic diagram of PMT based detectors [105, 106].*

The circuit diagram of DSCU has been built around microcontroller 89V51RD2 [91] and is depicted in Fig. D.2.

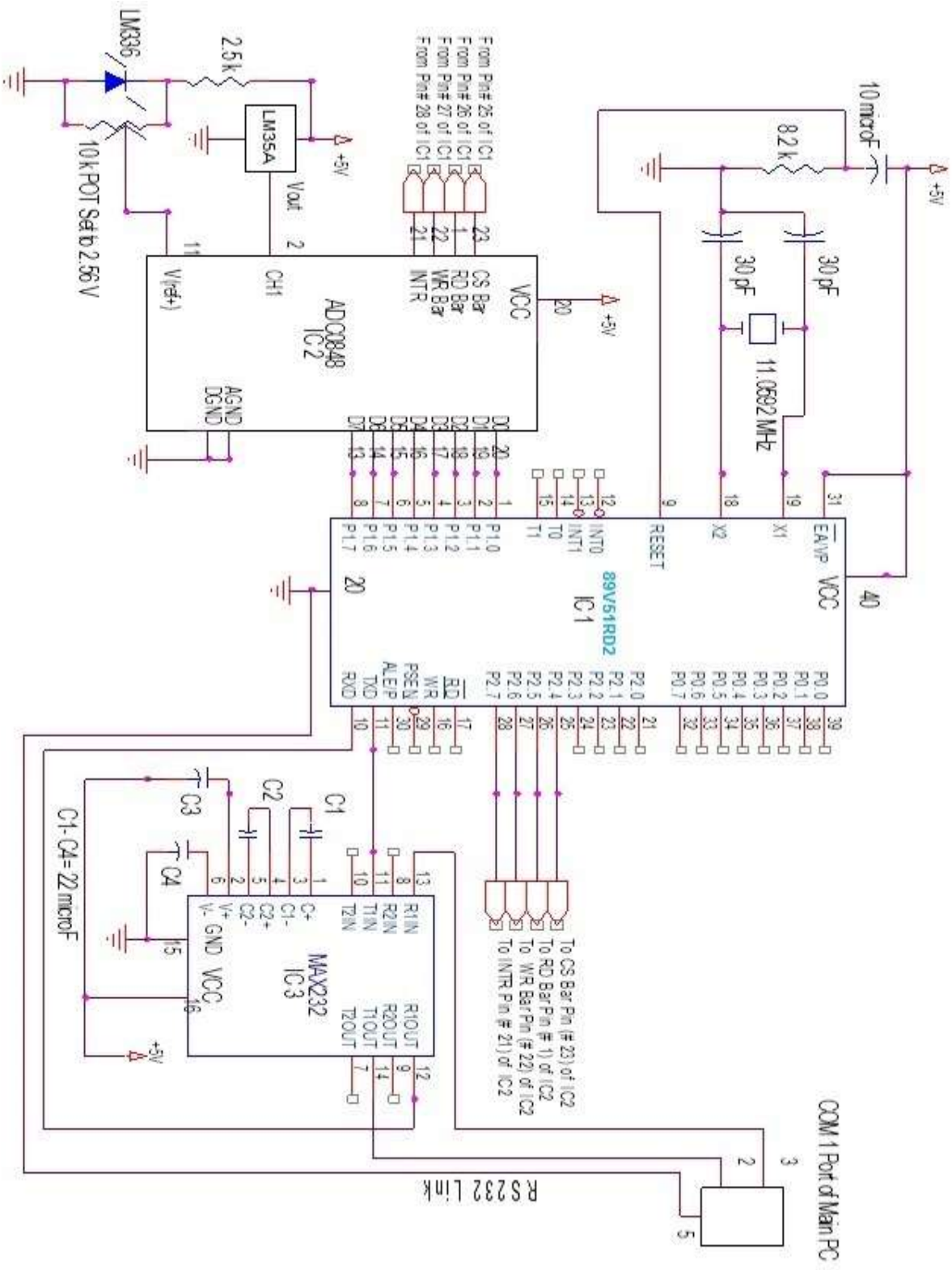


*Fig. D.2. Circuit diagram of dynamic self-calibration unit (DSCU).*

# REFERENCES

[1] Thorsen N., “Fiber Optics & the Telecommunication Explosion,” Pretice Hall PTR, Upper Saddle River, NJ, 1998, Chapter 2.

[2] Culshaw B., “Basic concepts of optical fiber sensors,” In: Dakin J., Culshaw B. (eds.), “Optical Fiber Sensors: Principle and components - vol. 1,” Artech House Inc., Norwood, MA, 1998.

[3] Culshaw B., “Optical Fiber Sensor Technologies: Opportunities and-perhaps-pitfalls,” Journal of Lightwave Technology 22 (1) (2004), pp. 39-50.

[4] Krohn D. A., “Fiber Optic Sensors: Fundamentals and Applications,” Instrument Society of America, Research B, Triangle Park, NC, 1998. pp. 7-13.

[5] Grattan K. T. V., Sun T., “Fiber optic sensor technology: Introduction and overview,” In: Grattan K. T. V. (eds.), “Optical Fiber Sensor Technology,” Kluwer Academic, London, 2000, Chapter 1.

[6] Grattan K. T. V., Sun T., “Fiber optic sensor technology: An overview,” Sensors and Actuators 82 (2000), pp. 40–61.

[7] Krohn D. A., “Fiber Optic Sensors: Fundamentals and Applications,” Instrument Society of America, Research B, Triangle Park, NC, 1998, Chapter 7.

[8] Culshaw B., Kersey A., “Fiber-optic sensing: A historical perspective,” Journal of Lightwave Technology 26 (2008), pp. 1064-1078.

[9] Long D. A., “The Raman Effect,” John Wiley, England, 2002, pp. 49-131.

[10] Dakin J. P., “Distributed optical fiber sensor systems,” In: Culshaw B., Dakin J. (eds.) “Optical Fiber Sensors: Systems and Applications - vol. 2,” Artech House Inc., Norwood, MA, 1989, pp. 575-597.

[11] Zhao X. F., Li L., Ba Q., Ou J. P., “Scour monitoring system of subsea pipeline using distributed Brillouin optical sensors based on active thermometry,” Optics & Laser Technololgy 44 (2012), pp. 2125-2129.

[12] Rogers A. J., “Distributed optical-fiber sensors for the measurements of pressure, strain and temperature,” Physics Reports 169 (1988), pp. 99-143.

[13] Yilmaz G., Karlik S. E., “A distributed optical fiber sensor for temperature detection in power cables,” Sensors & Actuators A Physical 125 (2006), pp. 148-155.

[14] Hurtig E., Großwig S., Kühn K., “Fiber optic temperature sensing: Application for subsurface and ground temperature measurements,” Tectonophysics 257 (1996), pp. 101-109.

[15] Höbel M., Ricka J., Wüthrich M., Binkert Th., “High-resolution distributed temperature sensing with the multiphoton-timing technique, Applied Optics 34 (1995), pp. 2955-2967.

[16] Lopez R. M., Spirina V. V., Miridonova S. V., Shlyagina M. G., Beltran G., Kuzin E. A., “Fiber optic distributed sensor for hydrocarbon leak localization based on transmission/ reflection measurement,” Optics & Laser Technology 34 (2012), pp. 465-469.

[17] Pandian C., “Single fiber grid with improved spatial resolution in distributed optical fiber sensor system,” IGC Newsletter 83 (2010), pp. 11-12. (http://www.igcar.ernet.in/lis/nl83/igc83.pdf)

[18] Baronski M. K., Jensen S. M., “Fiber waveguides: A novel technique for investigating attenuation characteristics,” Applied Optics 15 (1976), pp. 2112-2115.

[19] Personick S. D., “Photon probe-an optical-fiber time domain reflectometre,” Bell System Technical Journal 56 (1977), pp. 355-366.

[20] Rogers A. J., “Polarization optical time domain reflectometry,” Electronics Letters 16 (1980), pp. 489-490.

[21] Dakin J. P., Pratt D. J., Bibby G. W., Ross J. N., “Distributed optical fiber Raman temperature sensor using a semiconductor light source and detectors,” Electronics Letters 21(13) (1985), pp. 569-570.

[22] The wavelet tutorial by Robi Poliker, Rowan University Glassboro, NJ. (http://users.rowan.edu/~polikar/wavelets/wttutorial.html)

[23] Cohen L., “Time-Frequency Analysis,” Prentice Hal PTR, New Jersey, 1995, Chapter 7.

[24] Allen J. B., Rabiner L. R., “A unified approach to STFT analysis and synthesis,” In: Proceedings of the IEEE, 65 (1977), pp. 1558-1564.

[25] Portnoff M. R., “Time-frequency representation of digital signals and systems based on short-time Fourier analysis,” IEEE Transaction on Acoustics, Speech and Signal Processing. 28 (1980), pp. 55-69.

[26] Mallat S. G., “A theory for multiresolution signal decomposition: The wavelet representation,” IEEE Transaction on Pattern Analysis & Machine Intelligence 11 (1989), pp. 674-693.

[27] Ocak H., “Automatic detection of epileptic seizures in EEG using discrete wavelet transform and approximate entropy,” Expert System with Applications 36 (2009), pp. 2027-2036.

[28] Huang N. E., Shen Z., Long S. R., Wu M. C., Shih H. H., Zheng Q., *et al.*, “The empirical mode decomposition and Hilbert spectrum for nonlinear and nonstationary time series analysis.” Proceedings of the Royal Society A 454 (1998), pp. 903-995.

[29] Lee C. E., “Self-calibrating technique enables long-distance temperature sensing,” Laser Focus World 43 (2007), pp. 101-117.

[30] Chakraborty A. L., Kher S., Chaubey S., Nathan T. P. S., “Bidirectional frequency-domain digital filtering to simultaneously improve temperature resolution and eliminate spatial inaccuracy of a distributed temperature sensor,” Optical Engineering 43(2004), pp.

2724-2729.

[31] Hwang D., Yoon D. J., Kwon I. B., Seo D. C., Chung Y., " Novel auto-correction method in a fiber-optic distributed-temperature sensor using reflected anti-Stokes Raman scattering," Optics Express 18 (2010), pp. 9747-9754.

[32] Saxena M. K., Raju S. D. V. S. J., Arya R., Ravindranath S. V. G., Kher S., Oak S. M., "Optical fiber distributed temperature sensor using short term Fourier transform based simplified signal processing of Raman signals," Measurement 47 (2014), pp. 345-355.

[33] Saxena M. K., Raju S. D. V. S. J., Arya R, Pachori R. B., Ravindranath S. V. G., Kher S., Oak S. M., "Raman optical fiber distributed temperature sensor using wavelet transform based simplified signal processing of Raman backscattered signals," Optics & Laser Technology 65 (2014), pp. 14-24.

[34] Saxena M. K., Raju S. D. V. S. J., Arya R., Pachori R. B., Ravindranath S. V. G., Kher S., Oak S. M., "Empirical mode decomposition based dynamic error correction in SS covered 62.5/125 μm optical fiber based distributed temperature sensor," Optics & Laser Technology 67 (2015), pp. 107-118.

[35] Saxena M. K., Raju S. D. V. S. J., Arya R., Pachori R. B., Ravindranath S. V. G., Kher S., Oak S. M., "Microcontroller based Raman optical fiber distributed temperature sensor and alarm system," Journal of the Instrument Society of India 44 (1) (2014), pp. 28-31.

[36] Saxena M. K., Raju S. D. V. S. J., Arya R., Pachori R. B., Ravindranath S. V. G., Kher

S., Oak S. M., "Empirical mode decomposition-based detection of bend-induced error and its correction in a Raman optical fiber distributed temperature sensor," IEEE Sensors Journal 16 (5) (2016), pp. 1243-1252.

[37] Donghoh K. and Hee-Seok O., "EMD: A Package for empirical mode decomposition and Hilbert Spectrum," The R. Journal 1 (1) (2009), pp. 40-46. (http://journal.r-project.org/archive/2009-1/RJournal_2009-1_Kim+Oh.pdf)

[38] Gupta S. L., Kumar V., Sharma R. C., "Elements of Spectroscopy," Pragati Prakashan, Meerut, 2010, Chapter 4.

[39] Stoddart P. R., Cadusch P. J., Pearce J. B., Vukovic D., Nagrajah C. R., Booth D. J., "Fiber optic distributed temperature sensor with an integrated background correction function," Measurement Science & Technology 16 (6) (2005), pp. 1299-1304.

[40] Fernandez A. F., Rodeghiero P., Brichard B., Berghmans F., Hartog A. H., Hughes P., Williams K., Leach A. P., "Radiation-tolerant Raman distributed temperature monitoring system for large nuclear infrastructures," IEEE Transactions on Nuclear Science 52 (2005), pp. 2689-2694.

[41] Suh K., Lee C., "Auto-correction method for differential attenuation in a fiber-optic distributed-temperature sensor," Optics Letters 33 (2008), pp. 1845-1847.

[42] Soto M. A., Signorini A., Nannipieri T., Faralli S., Bolognini G., "Impact of loss variations on double-ended distributed temperature sensors based on Raman anti-Stokes

signal only," Journal of Lightwave Technology 30 (2012), pp. 1215-1222.

[43] Guang-yong X., Jian-ping Y., Kun-jun Z., Wen M., "Monitoring data processing of distributed optical fiber temperature sensor based on multi-wavelet," In: Proceedings of the International Workshop on Education Technology and Training & International Workshop on Geoscience and Remote Sensing 2008, pp. 203-206. (doi: 10.1109/ETTandGRS.2008.60)

[44] Xiaobing L., Jiangtao G., "Wavelet analysis in distributed optical fiber temperature sensor," Proceedings of the Asia Communications and Photonics Conference (ACP/IPOC) 2013, paper code AF21.3.

[45] Wang Z., Chang J., Zhang S., Luo S., Jia C., Sun B., Jiang S., Liu Y., Liu X., Lv G., Liu Z., "Application of wavelet transform modulus maxima in Raman distributed temperature sensors," Photonic Sensors 4 (2014), pp. 142-146.

[46] Hou S., Jian Y., Chen Y., Han L., "Signal processing of single-mode fiber sensor system based on Raman scattering," In: Proceedings of the 2nd International Conference on Advanced Computer Control 2010, pp. 176-181.

[47] Henderson R. D., Day-Lewis F. D., Harvey C. F., "Investigation of aquifer-estuary interaction using wavelet analysis of fiber-optic temperature data," Geophysics Research Letters 36 (2009), pp. 1-6. (doi:10.1029/2008GL036926) .

[48] Chakraborty A. L., Sharma R. K., Saxena M. K., Kher S., "Compensation for

temperature dependence of Stokes signal and dynamic self-calibration of a Raman distributed temperature sensor," Optics Communication 274 (2007), pp. 396-402.

[49] Wong A. C. L., Peng G. D., "Applications of discrete wavelet transform in optical fiber sensing," In: Olkkonen H. (ed.), "Discrete Wavelet Transforms-Biomedical Applications," In Tech, Shanghai, 2011, pp. 221-248.

[50] Bahrampour A. R., Maasoumi F., "Resolution enhancement in long pulse OTDR for application in structural health monitoring," Optical Fiber Technology 16 (2010), pp. 240-249.

[51] Bahrampour A. R., Moosavi A., Bahrampour M. J., Safaei L., "Spatial resolution enhancement in fiber Raman distributed temperature sensor by employing ForWaRD deconvolution algorithm," Optical Fiber Technology 17 (2011), pp. 128-134.

[52] Bazzo J. P., Pipa D. R., Martelli C., Vagner da Silva E., Cardozo da Silva J. C., "Improving spatial resolution of Raman DTS using total variation deconvolution," IEEE Sensors Journal 16 (11) (2016), pp. 4425-4430.

[53] Soto M. A., Ramírez J. A., The´venaz L., "Intensifying the response of distributed optical fibre sensors using 2D and 3D image restoration," Nature Communications 7 (2016), Article No. 10870. (doi: 10.1038/ncomms10870)

[54] Zhong Y. P., Zhang Q., Zhou D., "Distributed optical fiber Raman signal noise cancellation based on empirical mode decomposition," Applied Mechanics and Materials

198 (2012), pp. 1621-1626.

[55] Pandian C., Kasinathan M., Sosamma S., Babu Rao C., Jayakumar T., Murali N., Raj B., “Looped back fiber mode for reduction of false alarm in leak detection using distributed optical fiber sensor,” Applied Optics 49 (20) (2010), pp. 3869-3874.

[56] Ravet F., “Submillimeter crack detection with Brillouin-based fiber-optic sensors,” IEEE Sensors Journal 9 (2009), pp. 1391-1396.

[57] Horiguchi T., Shimizu K., Kurashima T., Tateda M., Koyamada Y., “Development of a distributed sensing technique using Brillouin scattering,” Journal of Ligthwave Technology 13 (1995), pp. 1296-1302.

[58] Ifeachor E. C., Jervis B. W., “Digital Signal Processing: A Practical Approach,” Pearson Education, Singapore, 2004, pp. 111-135.

[59] Etter D. M., “Introduction to MATLAB for Engineers and Scientists,” Prentice Hall, Upper Saddle River, New Jersey, 1996.

[60] Mitra S. K., “Digital Signal Processing: A Computer-Based Approach,” Tata McGraw-Hill, New Delhi, 2001, Chapter 8.

[61] Kher S., Srikanth G., Chaube S., Chakraborty A. L., Nathan T. P. S., D. D. Bhawalkar, “Design, development and studies on Raman based fiber-optic distributed temperature sensor,” Current Science 83 (11) (2002), pp. 1365-1368.

[62] Kher S., Srikanth G., Saxena M. K., Nathan T. P. S., “Development of distributed fiber optic temperature sensor with sub-meter resolution,” Current Science 86 (9) (2004), pp. 1202-1204.

[63] Abbott D., “PCI Bus Demystified,” Elsevier, Amsterdam, 2004.

[64] Fukuzawa T., Shida H., Oishi K., Takeuchi N., Adachi S., “Performance improvements in Raman distributed temperature sensor,” Photonic Sensors 3 (2013), pp. 314-319.

[65] Wang Z. L., Chang J., Zhang S. S., Lv G. P., Wang W. J., Jiang S., *et al.*, “Spatial resolution improvement of distributed Raman temperature measurement system,” IEEE Sensors Journal 13 (2013), pp. 4271-4278.

[66] Vo T. D., He J., Magi E., Collins M. J., Clark A. S., Ferguson B. G., Xiong C., Eggleton B. J., “Chalcogenide fiber-based distributed temperature sensor with sub-centimeter spatial resolution and enhanced accuracy,” Optics Express 22 (2014), pp.1560-1568.

[67] Mix D. F., “Elements of Wavelets for Engineers and Scientists,” Wiley- Interscience, New Jersey, 2003.

[68] Fugal D. L., “Conceptual wavelets in Digital Signal Processing,” Space and Signal Technical Publication. San Diago, California, 2009.

[69] Gadre V. M., “Advanced Digital Signal Processing - Multirate and Wavelets,” Lecture Notes, NPTEL, IITM.

(http://nptel.ac.in/downloads/117101001/).

[70] Mallat S., “A Wavelet Tour of Signal Processing: The Sparse Way,” Academic, Burlington, Academic, 2009.

[71] Vetterli M., Herley C., “Wavelets and filter banks: Theory and design,” IEEE Transactions on Signal Processing 40 (9) (1992), pp. 2207-2232.

[72] Ifeachor E. C., Jervis B. W., “Digital Signal Processing: A Practical Approach,” Pearson Education, Singapore, 2004, pp. 141-151.

[73] Jirasek A., Schulze G., Yu M. M. L., Blades W., Turner R. F. B., “Accuracy and precision of manual baseline determination,” Applied Spectroscopy 58(12) (2004), pp. 1488-1499.

[74] Zhao J., Lui H., McLean D. I., Zeng H., “Automated autofluorescence background subtraction algorithm for biomedical Raman spectroscopy,” Applied Spectroscopy 61 (2007), pp.1225-1232.

[75] Alsberg B. K., Woodward A. M., Kell D. B., “An introduction to wavelet transforms for chemometricians: A time-frequency approach,” Chemometrics and Intelligent Laboratory Systems 37 (1997), pp. 215-239.

[76] Donoho D. L., “De-noising by soft-thresholding,” IEEE Transaction on Information Theory 41 (3) (1995), pp. 613-627.

[77] Donoho D. L., Johnstone I. M., “Adapting to unknown smoothness via wavelet shrinkage,” Journal of the American Statistical Association 90 (432) (1995), pp. 1200- 1224.

[78] Daubechies I., “Ten Lectures on Wavelets,” Society for Industrial and Applied Mathematics, Philadelphia, 1992.

[79] Venkataraman P., “Applied Optimization with MATLAB Programming,” Wiley-Interscience, USA, 2001, Chapter 2.

[80] Wu M. C., Huang N. E., “Biomedical data processing Using HHT: A review,” In: A. Naït Ali (ed.), “Advanced Biosignal Processing,” Springer-Verlag, Heidelberg, 2009, pp. 335-352.

[81] Wu Z., Huang N. E., Long S. R., Peng C., “On the trend, detrending, and variability of nonlinear and nonstationary time series,” Proceedings of the National Academy of Sciences of the USA 104 (2007), pp. 14889-94.

[82] Li C., Liang M., “Oil debris signal detection based on integral transform and empirical mode decomposition,” World Academy of Science, Engineering and Technology 76 (2011), pp. 190-194.

[83] Wu S., Liu Z., Liu B., “Enhancement of lidar backscatters signal-to-noise ratio using empirical mode decomposition method,” Optics Communication 267 (2006), pp. 137-144.

[84] Parey A., Pachori R. B., “Variable cosine windowing of intrinsic mode functions:

Application to gear fault diagnosis." Measurement 45 (2012), pp. 415-426.

[85] Huang H., Pan J., "Speech pitch determination based on Hilbert-Huang transform," Signal Processing 86 (2006), pp.792-803.

[86] Pachori R. B., Hewson D., Snoussi H., Duchene J., "Postural time-series analysis using empirical mode decomposition and second-order difference plots," In: Proceedings of the IEEE International Conference on Acoustics, Speech, and Signal Proceessing, Taipei, 2009, pp. 537-540.

[87] Pachori R. B., "Discrimination between ictal and seizure-free EEG signals using empirical mode decomposition," Research Letters in Signal Processing 293056 (2008), pp. 1-5.

[88] Ishii H., Kawamura K., Ono T., Megumi H., Kikkawa A., "A fire detection system using optical fibers for utility tunnels," Fire Safety Journal 29 (1997), pp. 87-98.

[89] Bolognini G., Hartog A., "Raman-based fiber sensors: Trends and applications," Optical Fiber Technology 19 (2013), pp. 678-688.

[90] Perez-Herrera R. A., Lopez-Amo M., "Fiber optic sensor networks," Optical Fiber Technology 19 (2013), pp. 689-699.

[91] Data Sheet 89V51RD2
(http://netmedia.com/siteplayer/telnet/documents/p89v51rb2.p89v51rc2.p89v51rd2.pdf)

[92] Mazidi M. A., Mazidi J. G., McKinlay R. D., “The 8051 Microcontroller and Embedded Systems using Assembly and C,” PHI, New Delhi, 2006, Chapter 13.

[93] Pachori R. B., Avinash P., Shashank K., Sharma R., Acharya U. R., “Application of empirical mode decomposition for analysis of normal and diabetic RR-interval signals,” Expert Systems with Applications 9 (1) (2015), pp. 4567–4581.

[94] Pachori R. B., Bajaj V., “Analysis of normal and epileptic seizure EEG signals using empirical mode decomposition,” Computer Methods and Programs in Biomedicine 104 (2011), pp. 373–381.

[95] Bajaj V., Pachori R. B., “Epileptic seizure detection based on the instantaneous area of analytic intrinsic mode functions of EEG signals,” Biomedical Engineering Letters, 3 (1) (2013), pp. 17-21.

[96] Jahanadan S., Munajat Y., “The usage of optical coupler and its optimization signal in modified optical time domain reflectometer,” Journal of Fundamental Science 7 (2011), pp. 31-34.

[97] Tateda M., Horiguchi T., “Advances in optical time-domain reflectometry,” Journal of Lightwave Technology 8 (1989), pp. 1217-1224.

[98] Lai Y. C., Ye N., “Recent developments in chaotic time series analysis,” International Journal of Bifurcation Chaos 13 (2003), pp. 1383-1422.

[99] Cohen M. E., Hudson D. L., Deedwania P. “Applying continuous chaotic modeling to cardic signal analysis,” IEEE Engineering in Medicine and Biology Magazine 15 (1996), pp. 97-102.

[100] Freund R. J., Wilson W. J., Mohr D. J., “Statistical Methods,” Academic, Burlington, MA, USA, 2010.

[101] Selesnick I. W., Baraniuk R. G., Kingsbury N. G., “The dual-tree complex wavelet transform,” IEEE Signal Processing Magazine 1053-5888/05/ (2005), pp. 123-151.

[102] Pandian C., Kasinathan M., Sosamma S., Babu Rao C., Murali N., Jayakumar T., Raj B., “One-dimensional temperature reconstruction for Raman distributed temperature sensor using path delay multiplexing,” Journal of Optical Society of America B 26 (12) (2009), pp. 2423-2426,

[103] Soman K. P., Ramachandran K. I., Resmi N. G., “Insight into Wavelets: From Theory to Practice,” PHI Learning, New Delhi, 2011.

[104] Rao R. M., Bopardikar A. S., “Wavelet Transforms: Introduction to Theory and Applications,” Pearson, New Delhi, 2011.

[105] Data sheet PMT R5108. (https://www.hamamatsu.com/us/en/R5108.html)

[106] Data sheet C4900. (https://www.hamamatsu.com/us/en/C4900.html)